# BULLETIN OF THE
# LABORATORY FOR ZERO-CARBON ENERGY

▼

VOL. 1
2022

Laboratory for Zero-Carbon Energy (ZC)
Institute of Innovative Research
Tokyo Institute of Technology

# BULLETIN OF THE LABORATORY FOR ZERO-CARBON ENERGY

## (Formerly, BULLETIN OF THE LABORATORY FOR ADVANCED NUCLEAR ENERGY)

Abbreviation of the ″**BULLETIN OF THE LABORATORY FOR ZERO-CARBON ENERGY**″ is "**BULL. LAB. ZC. ENERGY**"

BULLETIN OF THE LABORATORY FOR ZERO-CARBON ENERGY
*BULL. LAB. ZC. ENERGY, Vol.1, 2022*

## CONTENTS

## IV. Co-operative Researches

## V. List of Publications

# Research staffs of
## THE LABORATORY FOR ZERO-CARBON ENERGY,
## TOKYO INSTITUTE OF TECHONOGY
### AS OF 2022 JAPANESE FISCAL YEAR

**Director**

| | |
|---|---|
| Yukitaka Kato | Professor |

**Future Energy Division**

| | |
|---|---|
| Junichiro Otomo | Professor |
| Takehiko Tsukahara | Professor |
| Yoichi Murakami | Professor |
| Hiroki Takasu | Associate Professor |
| Toshiyuki Yokoi | Associate Professor |
| Takao Kashiwagi | Institute Professor |
| Ryoji Kanno | Institute Professor |
| Hiroshi Asano | Specially Appointed Professor |
| Takuya Oda | Specially Appointed Professor |
| Ken Koyama | Specially Appointed Professor |
| Tsuyoshi Fujita | Specially Appointed Professor |
| Atsushi Morihara | Specially Appointed Professor |

**Nuclear Energy Division**

| | |
|---|---|
| Yoshiyuki Oguri | Professor |
| Toru Obara | Professor |
| Yoshinao Kobayashi | Professor |
| Satoshi Chiba | Professor |
| Noriyasu Hayashizaki | Professor |
| Yoshihisa Matsumoto | Professor |
| Hiroshi Akatsuka | Associate Professor |
| Tatsuya Katabuchi | Associate Professor |
| Hiroshige Kikura | Associate Professor |
| Masatoshi Kondo | Associate Professor |
| Hiroshi Sagara | Associate Professor |
| Koichiro Takao | Associate Professor |
| Hiroaki Tsutsui | Associate Professor |
| Jun Hasegawa | Associate Professor |
| Katsumi Yoshida | Associate Professor |
| Chikako Ishizuka | Assistant Professor |
| Naokazu Idota | Assistant Professor |
| Hanna Hubarevich | Assistant Professor |
| Mikio Shimada | Assistant Professor |
| Masahiko Nakase | Assistant Professor |
| Jun Nishiyama | Assistant Professor |
| Shintaro Yasui | Assistant Professor |

**Other Faculties**

| | |
|---|---|
| Kenji Takeshita | Specially Appointed Professor |
| Hiroyasu Mochizuki | Specially Appointed Professor |
| Tadashi Narabayashi | Specially Appointed Professor |
| Masahiro Okamura | Specially Appointed Professor |
| Satoru Tsushima | Specially Appointed Associate Professor |
| Sunil Chirayath | Specially Appointed Associate Professor |
| Daisuke Nagae | Specially Appointed Associate Professor |
| Chi Young Han | Specially Appointed Associate Professor |
| Ayumi Ito | Specially Appointed Assistant Professor |
| Aki Murata | Specially Appointed Assistant Professor |
| Hidekazu Asano | Visiting Professor |
| Kenji Nishihara | Visiting Professor |
| Tatsuro Matsumura | Visiting Professor |
| Takatoshi Takemoto | Visiting Associate Professor |

**Technical Staffs**

| | |
|---|---|
| Isao Yoda | Senior Technical Specialist |
| Kazuo Takezawa | Senior Technical Specialist |
| Ken-ichi Tosaka | Senior Technical Specialist |
| Atsushi Nezu | Senior Technical Specialist |
| Hitoshi Fukuda | Senior Technical Specialist |
| Yuko Suzuki | Senior Technical Specialist |

# I. Vision for Green Transformation of Laboratory of Zero-Carbon Energy

# I.

# Vision for Green Transformation of Laboratory of Zero-Carbon Energy

Yukitka Kato

## 1. Introduction

Laboratory for Zero-Carbon Energy (ZC Lab), Institute of Innovative Research, Tokyo Institute of Technology, was established in June 2021 with the aim of contributing to a carbon neutrality (CN) society through technology using zero carbon energy[1]. This paper introduces the vision that ZC Labs is aiming for, the challenges to realize it, and the efforts to solve the challenges.

## 2. Realization of carbon neutrality

Reduction of carbon dioxide ($CO_2$) emissions is necessary to mitigate global warming. On the other hand, the world requires for a modern and prosperous society. Green Transformation (GX) can be defined as a social transformation toward the realization of a green society using zero-carbon energy. At the establishment of ZC Lab, we defined the ideal green society vision and extracted the issues for its realization. At our laboratory, we are developing activities with the aim of realizing GX technology for problem solving.

CN is correct as a goal, but it seems very difficult to achieve. In particular, Japan's energy environment is different from that of other countries, and we believe it is necessary to share the awareness that it will be difficult to achieve this simply by imitating other countries' examples. The Japanese government aims to achieve CN by 2050. Figure 1 shows ZC Lab's strategy for realizing a CN society in 2050 in terms of (1) energy supply and (2) energy use [1].

85% of primary energy is fossil fuel, 15% of one is non-fossil energy (zero carbon energy), that is, renewable energy includes photovoltaic, wind and hydroelectric power generation, and nuclear power. In the future, achieving CN will require a drastic reduction in fossil fuels and zero-carbon energy to replace them. On the other hand, in recent years, power shortages have frequently occurred throughout the country due to factors such as non-operation of renewable energy sources and an increase in electricity demand due to the atmospheric temperature steep fluctuations. In addition, the issue of energy supply security has become more apparent, and the use of domestic primary energy and its application technology continue to be desired.

Energy users are classified into power and non-power. Electric power accounts for less than 30% based on the enthalpy base, and the majority is in the non-electric power sector. In the non-electric field, fuel is converted into heat, and the enthalpy is used in Japan's key industries such as transportation, steel and chemical industries. CN in the non-electric field is quantitatively important, and GX technologies such as energy networks, carbon recycling, and energy storage are required.

## 3. Vision for a Green Society of ZC Lab

It is difficult to achieve CN by applying conventional technology, and GX will be required as a non-linear technological and social reform. Fig. 2 shows the green society vision proposed by ZC Labs. In 20th century, fossil energy has been the main source of conventional primary energy, and there was no limit to $CO_2$ emissions, resulting in global warming. To overcome this problem, it is necessary to convert primary energy to zero-carbon energy and to use green energy in society in the new era.

Energy storage is essential for stable use of fluctuating renewable energy output. The use of secondary batteries, which is currently leading the way, poses a raw material supply risk with high-cost, and it is predicted that other energy storage options
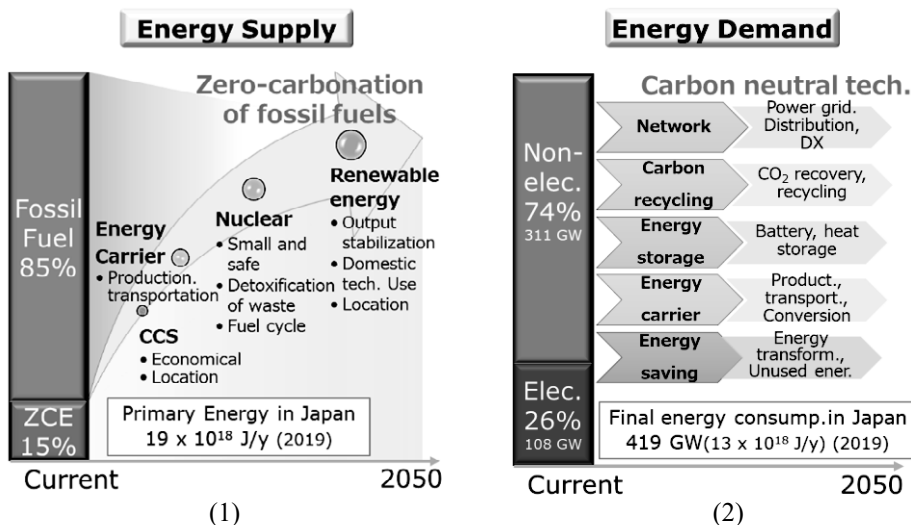
Fig.1 Strategy for attainment of Carbon Neutrality by 2050 in Japan, (1) Roadmap for the transition from fissile fuels to zero-carbon energy for primary energy in Japan, (2) Final energy consumption and introduction of carbon neutral technologies for CN society in Japan

will be necessary. Heat storage has potential as a large-volume, low-cost storage technology. Furthermore, energy carrier conversion such as hydrogen production by electrolysis using renewable energy, ammonia production, and material conversion to methanation and synthetic fuel for e-fuel and SAF (sustainable aviation fuel) are also important as energy storage. Electrification is required on the energy user side. On the other hand, carbon has had an affinity with mankind since ancient times, and decarbonization is expected to reach a limit, and a society that can use carbon as an energy source is highly robust and continues to be desired. It is possible to achieve CN while allowing the consumption of carbon by recovering the $CO_2$ generated by the consumption of carbon substances and reusing them as energy carriers and carbon substances for recycling use. It is desired to create new GX technology for energy storage and carbon cycle in CN.

Nuclear power generation (nuclear power) is also an important option for zero-carbon energy. The EU has recognized the need for nuclear power plants in 2021, with plans to build eight in the UK and 14 in France. Germany, which is proceeding with the decommissioning of nuclear power plants, is also accepting cheap and stable electricity from nuclear power plants in neighboring countries, and the use of nuclear power will continue in the future. Nuclear power plants are being pursued for safety and economic efficiency, and various countries are considering small modular reactors (SMRs) and high-temperature gas-cooled reactors. Japan also needs to secure the possibility of nuclear power. The mission of ZC Lab is to realize the three required GX technologies for zero-carbon energy, energy storage and carbon recycling.

## 4. Tokyo Tech GXI

The Green Transformation Initiative (Tokyo Tech GXI) project founded by MEXT was launched with ZC Lab as its headquarters in April, 2022. GXI aims to lead GX technology for structural changes in industry and society in response to the shift to CN. GXI has organized an industry-academia collaboration committee (corporate consortium) together with energy-related companies, local governments and citizens, and is working to solve problems through open innovation by collaboration between 400 faculty members related to energy research and the member companies and organizations and fostering GXI joint research projects. The GXI Ookayama Laboratory will be set up as a demonstration research facility, where research on social implementation of carbon rcycling green industrial systems will be consolidated, and we plan to make it a research base for GX innovation by university researchers and corporate
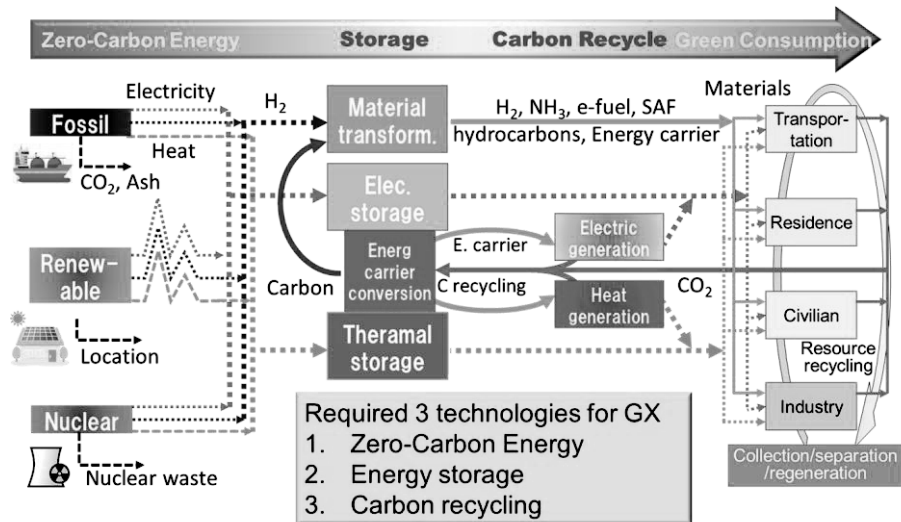


Fig.2 Vision of a Green Society of ZC Lab

committee members. The Laboratory plans will be expanded wider for GXI subjects.

## 5. Conclusion

Aiming for CN realization in Japan, ZC Lab intends to show the problem from an engineering point of view and develop GX technology to solve it. Based on the Tokyo Tech GXI project, we aim to promote industry-university collaboration, orgaize it as an international base for GX research, and contribute to the realization of a CN society. The scale of GX technology for CN is very large. We would like to ask for your cooperation in the social implementation of GX technology, and we would appreciate your continued guidance and encouragement.

## Reference

1. Overview of ZC, Tokyo Tech, http://www.zc.iir.titech.ac.jp/jp/events/publications/files/Overview_ZC_2021.pdf
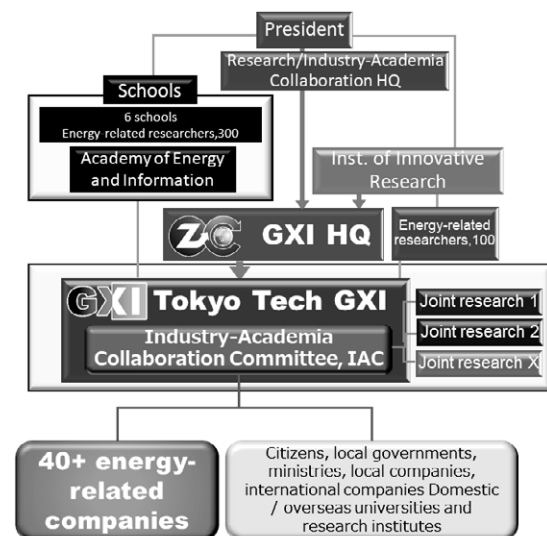


Fig.3 Tokyo Tech GXI open-innovation network

# II. Special Articles in Commemoration of Retiring Professors

# II. 1        Study of nuclear fission, nuclear data and their application

Satoshi Chiba

## 1. Introduction

Nuclear fission, which proceeds as shown in Fig. 1, is the most fundamental physics process underlying nuclear energy, which is now recognized widely as an important source of zero-carbon energy. Nuclear fission makes the stable operation of nuclear reactors possible through a chain reaction mediated by fission neutrons, generating heat at the same time. Furthermore, nuclear fission populates a number of radioactive fission products, and the treatment of the radioactive wastes is one of the key issues in the utilization of nuclear energy. On the other hand, some of the fission products like $^{99}$Tc have been used as important radioactive materials for, e.g., medical applications. Moreover, nuclear fission takes place in r-process nucleosynthesis in merger events of 2 neutron stars or between a neutron star and a blackhole, which determines the abundance of medium to heavy nuclei through fission recycling. Therefore, information on nuclear fission is crucial in accurate design of nuclear systems, medical applications and in understanding origin of matter in the cosmos.

Nuclear fission has been studied for more than eighty years since its discovery. However, fundamental aspects of nuclear fission still remain to be a mystery due to its sophisticated nature as a large-amplitude collective motion of a system including finite number of nucleons [1]. Indeed, we still cannot explain the whole property of nuclear fission even for the n+$^{235}$U reaction with sufficient predictive power, although experimental data and/or empirical models have been applied for practical use. Such practical methods may work properly in the case of well examined n-induce fission of $^{235}$U and $^{239}$Pu. In order to develop a new system such as Accelerator-driven Systems (ADS) and Fast Reactors (FR) which may act as a transmuter of the TRU wastes, we need high quality nuclear data on minor actinides (MA), which are fissile or fissionable nuclei. Experiments to obtain fission data for MA and long-lived fission products (LLFP) have been performed in various facilities. But it is still difficult to cover whole fission data, such as fission fragment mass distributions (FFMDs), total kinetic energy (TKE), number of prompt and delayed neutrons, decay heat, and emission of anti-electron neutrinos from the fission products. We have developed a comprehensive set of nuclear models which can reproduce and predict the physical quantities on nuclear fission.

In addition to the above fundamental approaches, we are also working on the reduction of long-lived fission products, research on the effects of uncertainty of nuclear data on properties of nuclear systems, and the influence of nuclear data on the clearance problem of decommissioning by developing a computational scheme of high-quality nuclear data. The aim of Chiba laboratory is the improvement of nuclear data starting from a fundamental research to

application, placing emphasis on fission-related nuclear data.
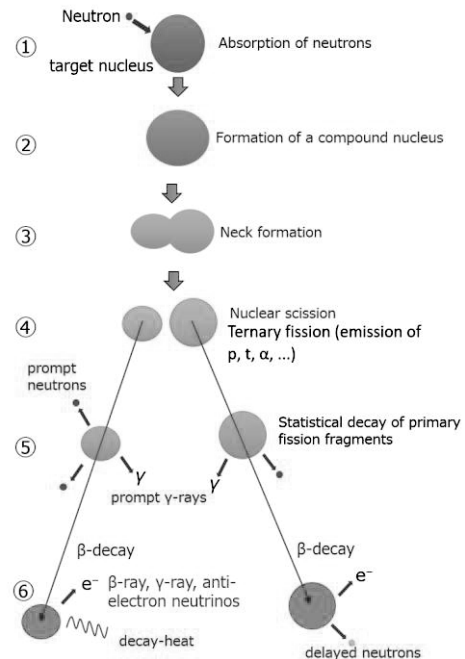


Fig. 1 Schematic view of nuclear fission process.

## 2. Fundamental studies for nuclear fission [2-22]

Nuclear fission we consider is initiated by absorption of neutrons by heavy nuclei like $^{235}$U and $^{239}$Pu, the process ① in Fig. 1, which can be described by a standard method like the optical model or the coupled-channels theory. However, it is still difficult to describe the whole feature of a nuclear fission process starting at ② with a single model due to the fact that nuclear force is still unclear as well as it consists of several parts which have completely different time scales ranging from $\sim 10^{-20}$ second to $\sim 10^6$ years. Indeed, there is no theoretical model which can simulate the whole process of nuclear fission shown in Fig.1. Therefore, we have developed different models depending on our purpose. In our laboratory, we have studied the fundamental mechanism of nuclear fission at low energies with models such as a 4-dimensional Langevin model, the Anti-symmetrized Molecular Dynamics, relativistic and non-relativistic density functional theories to describe the process ② to ④ in Fig. 1. As a result of this process, about 1,300 different primary fission fragments are formed at stage ④ from a single fissioning system, and we need to specify the yield, distributions of kinetic energy, excitation energy and spin-parity to each of the populated fragment, which is a formidable task. Furthermore, we have used the Hauser-Feshbach theory to describe the statistical

decay of the primary fission fragments (process ⑤) to lead to the population of independent fission products and emission of prompt neutrons, and the gross theory of beta-decay and summation method to investigate the final $\beta$-decay process (process ⑥) which leads to the generation of delayed neutrons, decay heat, and emission of anti-electron neutrinos.

## 2.1. Fission properties studied by the Langevin equation

Langevin dynamical model can reproduce and predict not only the fission fragment mass yields but also the total kinetic energies of the fission fragments of various actinides very accurately. In the Langevin model, a nuclear fission process is regarded as a time-evolution of the nuclear shape of a compound nucleus, which is formed via neutron absorption by a target in a neutron-induced reaction, following the equation of motion under the friction force and the random force (so called the Langevin equation). We have developed a 4-dimensional Langevin model [9] by extending degree of freedom to describe a realistic nuclear-shape leading to nuclear scission, and by introduction of quantal effects to the free energy, the zero-point energy correction to each of the collective coordinate, and also by introducing microscopic transport coefficients based on the linear response theory.

Figure 1 shows calculated mass distributions of fission fragments (black histograms) compared with experimental data (red circles) at excitation of 20 MeV as representatives of compound nuclei populated by neutrons. In contrast, Fig. 2 compares calculated mass-TKE correlation of fission fragments (left panel) with experimental data (right panel). The gray histogram in the upper-left panel of Fig. 1 shows a calculation without quantal effects yielding only 1-peak in mass distribution. These figures show how our 4D Langevin model can describe known properties of nuclear fission by taking account of the quantal effects properly into the thermodynamic approach represented by the Langevin equation. Verified by this quantitative agreement, we have made a systematic calculation of fragments-mass v.s. TKE correlation for actinides as shown in Fig. 3[14]. We notice

that, starting from the left-bottom to the right-upper panel, the TKE of the symmetric component makes a sudden jump to higher values at mass number of 250 to 254 which is an indication of transition of the symmetric mode from superlong to supershort mode. Furthermore, the dominant mode, shown by red dots, moves from the asymmetric mode to the symmetric mode at A=257 to 258, then moves back to the asymmetric mode at $^{260}$Md to $^{256}$No, making mass distribution to change from 2-peak structure to 1-peak, then to 2 peak again. Such a "correlated transition" of 2 physical quantities were effective in understanding
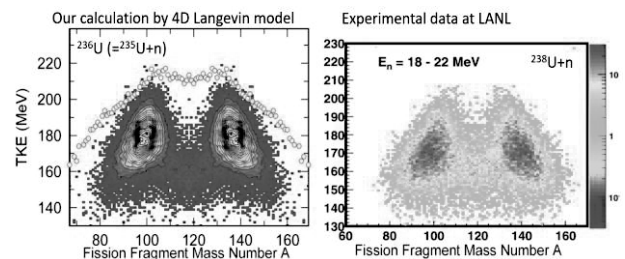


Fig. 2 Mass-TKE correlation of fission fragments (left: our calculation, right: experimental data).

systematical and anomalous trends in the fission mechanisms of actinide nuclei in a unified manner.
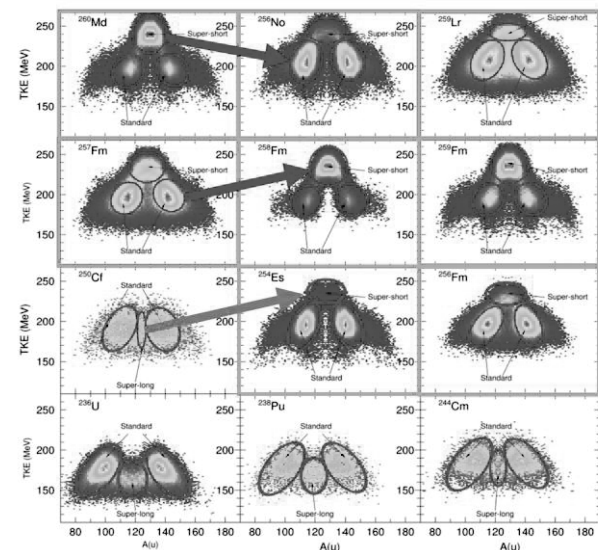


Fig. 3 Mass-TKE correlation of fission fragments for a series of actinide nuclei arranged in increasing order of $Z^2/A^{1/3}$ of fissioning nucleus starting from the leftmost-bottom panel to the rightmost upper panel.

Then, based on this success, we have extended our calculation to superheavy nuclei [15]. A result is shown in Fig. 4 for the fragment-mass v.s. TKE correlation of $^{294}$Og (Z=118). We can notice that this correlation pattern is much more complicated than that of the actinide region shown in Figs. 2 and 3. We have found that the shell of $^{208}$Pb plays a dominant role in the fission mechanisms of superheavy nuclei to form the "superaymmetric" component.



Fig. 1 Calculated mass distribution of fission fragments (black histograms) compared to experimental information (right circles).
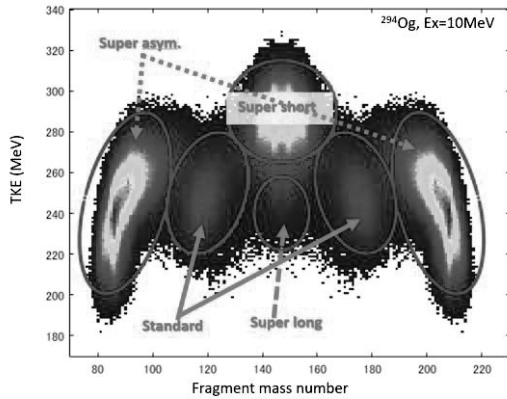
Fig. 4 Predicted mass-TKE correlation of fission fragments for $^{294}$Og.



Fig. 6 Fragment mass-TKE correlation of $^{236}$U. Color contour: experimental data, white circles : AMD calculation.

## 2.2. Application of Anti-symmetrized Molecular Dynamics (AMD) to study of nuclear fission

While we understood that Langevin model gives rather accurate results to describe various properties of nuclear fission, it is based on a macroscopic-microscopic approach, and it lacks full microscopic description of the fission process, which is becoming a major trends in this field. Then, we also have investigated the fission reaction based on the Anti-symmetrized Molecular Dynamics (hereafter AMD). In AMD, a nucleus can be microscopically described by a Slater determinant consisting of Gaussian wave packets chosen as variational functions to represent single-particle states. AMD has been widely used to study nuclear reactions and nuclear structures for light nuclei, but we are the only one group to apply AMD to fission study. From this study, we expect to get aspects of nuclear fission that cannot be obtained from the Langevin model.

In Fig. 5, we show snapshots of nucleon density distributions during the fission of $^{236}$U (= compound nucleus of n + $^{235}$U reaction), where degree-of-freedom of 92 protons and 144 neutrons are explicitly considered. We have adopted SLy4 effective interaction acting among nucleons, NN collision by Li-Machleit parameterization. and the fission was initiated by a technique called "symmetric boost mechanism". By repeating such calculations, we can obtain distributions of isotopes, TKE and spin of fission fragments.
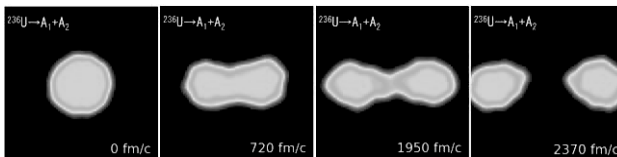


Fig. 5 Snapshots of time evolution of nucleon density during fission of $^{236}$U.

In Fig. 6, we plotted mass-TKE correlation of fission fragments originated from $^{236}$U compound nucleus. The color contour shows data estimated from experimental information, while circles are the results of AMD calculation, which corresponds to symmetric fission mode. We notice that the AMD calculation can describe the TKEs of symmetric fission components quite accurately.
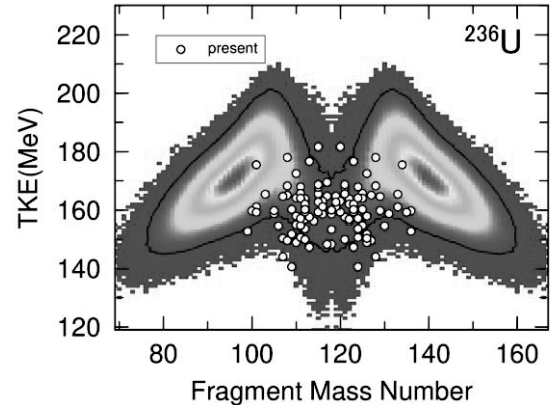
Through such simulations, we could draw conclusions on the spin distribution and mechanisms of ternary fission in quantitative manner.

### 2.3 Relativistic and non-relativistic density functional theories

Other microscopic approaches used in our laboratory are relativistic and non-relativistic density functional theories. These models can provide detailed information on potential energy surfaces as a function of nuclear deformations and on fission barrier height. Nevertheless, there is no effective interaction designed for nuclear fission itself. In our laboratory, we have investigated how the pairing interaction affects the fission barrier height in both models, and found that about 20% increase in the pairing strength drastically improves reproduction of fission barrier heights [17,19,20]. Our study on the pairing interaction is based on a consideration including the pairing rotational energy, which confirms the validity of our conclusions. Furthermore, we found that triaxiality has a dominant role in the height of outer fission barrier.

### 3. Beta decay of fission products [6,13,23]

After prompt neutrons and gammas emitted from the fission fragments, the beta-decays of these nuclei will occur. Anti-electron neutrinos (abbreviated as neutrinos for simplicity) produced by the beta-decay process play a significant role in the surveillance and in-service inspection of nuclear power plants, which can serve as a novel method of nuclear safeguards. They are also used to establish neutrino oscillations, and such a study eventually leads to discovery of exotic particles such as sterile neutrinos.

In our laboratory, we have studied the antineutrino spectrum from aggregate beta-decay of fission products based on summation calculation and the gross theory. Figure 7 shows a comparison of antineutrino spectra emitted from $\beta$-decay of $^{92}$Rb calculated by Gross Theory 2 (red line) and experimental data (triangles). We have performed such calculations for about 1,000 FP nuclei, and constructed an original database. Then, fig. 8 compares aggregate and independent neutrino spectra emitted from

fission products populated in the fission of thermal neutron + $^{235}$U system. The aggregate spectra are made by superposition of about 1,000 fission products. The calculation was done by using JENDL Decay Data Library 2011 and FPY (Fission Product Yield) from FPY2011 and that in JENDL-5 (FPY2020). We notice that the difference of the FPY data makes a difference in the neutrino spectra above 8 MeV, where only several nuclei like $^{92,95}$Rb and $^{96}$Y, having large $Q_\beta$ values, contribute. Even though the calculation seems to reproduce the measured data, the accuracy of such a computational method must be further improved for practical applications. Anyhow, we have established the basis of such a computational method.
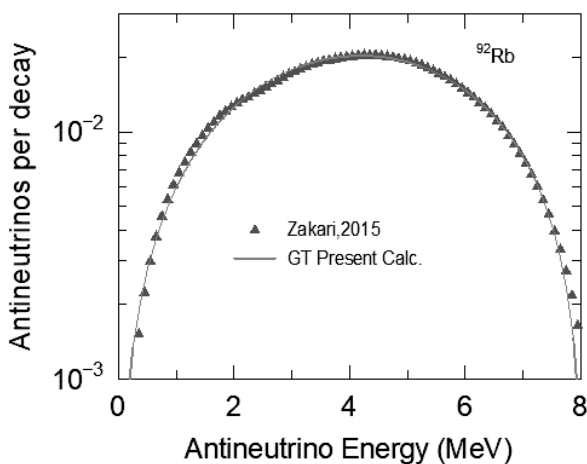


Fig. 7 Comparison of antineutrino energy spectra emitted from $\beta$-decay of $^{92}$Rb calculated by Gross Theory 2 (red line) and experimental data (triangles).
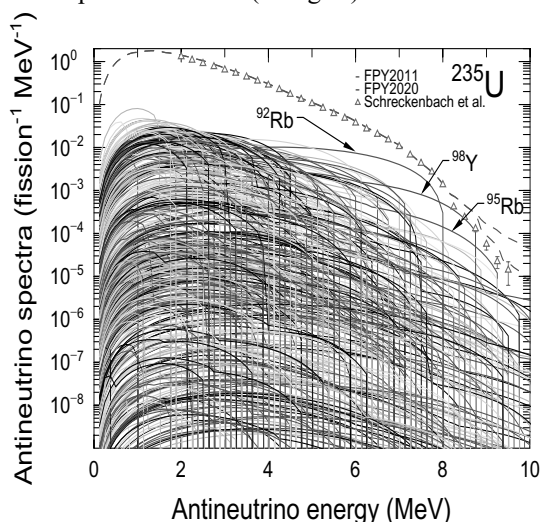


Fig. 8 Aggregate and independent neutrino spectra emitted from fission products populated in fission of n + $^{235}$U system. The triangles are experimental data, while the total and independent neutrino spectra are shown by lines.

## 4. Evaluation of nuclear data and its impact on

integral system

### 4.1: Development of fission yield data library for various applications

High precision nuclear data on the fission product yield (FPY) is necessary to evaluate the inventory of radioactive materials in spent nuclear fuel, total decay heat from the fission products and their toxicity. Historically, FPY data in JENDL have been borrowed from U.S. evaluation ENDF. Fortunately, a number of measurements of fission products yields (FPYs) have been accumulated since the last major evaluation was performed in ENDF library.

In our laboratory, we have developed a FPY library based on the original evaluation method of experimental data, guided by all the fundamental research on nuclear fission we have carried out [24]. Our FPY library contains not only yields such as independent yields and cumulative yields, but also the covariance information on uncertainty in each data. Recently, such covariance data has been necessitated significantly for V&V (Validation and Verification) purposes. To develop the new library, we first gathered and evaluated experimental data from EXFOR database, and then developed a semi-phenomenological FPY model based on the recent knowledge of the shell effects including the even-odd staggering. The semi-phenomenological model is necessary to estimate the FPYs where no measured data exist. Hauser-Fechbach theory[12] was also applied to estimate unknown isomer ratios. The covariance was obtained by a generalized least-squares analysis containing minimal physics constraints. In this manner, we constructed a brand-new FPY library for the first time in Japan [24]. Our FPY library was adopted in JENDL-5 as a national nuclear database.

### 4.2: Impact of uncertainty of nuclear data on integral system

The uncertainty in various quantities relating to nuclear reactors becomes necessary information. Especially, the uncertainty in the evaluation for radioactivity due to neutron irradiation is strongly required by nuclear regulation procedures.

We have evaluated the uncertainty of the cross sections of some LLFP nuclides in JENDL-4.0 by use of T6 code which evaluates the nuclear data employing the Bayesian Monte Carlo calculations [25,26]. Using these methods, we have investigated the uncertainty of the neutron spectra after deep penetration and found that the correlation of the total cross section and forward elastic angular distribution plays a crucial role [27].

## Reference

1. Future of Nuclear Fission Theory, Michael Bender, Remi Bernard, George Bertsch, Satoshi Chiba, Jacek Dobaczewski, Noel Dubray, Samuel A. Giuliani, Kouichi Hagino, Denis Lacroix, Zhipan Li, Piotr Magierski, Joachim Maruhn, Witold Nazarewicz, Junchen Pei, Sophie Peru, Nathalie Pillet, Jorgen Randrup, David Regnier, Paul-Gerhard Reinhard, Luis M. Robledo, Wouter Ryssens, Jhilam Sadhukhan, Guillaume Scamps, Nicolas Schunck, Cedric Simenel, Janusz Skalski, Ionel Stetcu, Paul Stevenson, Sait Umar, Marc Verriere, Dario Vretenar, Michaa Warda, Sven Aberg, Journal of Physics G: Nuclear and Particle Physics, 47, No. 11, 113002(2020).

2. Scission-point configuration within the two-center shell model shape parameterization, Fedir A. Ivanyuk, Satoshi Chiba, Yoshihiro Aritomo, Physical Review C 90, 054607(2014).

3. A Comprehensive Approach to Estimate Delayed-neutron Data of Actinides and Minor-actinides, Satoshi Chiba, Nishio, K., Aritomo, Y., Koura, H., Iwamoto, O., Kugo, T., Energy Procedia, 71, pp. 205-212(2015).

4. The transport coefficient of collective motion within the two-center shell model shape parameterization, Fedir A. Ivanyuk, Satoshi Chiba, Yoshihiro Aritomo, Journal of Nuclear Science and Technology, 53, 6, pp. 737-748(2015).

5. A Comprehensive Approach to Determination of Nuclear Data of Unstable Nuclei, Satoshi Chiba, Katsuhisa Nishio, Yohihiro Aritomo, Hiroyuki Koura, Osamu Iwamoto, Hiroyuki Makii, Ichiro Nishinaka, Kentaro Hirose, EPJ Web of Conferences, 106, No. 9, 04004(2016).

6. Composition, decomposition and analysis of reactor antineutrino and electron spectra based on gross theory of $\beta$-decay and summation method, Tadashi Yoshida, Takahiro Tachibana, Naoto Hagura, Satoshi Chiba, Progress in Nuclear Energy, Vol. 88, pp. 175-182(2016).

7. Effects of microscopic transport coefficients on fission observables calculated by the Langevin equation, Mark Dennis Usang, Fedir A. Ivanyuk, Chikako Ishizuka, Satoshi Chiba, Physical Review C, 94, No. 4, Page 044602(2016).

8. CHARGE POLARIZATION AND THE ELONGATION OF THE FISSIONING NUCLEUS AT SCISSION, Chikako Ishizuka, Satoshi Chiba, Nicolae Carjan, Romanian Reports in Physics, 70, page 202(2017).

9. Four-dimensional Langevin approach to low-energy nuclear fission of $^{236}$U, Chikako Ishizuka, Mark Dennis Usang, Fedir A. Ivanyuk, Joachim A. Maruhn, Katsuhisa Nishio, Satoshi Chiba, Physical Review C 96, 6, 064616(2017).

10. Analysis of the total kinetic energy of fission fragments with the Langevin equation, Mark Dennis Usang, Fedir A. Ivanyuk, Chikako Ishizuka, Satoshi Chiba, Phys. Rev. C, 96, page 064617-1-13(2017).

11. Temperature dependence of shell corrections, Fedir A. Ivanyuk, Chikako Ishizuka, Mark Dennis Usang, Satoshi Chiba, Phys. Rev. C, 97, page 054331(2018)

12. $^{235}$U(n,f) Independent Fission Product Yield and Isomeric Ratio Calculated with the Statistical Hauser-Feshbach Theory, Shin Okumura, Toshihiko Kawano, Patrick Jaffke, Patrick Talou, Satoshi Chiba, Journal of Nuclear Science and Technology, 55, Issue 9, pp. 1009-1023(2018).

13. Spectral anomaly of reactor antineutrinos based on theoretical energy spectra, Tadashi Yoshida, Takahiro Tachibana, Shin Okumura, Satoshi Chiba, Physical Review C 98, Page 041303(R)(2018).

14. Correlated transitions in TKE and mass distributions of fission fragments described by 4-D Langevin equation, Mark Dennis Usang, Fedir A. Ivanyuk, Chikako Ishizuka, Satoshi Chiba, Scientific Reports, 9, Page 1525(2019)

15. Effect of the doubly magic shell closures in $^{132}$Sn and $^{208}$Pb on the mass distributions of fission fragments of superheavy nuclei, Chikako Ishizuka, X. Zhang, Mark Dennis Usang, Fedir A. Ivanyuk, Satoshi Chiba, Physical Review C 101, 011601(R)(2020).

16. Dependence of total kinetic energy of fission fragments on the excitation energy of fissioning systems, Kazuya Shimada, Chikako Ishizuka, Fedir Ivanyuk, Satoshi Chiba, Physical Review C, 104, 054609(2021).

17. Pairing strength in the relativistic mean-field theory determined from the fission barrier heights of actinide nuclei and verified by pairing rotation and binding energies, Taiki Kouno, Chikako Ishizuka, Tsunenori Inakura, Satoshi Chiba, Progress of Theoretical and Experimental Physics, 2022 023D02(2021)

18. The memory effects in the Langevin description of nuclear fission, Fedir Ivanyuk, S.V.Radionov, Chikako Ishizuka, Satoshi Chiba, Nuclear Physics A, 1028, p. 122526(2022)

19. Energy competition and pairing effect for the fission path with a microiscopic model, Kazuki Fujio, Shuichiro Ebata, Tsunenori Inakura, Chikako Ishizuka, Satoshi Chiba, Frontiers in Physics, DOI 10.3389/fphy.2022.986488(2022).

20. Effects of triaxiality and pairing interaction on fission barriers of actinide nuclei, Taiki Kouno, Chikako Ishizuka, Kazuki Fujio, Tsunenori Inakura, Satoshi Chiba, International Journal of Modern Physics E, accepted for publication (2022).

21. Spin-dependent observables in surrogate reactions, Satoshi Chiba, Osamu Iwamoto, Yoshihiro Aritomo, Physical Review C 84, 054602(2011).

22. Surrogate Reactions Research at JAEA/Tokyo Tech, Satoshi Chiba, Katsuhisa Nishio, H. Makii, Yoshihiro Aritomo, I. Nishinaka, T. Ishii, K. Tsukada, M. Asai, K. Furutaka, S. Hashimoto, H. Koura, K. Ogata, T. Otsuki, T. Nagayama, Nuclear Data Sheets, 119, pp. 229-232(2014).

23. Improvement to the gross theory of $\beta$ decay by inclusion of change in parity, Hiroyuki Koura, Satoshi Chiba, Phys. Rev. C, 95, 064304-1-6(2017).

24. Evaluation of fission product yields and associated covariance matrices, Kohsuke Tsubakihara, Shin Okumura, Chikako Ishizuka, Tadashi Yoshida, Futoshi Minato, Satoshi Chiba, Journal of Nuclear Science and Technology, 58:2, 151-165(2021).

25. Method to Reduce Long-lived Fission Products by Nuclear Transmutations with Fast Spectrum Reactors, Satoshi Chiba, Toshio Wakabayashi, Yoshiaki Tachi, Naoyuki Takaki, Atsunori Terashima, Shin Okumura, Tadashi Yoshida, Scientific Reports, 7, 13961(2017).

26. Estimation of uncertainty in transmutation rates of LLFPs in a fast reactor transmutation system via an estimation of the cross-section covariances, Naoki Yamano, Tsunenori Inakura, Chikako Ishizuka, Satoshi Chiba, Journal of Nuclear Science and Technology, 58, 5, pp. 567-578(2020)

27. Crucial importance of correlation between cross sections and angular distributions in nuclear data of 28Si on estimation of uncertainty of neutron dose penetrating a thick concrete, Naoki Yamano, Tsunenori Inakura, Chikako Ishizuka, Satoshi Chiba, Journal of Nuclear Science and Technology, 59, pp. 641-646(2021).

# II. 2                  Applied Research at IIR/Tokyo Tech
## Heavy-Ion Accelerator System

### Yoshiyuki Oguri

## 1. Introduction

The heavy-ion accelerator system at the IIR, Tokyo Tech, began operating in 1984. Since then, it has been utilized for various kinds of scientific research activities as well as for teaching graduate and undergraduate students. In September 2022, the operation of the accelerator was stopped and decommissioning of the radiation facility began. The following lists all of the experimental research projects carried out at this facility over the past 25 years.

## 2. Heavy-ion fusion research

### 2.1. Beam-plasma interaction

Precise quantitative data on the stopping power of heavy ions in hot plasma is required for developing inertial-confinement heavy-ion fusion (HIF) since the fusion fuel target design is highly dependent on the energy deposition profile of the incident ions. To collect these data for $\approx 100$-keV/u projectiles, we created a laser-produced plasma target. To increase the plasma ionization degree, the target material should consist of light elements. As a result, lithium hydride (LiH) was selected. To guarantee isotropy of the target density distribution, the plasma was created by irradiating a LiH particle smaller than the size of the laser focal spot [1,2]. A Q-switched Nd-glass laser was employed for this irradiation. The density and morphology of the plasma were quantified by laser interferometry [2,3] and refractometry [4], respectively. The energy loss of the incident ions in the target was assessed by a time-resolved TOF spectrometer [5]. By utilizing this plasma target, interaction tests with $^{16}O$ [3,5–7] and $^{28}Si$ [5,8] projectiles were carried out. To calculate the Coulomb logarithm of the interaction, the stopping power of protons with the same speed was also measured separately [7]. We were able to successfully observe the increase in stopping cross sections for the plasma target concerning these projectile ions when compared to the cold equivalent. The incident energy dependence of the stopping power was examined in the projectile energy range of 150–350 keV/u. The measured energy dependence was in good agreement with the theoretical estimation based on a modified Bohr equation with corrections at low velocities [9]. Additionally, the charge-state distribution of ions ($^{12}C$, $^{16}O$, and $^{19}F$) after passing through the plasma was determined using a time-resolved magnetic spectrometer with plastic scintillators as the detector. In comparison with cold gas targets, the average charge of the projectile ions increased, which is why the stopping cross section rose in the plasma target [4,10].

In order to prepare plasma targets with higher densities, another form of target plasma was created by irradiating solid plates of graphite and polyethylene with a TEA–$CO_2$ laser. The energy loss and effective charge of $^{16}O$ projectiles in the polyethylene plasma were measured, and both parameters increased when compared to the cold equivalent target [11]. The analysis of the charge-state distribution of $^{7}Li$ ions following their passage through the plasma additionally demonstrated a potent stripping capacity of the ionized matter, whereby electron capture by the projectiles was suppressed [12]. Additionally, to increase the ionization degree of the target plasma and minimize the atomic process complexity, a laser plasma created from cryogenic solid hydrogen was constructed. The electron density and temperature of this hydrogen plasma were measured using optical spectrometry [13].

In indirectly driven HIF scenarios, X-ray converter plasmas created by heavy-ion beams maintain strong coupling between plasma particles as well as between projectiles and plasma particles during the beam irradiation. To reproduce such a condition, a nonideal hydrogen plasma target based on the shock approach was created [14–17], which can produce relatively cold, but dense plasmas compared with discharge or laser irradiation. This technique was also applied to create a dissociated hydrogen atomic gas target, which is a transitional state between the cold gas and highly ionized plasmas [18–20]. In addition, an electromagnetic shock tube was constructed, and the discharge circuit, as well as the arrangement of the discharge electrodes, was modified to increase the shock speed and plasma duration. The shock speed was measured using a TOF approach based on the refraction of He–Ne lasers and streak photography. Besides, the axial and azimuthal distributions of the plasma in the tube were observed using a framing camera [21]. Also, the strong coupling effect, which results in a nonlinear dielectric response of the stopping medium, was assessed using the beam-plasma coupling constant [22]. The energy loss of ions behind the target was quantified by detecting single ions using a Si surface-barrier detector synchronized with the passing of the shock [22,23]. Additionally, the energy loss of heavy ions was successfully determined in these shock-driven targets. However, the energy and time resolution were insufficient to quantitatively evaluate the difference in the stopping cross sections between these hot targets and the cold equivalent matter [24].

### 2.2. High-current ion source development

In scenarios of HIF based on induction linacs, ion sources must provide $10^{13}$–$10^{14}$ ions within $\approx 10$ μs to the accelerator system. The corresponding beam current is 0.1–1 pA (particle amperes). Laser-produced plasmas are possible sources of high-intensity pulsed ion beams that can meet this criterion. We created a plasma source by

irradiating a solid Cu block with a Nd:YAG laser of $10^8$–$10^9$-W/cm² intensity. To increase the fraction of singly or doubly charged ions (Cu⁺ and Cu²⁺), the second harmonic ($\lambda$ = 532 nm) of this laser was used. Ions were extracted using a pulsed voltage generated by an induction accelerator module. A time-resolved emittance monitor was developed for such a single-shot pulsed, high-current ion beam [25]. Ion fluxes greater than $10^{14}$ cm$^{-2}$ were recorded per laser shot. The extracted ion current density reached 0.1 A/cm² [26,27]. To focus the beam while being subjected to a significant space-charge force during extraction, the ability of a spherical diode construction made of two stainless-steel hemispherical shells has been tested. Using multiaperture extraction with this shape and a biased control grid on the anode holes, well-focused Cu⁺ beams with a current of $\approx$ 0.1 A were successfully extracted behind the cathode [28]. Such a grid-controlled extraction was also applied to a KrF-laser-driven ion source in the over-dense domain, and the beam current waveform could be stabilized [29,30].

### 3. Ion beam analysis

#### 3.1. Proton-induced X-ray emission analysis

Over other analytical techniques based on X-ray spectrometry, the benefits of proton-induced X-ray emission (PIXE) analysis include its quick measurement time, multielemental capabilities, little sample requirement, and low detection limit. To fully take use of these benefits, we carefully planned and built a PIXE analysis system based on energy-dispersive spectrometry using a Si(Li) semiconductor X-ray detector. By using this setup, environmental samples, including atmospheric aerosol [31], roadside soil [32], and rainwater collected close to the Tokyo Tech Ookayama campus, were measured. The measurements demonstrated that the technology might be used to address regional environmental problems. Additionally, utilizing ion-exchange filter paper, high-sensitivity valence-state-selective PIXE analysis of metallic elements in water was also created [33–35]. Additionally, samples relating to materials science [36] and medical sciences [36] were measured, and the analytical performances in these domains were examined. The use of PIXE analysis to developing and assessing environmental decontamination strategies, such as phytoremediation and electrokinetic removal [38] of the soil, was demonstrated using simulated decontamination setups. With regard to assessing priceless cultural heritage materials, the radiation damage of samples caused by proton irradiation during analysis was also examined by FT-IR spectroscopy [39].

To identify the chemical state of elements in the sample, a high-resolution wavelength-dispersive X-ray spectrometer was created for the PIXE study [40–42]. By using a crystal spectrometer with the von Hamos geometry and a low-noise liquid-N₂-cooled X-ray CCD camera, high energy resolution and sensitivity could be achieved simultaneously. Using this setup, chemical state measurements of environmental materials, including lake sediments [43], organic Cl compounds in the atmospheric

particulate matter [44], and combustion products [45], were implemented. Additionally, it was discovered that the shift of K$_\beta$X-ray energy could be used to determine the chemical state of Cl. Additionally, the change in the valence state of the elements in the samples brought about by proton irradiation was also observed effectively [46–48]. Additionally, the valence state of S absorbed by activated carbon [49] and in polymer electrolyte fuel-cell samples [50] has been successfully assessed.

As a small, affordable device for creating MeV-proton microbeams, glass capillary optics has been designed [51], and the effects of the wall material and capillary shape on the focusing performance have been experimentally investigated [52]. Additionally, the transport process of protons in tapered capillaries has been studied based on numerical simulation, including scattering and energy loss of protons in the wall material [53]. In order to illustrate the use of this microbeam, X-ray radiography has been demonstrated, where a metallic plate was exposed to a proton microbeam that was focused using the technique described above to create a pointlike quasimonochromatic X-ray source [54]. The feasibility of focusing on powerful heavy-ion beams for warm-dense matter experiments has also been numerically investigated [55].

#### 3.2. Application of proton-induced quasimonochromatic X-rays

By bombarding a single-element solid target with MeV protons, X-rays consisting primarily of characteristic line emissions can be efficiently produced. Such quasimonochromatic radiation has the ability to deposit energy onto some materials that have an absorption-edge with slightly lower energy than the incident X-ray energy. Such quasimonochromatic X-rays can be produced by MeV-proton irradiation onto various metallic targets. The X-ray photon energy can be adjusted by changing the target atomic species. Using X-ray photons with two different energies produced by two separate metallic objects, a subtraction imaging of a plastic phantom filled with contrast medium for background reduction has been tested [56]. Additionally, the viability of using low-dose high-contrast radiography with iodinated contrast media for medical applications has been researched [57,58]. Additionally, by employing a rotational target with two metallic plates, a digital subtraction cineangiography of a moving object was demonstrated [59].

Based on the aforementioned findings, we created a syringe-needle-shaped proton-induced X-ray source that can be inserted into the human body [60]. The three-dimensional dosage distribution around the needle's point was assessed using a CdTe X-ray detector [61] and a liquid scintillator connected to a high-sensitivity electron-multiplying CCD camera [62]. These outcomes were in line with Monte Carlo simulations by PHITS [61] and Geant4 [63]. Additionally, we looked at the viability of using this X-ray source for applications to cancer therapy using nanoparticle sensitizers [64], as well as conventional brachytherapy of prostate cancer [61–63].

The low-dose and low-background feature of proton-

induced quasimonochromatic X-rays was also investigated using X-ray fluorescence (XRF) analysis. A Cu target was bombarded with 2.5-MeV protons to produce Cu-$K_\alpha$X-rays (8.04 keV) as primary photons. These X-rays were focused by a polycapillary X-ray lens onto the sample, and the XRF measurements were carried out [65]. Using this setup, because of the extremely low primary X-ray dosage, we were able to evaluate the uptake of Co *in vivo* (K-absorption-edge energy = 7.71 keV) by plant samples [66,67].

## 4. Astrobiological study

It is suggested that extraterrestrial organics could be sources of the first life on Earth [68,69]. These materials are thought to be carried by carbonaceous chondrites and comets to the early Earth. A gas combination of CO, $NH_4$, and $H_2O$ created as an interstellar ice analog was irradiated using MeV protons, which replicated cosmic rays. By this irradiation, complex amino acid precursors were created in the gas mixture. In order to validate the stability of these precursors in space, the irradiated gas was subjected to heavy-ion- and $\gamma$-ray irradiation [70], high-temperature mimicking conditions in meteorite parent bodies [71], and space environments in the Earth orbit [72]. According to the investigation, which included high-performance liquid chromatography and ultraviolet–visible light (UV–Vis) spectroscopy, it was revealed that the complex amino acid precursors were stable against space environments while being transported to the early Earth [72].

According to estimates, the early Earth's atmosphere was slightly reducing. We investigated the potential synthesis of amino acids from such mildly reducing gas combinations by using ionizing radiation to imitate the impact of galactic and solar cosmic rays [73,74]. $N_2$, $CO_2$, and $CH_4$ mixtures with pure water were exposed to 2.5-MeV protons. For comparison, the identical gas combinations were subjected to spark discharges [74]. Amino acids were found in the samples that had been bombarded with the protons, whereas in the case of spark discharges, amino acids were not detected when the $CH_4$ concentration was low. These findings imply that galactic cosmic rays may be more effective at generating N-containing organics than energy sources, like thundering or solar UV emissions.

Titan is the largest satellite of Saturn, and its atmosphere is primarily made up of $N_2$ and $CH_4$, suggesting that it is comparable to that of the early Earth. A gas combination of $N_2$ and $CH_4$ in order to simulate the Titan atmosphere was irradiated using the 2.5-MeV protons. Additionally, the samples following proton irradiation included amino acid precursors, according to the ESI-MS analysis [75].

## Acknowledgment

## References

1. Y. Oguri: Diagnostics of a Laser-Ablated Plasma for Beam-Plasma Interaction Experiments; US-Japan Workshop on Heavy-Ion Fusion and Related Topics, Claremont Hotel, Berkeley, California, USA, November 12-14, 1997, UCRL-MI-129243 (1997).
2. Y. Oguri et al.: Development of a Laser-Produced Plasma Target for Beam-Plasma Interaction Researches; Nucl. Instrum. Methods. Phys. Res. A, Vol. 415, pp. 657-661 (1998).
3. A. Sakumi et al.: Experiments on the Interaction of Fast Heavy Ions with a Laser-Plasma Target; Nucl. Instrum. Methods. Phys. Res. A, Vol. 415, pp. 648-652 (1998).
4. K. Shibata et al.: Experimental Study on the Feasibility of Hot Plasmas as Stripping Media for MeV Heavy Ions; J. Appl. Phys., Vol. 91, pp. 4833-4839 (2002).
5. K. Shibata et al.: A TOF System to Measure the Energy Loss of Low Energy Ions in a Hot Dense Plasma; Nucl. Instrum. Methods. Phys. Res. B, Vol. 161-163, pp. 106-110 (2000).
6. A. Sakumi et al.: Stopping Power Measurement of 225 keV/u Oxygen Ions in Laser-Produced Lithium Hydride Plasma; Nucl. Sci. Technol., Vol. 36, pp. 326-331 (1999).
7. K. Shibata et al.: Experimental Investigation of the Coulomb Logarithm in Beam-Plasma Interaction; Nucl. Instrum. Methods. Phys. Res. A, Vol. 464, pp. 225-230 (2001).
8. K. Shibata et al.: Energy Loss of 180 keV/u $^{28}$Si ions in a Hot Dense Plasma; Proc. IAEA Technical Committee Meeting on Research Using Small Fusion Devices, October 26-28, 1998, Shonan-Village Center, Japan, F1-TC-536-14, pp. 63-70 (1998).
9. A. Sakumi et al.: Energy Dependence of the Stopping Power of MeV $^{16}$O Ions in a Laser-Produced Plasma; Nucl. Instrum. Methods. Phys. Res. A, Vol. 464, pp. 231-236 (2001).
10. Y. Oguri et al.: Heavy Ion Stripping by a Highly-Ionized Laser Plasma; Nucl. Instrum. Methods. Phys. Res. B, Vol. 161-163, pp. 155-158 (2000).
11. K. Nishigori et al.: Energy Loss and Effective Charge of Low-Energy Oxygen Ions in Partially Ionized Plasma; Laser Part. Beams, Vol. 18, pp. 639-646 (2000).
12. U. Neuner et al.: Performance of a Carbon Plasma Stripper for Intense Beams; Fusion Eng. Design, Vol. 44, pp. 285-286 (1999).
13. M. Kojima et al.: Laser Plasma Induced from Solid Hydrogen for Beam-Plasma Interaction; Nucl. Instrum. Methods. Phys. Res. A, Vol. 464, pp. 262-266 (2001).
14. Y. Oguri: Development of a Shock-Produced Plasma Target for Nonlinear Beam-Plasma Interaction Experiments; U.S.-Japan Workshop on Heavy Ion Fusion and High Energy Density Physics, September 28-30, 2005, Academia Hall, Utsunomiya University, Japan (2005).
15. K. Katagiri et al: Development of a Non-Ideal Plasma Target for Non-Linear Beam-Plasma Interaction Experiments; Nucl. Instrum. Methods. Phys. Res. A, Vol. 577, pp. 303-308 (2007).
16. K. Katagiri et al.: Time-Resolved Measurement of a Shock-Driven Plasma Target for Interaction Experiments between Heavy-Ions and Plasmas; J. Appl. Phys., Vol. 102, pp. 113304-1-8 (2007).
17. K. Katagiri et al.: Development of a Coaxial Tapered Electromagnetic Shock Tube for Beam-Plasma Non-Linear Interaction Experiments; Nucl. Instrum. Methods. Phys. Res. B, Vol. 266 pp. 2161-2164 (2008).
18. K. Kondo and Y. Oguri: Velocity Evolution of Electro-

Magnetically-Driven Shock Wave for Beam-Dissociated Hydrogen Interaction Experiment; The 8th International Conference on Inertial Fusion Sciences and Applications (IFSA 2013), the Nara Prefectural New Public Hall, September 8-13, 2013, Nara, Japan, P.Tu_38 (2013).

19. K. Kondo et al.: Velocity Measurement of Electro-magnetically-Driven Shock Wave to Produce a Dissociated Hydrogen Target for Beam Interaction Experiment; Energy Procedia, Vol. 71, pp. 268-273 (2015).

20. K. Kondo and Y. Oguri: Velocity Evolution of Electro-Magnetically-Driven Shock Wave for Beam-Dissociated Hydrogen Interaction Experiment; J. Phys.: Conf. Ser., Vol. 688, pp. 012052-1-4 (2016).

21. K. Kondo et al.: Well-Defined Atomic Hydrogen Target Driven by Electromagnetic Shock Wave for Stopping Power Measurement; Laser Part. Beams, Vol. 33, pp. 679-683 (2015).

22. J. Hasegawa et al.: Beam-Plasma Interaction Experiments Using Electromagnetically Driven Shock Waves; Nucl. Instrum. Methods. Phys. Res. A, Vol. 606, pp. 205-211 (2009).

23. S. Nishinomiya et al.: Experimental Apparatus for the Measurement of Non-Linear Stopping of Low-Energy Heavy Ions; Nucl. Instrum. Methods. Phys. Res. A, Vol. 577, pp. 309-312 (2007).

24. S. Nishinomiya et al.: Time-Resolved Measurement of Energy Loss of Low-Energy Heavy Ions in a Plasma Using a Surface-Barrier Charged-Particle Detector; Prog. Nucl. Energy, Vol. 50, pp. 606-610 (2008).

25. M. Yoshida et al.: A Simple Time-Resolved Emittance Measurement of a Laser Ion Source with a Digital Camera; Nucl. Instrum. Methods. Phys. Res. A, Vol. 464, pp. 582-586 (2001).

26. M. Yoshida et al.: Development of a High-Current Laser Ion Source for Induction Accelerators; Rev. Sci. Instrum., Vol. 71, pp. 1216-1218 (2000).

27. J. Hasegawa et al.: High-Current Laser Ion Source for Induction Accelerators; Nucl. Instrum. Methods. Phys. Res. B, Vol. 161-163, pp. 1104-1107 (2000).

28. Y. Oguri et al.: Extraction of High-Intensity Ion Beams from a Laser Plasma by a Pulsed Spherical Diode; Phys. Rev. ST Accel. Beams, Vol. 8, pp. 060401-1-8 (2005).

29. M. Yoshida et al.: Grid-Controlled Extraction of Low-Charged Ions from a Laser Ion Source; Jpn. J. Appl. Phys., Vol. 42, pp. 5367-5371 (2003).

30. J. Hasegawa et al.: Influence of Grid Control on Beam Quality in Laser Ion Source Generating High-Current Low-Charged Copper Ions; The 3rd International Conference on Inertial Fusion Sciences and Applications, September 7-12, 2003, The Double Tree Hotel and Conference Center in Monterey, California, USA, Inertial Fusion Sciences and Applications 2003, ISBN: 978-0-89448-682-1, pp. 706-709 (2003).

31. Y. Oguri et al.: PIXE Measurement of Atmospheric Particulate Matter in a Residential Area near a Major Urban Highway; Int. J. PIXE, Vol. 10, pp. 127-135 (2000).

32. Y. Oguri et al.: PIXE Analysis of Urban Roadside Soil; Int. J. PIXE, Vol. 11, pp. 71-78 (2001).

33. S. Thomyasirigul et al.: Application of Ion Exchange Paper to Preconcentration of Chromium (III) and Chromium (VI) in Water for PIXE Analysis; Int. J. PIXE, Vol. 18, pp. 13-19 (2008).

34. S. Thomyasirigul et al: Determination of Chromium (VI) in Water by PIXE Analysis Using Ion Exchange Paper - Limit of Detection and Interference by Coexisting Anions; Int. J. PIXE, Vol. 19, pp. 1-8 (2009).

35. S. Thomyasirigul et al.: Speciation and Determination of Cr(III) and Cr(VI) in Water by Energy-Dispersive PIXE Analysis; X-Ray Spectrom., Vol. 40, pp. 202-204 (2011).

36. N. Hayashi et al.: Synthesis of Nanosized FeCo Granular Alloys by Ion Implantation and TMR Effect; Nucl. Instrum. Methods. Phys. Res. B, Vol. 257, pp. 25-29 (2007).

37. S. Takahashi et al.: Surface Treatment of Sample Holders for Trace Element Analysis in Human Blood by Using Particle-Induced X-ray Emission; The 3rd International Symposium on Hybrid Materials and Processing, November 10-13, 2014, Busan, Korea, PA-032 (2014).

38. Y. Oguri et al.: Application of PIXE Analysis to the Study of Electrokinetic Removal of Cesium from Soil; Int. J. PIXE, Vol. 14, pp. 49-56 (2004).

39. Y. Oguri et al.: FT-IR Measurement on the Damage of Japanese Paper Induced by PIXE Analysis; Int. J. PIXE, Vol. 29, pp. 33-42 (2019).

40. J. Hasegawa et al.: Development of a High-Efficiency High-Resolution Particle-Induced X-ray Emission System for Chemical State Analysis of Environmental Samples; Rev. Sci. Instrum., Vol. 78, pp. 073105-1-6 (2007).

41. T. Tada et al.: Chemical Shift Measurements of Chlorine K X-ray Spectra Using a High-Resolution PIXE System; Nucl. Instrum. Meth. B, Vol. 266, pp. 2292-2295 (2008).

42. S. Wonglee et al.: Development of a Target Positioning System Based on a Laser Position Sensor for High-Efficiency Wavelength-Dispersive PIXE Analysis; Int. J. PIXE, Vol. 20, pp. 1-9 (2010).

43. T. Tada et al.: Application of a Wavelength Dispersive Particle Induced X-ray Emission System to Chemical Speciation of Phosphorus and Sulfur in Lake Sediment Samples; Spectrochim. Acta B, Vol. 65, pp. 46-50 (2010).

44. S. Wonglee et al.: Chemical Speciation of Chlorine in Particulate Matter by Wavelength-Dispersive PIXE Technique; Nucl. Instrum. Methods. Phys. Res. B, Vol. 269, pp. 3111-3114 (2011).

45. S. Wonglee et al.: Chemical Speciation of Chlorine Present in Particulate Combustion Products of Organic Chlorine Compounds by Employing High-Resolution PIXE Analysis; Int. J. PIXE, Vol. 21, pp. 55-62 (2011).

46. T. Tada et al.: Measurement of Chemical State Change of Phosphorus during MeV-Proton Irradiation by a High-Resolution Wavelength-Dispersive PIXE System; Int. J. PIXE, Vol. 19, pp. 9-15 (2009).

47. T. Tada et al.: In-Situ Observation of Chemical State Change of Sulfur in Solid Targets during MeV Proton Irradiation; X-Ray Spectrom., Vol. 38, pp. 200-204 (2009).

48. T. Tada et al.: Target Temperature Rise and Gas Emission during Chemical State Analysis by WD-PIXE Measurement; AIP Conf. Proc., Vol. 1221, pp. 18-23 (2010).

49. T. Tada et al.: Chemical Speciation of Sulfur in Activated Carbon by Wavelength-Dispersive PIXE Technique; X-Ray Spectrom., Vol. 38, pp. 239-243 (2009).

50. T. Kawabata et al.: Analysis of Sulfur in Polymer Electrolyte Fuel Cells Using Wavelength Dispersive Type-Particle Induced X-Ray Spectroscopy; Proc. 27th Symposium on Materials Science and Engineering Research Center of Ion Beam Technology, Hosei University, December 10, 2008, Hosei University, Tokyo Japan, pp. 63-66 (2008).

51. J. Hasegawa et al.: Transport Mechanism of MeV Protons in Tapered Glass Capillaries; J. Appl. Phys., Vol. 110, pp. 044913-1-9 (2011).

52. S. Jaiyen et al.: Effect of Wall Material and Shape on MeV Ion Focusing Ability of Tapered Capillary Optics; Nucl. Instrum Methods. Phys. Res B, Vol. 271, pp.13-18 (2012).

53. J. Hasegawa et al.: Development of a Micro-PIXE System Using Tapered Glass Capillary Optics; Nucl. Instrum. Meth. B,

Vol. 269, pp. 3087-3090 (2011).

54. J. Hasegawa et al.: A Compact Micro-Beam System Using a Tapered Glass Capillary for Proton-Induced X-ray Radiography; Nucl. Instrum. Methods. Phys. Res. B, Vol. 266, pp. 2125-2129 (2008).

55. J. Hasegawa et al.: Ion Beam Focusing with Cone Optics for WDM Experiments; Nucl. Instrum. Meth. Phys. Res. A, Vol. 733, pp. 32-38 (2014).

56. S. Iwatani et al.: Imaging by Using Proton-Induced Quasi-Monochromatic X-ray Emission; Sci. Tech. Adv. Mater., Vol. 5, pp. 597-602 (2004).

57. J. Hasegawa et al.: Imaging of Iodinated Contrast Medium Using Proton-Induced Quasi-Monochromatic X-ray Emission; UTTAC Annual Report 2005, UTTAC-75, ISSN: 1880-4748, pp. 47-48 (2006).

58. Y. Oguri et al.: A Phantom Test of Proton-Induced Dual-Energy X-Ray Angiography Using Iodinated Contrast Media; Int. J. PIXE, Vol. 17, pp. 11-21 (2007).

59. Y. Oguri et al.: Digital Subtraction Cineangiography Using Proton-Induced Quasi-monochromatic Pulsed X-rays; Int. J. PIXE, Vol. 23, pp. 21-29 (2013).

60. Y. Oguri et al.: Proton-Induced Characteristic X-ray Source for Deep-Seated Cancer Treatment Using a Syringe Needle; The 11th European Conference on Accelerators in Applied Research and Technology, September 8-13, 2013, Namur, Belgium, P99 (2013).

61. Y. Hu et al.: Experimental and Numerical Study of Dose Distribution around a Syringe Needle-Type Proton-Induced X-ray Source for Radiotherapy; Int. J. PIXE, Vol. 25, pp. 93-100 (2015).

62. Y. Hu et al.: Direct Observation of Dose Distribution around a Syringe-Needle Type Proton-Induced X-ray Source Using Liquid Scintillator and a CCD Camera; Int. J. PIXE, Vol. 26, pp. 53-60 (2016).

63. Y. Hu et al.: Evaluation of the X-ray Distribution of a Syringe-Needle Type Proton-Induced X-ray Source by Geant4 Simulation; X-Ray Spectrom., Vol. 46, pp. 356-360 (2017).

64. Y. Oguri et al.: Selective Internal Radiotherapy Using Proton-Induced Monochromatic X-rays and Cancer-Targeting Nanoparticle Sensitizers: Int. J. PIXE, Vol. 25, pp. 101-111 (2015).

65. K. Ploykrachang et al.: Production of Quasi-monochromatic X-ray Microbeams Using MeV-Protons and a Polycapillary X-ray Half Lens; Int. J. PIXE, Vol. 23, pp. 1-11 (2013).

66. K. Ploykrachang et al.: Development of a Micro-XRF system for Biological Samples Based on Proton-Induced Quasimonochromatic X-rays; Nucl. Instrum. Methods. Phys. Res. .Phys. Res., Sect. B, Vol. 331, pp. 261-265 (2014).

67. K. Ploykrachang et al.: Design of a Proton-Induced Quasimonochromatic Micro-XRF Setup for Wet Biological Samples; Energy Procedia, Vol. 71, pp. 252-260 (2015).

68. K. Kobayashi et al.: Evolution of Interstellar Organics to Meteoritic and Cometary Organics: Approaches by Laboratory Simulations; Proc. International Astrobiology Workshop 2013, November 28-30, 2013, Sagamihara, Japan, pp.34-35 (2013).

69. K. Kobayashi et al.: Evolution of Extraterrestrial Complex Amino Acid Precursors: From Interstellar Organics to Cometary / Meteoritic Organics; Origins 2014, the second ISSOL — the International Astrobiology Society and Bioastronomy (IAU C51) joint international conference, July 6-11, 2014, the Nara-ken New Public Hall, Nara, Japan (2014).

70. T Sato et al.: Stability of Amino Acid Precursors in Various Space Environments; Japan Geoscience Union-American Geophysical Union Joint Meeting 2017, May 20-25, 2017, Makuhari Messe, Chiba, Japan, BAO01-P02 (2017).

71. W. Elmasry et al.: Alteration and Stability of Complex Macromolecular Amino Acid Precursors in Hydrothermal Environments; Orig. Life Evol. Biosph., Vol. 50, pp. 15-33 (2020).

72. K. Kobayashi et al.: Space Exposure of Amino Acids and Their Precursors during the Tanpopo Mission; Astrobiology, Vol. 21, pp. 1479-1493 (2021).

73. T. Matsuda et al.: Formation of Complex Amino Acid Precursors from Possible Interstellar Media by Particles Irradiation; The 2015 International Chemical Congress of Pacific Basin Societies (PAC CHEM), December 15-20, 2015, Honolulu, Hawaii, USA (2015).

74. K. Kobayashi et al.: Prebiotic Formation of Amino Acid Precursors in Primitive Earth Atmosphere by Cosmic Rays and Solar Energetic Particles; Japan Geoscience Union-American Geophysical Union Joint Meeting 2017, May 20-25, 2017, Makuhari Messe, Chiba, Japan, BAO01-P04 (2017).

75. H. Abe et al.: Laboratory Simulations of Titan Tholins Formed by Cosmic Rays; Japan Geoscience Union Meeting 2016, May 22-26, 2016, Makuhari Messe, Chiba, Japan, BAO01-P01 (2016).

# II. 3       Nuclear Fuel Cycle Study in the Era of Carbon Neutrality

Kenji Takeshita

## 1. Personal Research History

### 1.1 Fuel Reprocessing Technology and Minor Actinide Separation[1]

I have conducted various research subjects on fuel reprocessing such as the separation of radioactive iodine from the dissolver off-gas, solvent extraction separation of minor actinoids (MA), rare earth elements and precious metals from high-level radioactive waste, MA separation by extraction chromatography technology, and MA separation using structural changes of separation agent molecules caused by external stimuli such as light, heat and acoustics. In particular, I was conducting research on multidentite extractants with many nitrogen donors for MA separation, and have designed the structure of extractant molecules that can encapsulate MA stably and selectively. As a result, I succeeded in synthesizing a highly selective extractant whose the separation coefficient of Am/Eu is 100 or more. These studies were mainly conducted under Nuclear System Research and Development Project supported financially by Ministry of Education, Culture, Sports, Science and Technology.

### 1.2 Fukushima Reconstruction and Revitalization Research[2]

By the accident at the Fukushima Daiichi Nuclear Power Plant following the Great East Japan Earthquake on March 11, 2011, I changed research direction from nuclear system development to Fukushima reconstruction and started new research subjects on Fukushima reconstruction and revitalization, such as environmental restoration in Fukushima, treatment of contaminated water and soil, and treatment of secondary waste from ALPS. We have developed a high-speed ion exchange method using subcritical water for the decontamination of soil with radioactive cesium, and have succeeded in completely recovering radioactive cesium in subcritical water from the contaminated soil under the conditions of 250ºC and 4Mpa. Furthermore, we have developed a cesium enrichment method using ferrocyanide and a low-temperature vitrification method in which cesium concentrated by ferrocyanide is confined stably in glass as pollucite at 900ºC. By the development of these cesium solidification methods, the large waste volume reduction of 1/10,000 or less has been achieved. These studies have been carried out through several large research projects financially supported by Ministry of the Environment such as the Demonstration Project for Volume Reduction of Contaminated Soil and the Environmental Research and Technology Development Fund. In 2020, I established the TEPCO Decommissioning Frontier Collaborative Research Center and the Fukushima Reconstruction and Revitalization Research Unit, and are currently conducting eight research subjects on the decommissioning of Fukushima Daiichi NPP.

### 1.3 Research on Nuclear Fuel Cycle for Sustainable Nuclear Energy Use[3]

Since 2017, I have resumed research on the nuclear fuel cycle which can smoothly promote the sustainable use of nuclear energy with the aim of building a carbon-neutral society. As a fuel cycle technology to smoothly utilize light water reactors which will continue for some time to come, I developed a simultaneous recovery process of PGMs (Pd, Ru, Rd) and Mo from HLLW. PGMs and Mo cause precipitation and phase separation inside the glass melter, respectively. By the recovery of PGMs and Mo from HLLW, the vitrification process which is the Achilles heel of spent nuclear fuel reprocessing can be operated smoothly. As conclusion, I found the HLLW content in vitrified bodies can be increased from the usual 22 wt% to 35 wt%, and the number of vitrified bodies generated can be halved. These results greatly contribute to reducing the load on final disposal sites.

Furthermore, with the aim of reducing the load on the final disposal site, co-workers in JAEA and I conducted a dynamic simulation of the nuclear fuel cycle by the middle of 22th Century using NMB 4.0. It was found that both the load on the final disposal site and the required amount of natural uranium were able to be reduced significantly by introducing light water reactor multicycle, fast reactor cycle and partitioning/transmutation process of MA, and optimizing the reprocessing conditions and disposal conditions of vitrified objects.

In the next section, as an example of fuel cycle study, I introduce a latest paper titled "Effect of Introduction of Simultaneous Adsorption System of Mo and PGMs from HLLW on Vitrification Process ", which was presented in Global 2022 held in July, 2022.

## 2. Effect of Introduction of Simultaneous Adsorption System of Mo and PGMs from HLLW on Vitrification Process

### 2.1. Research Background

Japan Nuclear Fuel Limited (JNFL) is developing a Liquid Fed Ceramic Melter (LFCM) system on the basis of the knowledge and experience of Tokai Vitrification Facility (TVF) development [4]. A glass frit layer called cold cap is formed on molten glass and play an important role for the production of stable vitrified objects. In the cold cap, most of metal nitrates containing HLLW are decomposed thermally in low temperature range below the softening point of the glass frit and change to metal oxides, which are penetrated from the surface of the soften glass frit above 800ºC, dissolved in the molten glass above 1000ºC and homogenized in the molten glass at 1200 ºC. The molten glass containing metal oxides is flowed down from the melter and solidified in a canister. Vitrified objects are

produced according to above steps.

However, platinum group metals (PGMs) such as Pd, Ru and Rh in HLLW form flocs, which consists of Pd metal and oxides of PGMs, in molten glass, because of low solubility of PGMs in molten glass. The flocs are deposited on the side wall of melter and cause the decrease of heating efficiency by the electric leakage. The apparent viscosity of molten glass is increased by the formation of flocs and the mobility of molten glass becomes worse. Therefore, the molten glass with flocs cannot be flown down stably from the melter and the stable operation of the melter is disturbed. Molybdenum (Mo) is also a trouble element, which is present as molybdate in molten glass and cause the formation of low viscous phase called yellow phase [5]-[7]. To avoid these problems, two special operations, such as the HLLW dilution and the melter washing, are carried out. By introducing these operations, the number of produced glass rods is increased to more than twice of those with no operations.

In this study, we are developing a simultaneous adsorption system of PGMs and Mo from HLLW for the decrease in the number of glass rods and the stable operation of glass melter. As shown in Fig.1, the proposed system consists of four steps, such as the simultaneous adsorption of Mo and PGMs from HLLW by metal ferrocyanides, the thermal decomposition of ferrocyanide adsorbing Mo and PGMs, the leaching of Mo and PGMs from the decomposed material by diluted $HNO_3$ and the separation of Mo and PGMs from the leachate by solvent extraction. In this paper, the simultaneous adsorption performance of Mo and PGMs by metal ferrocyanide was tested and the mass balance of the proposed system was calculated. From these results, the effect of the introduction of the simultaneous adsorption system of PGMs and Mo on the production of vitrified objects was discussed.
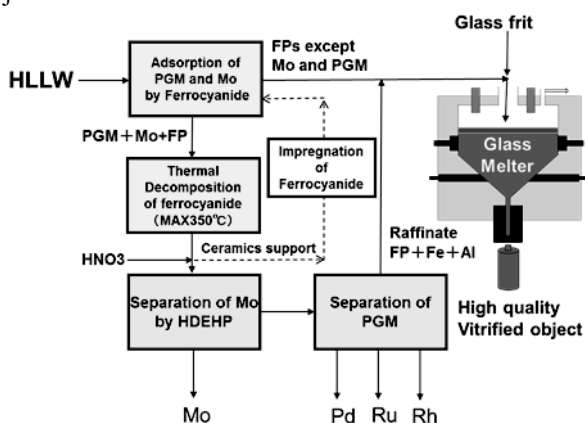


Fig.1 Simultaneous adsorption system of PGMs and Mo from HLLW

## 2.2 Simultaneous Adsorption of PGMs and Molybdenum from HLLW
### (1) Adsorption of PGMs and Molybdenum into Metal Ferrocyanides

We synthesized metal ferrocyanides by mixing $K_4[Fe(CN)_6]3H_2O$ and metal nitrates of Fe(III), Co(II),

Mn(II) and Al(III) vigorously at room temperature for 2 h. Precipitates of metal ferrocyanides obtained were separated by a centrifugal separator (3000 rpm, 30 min), washed 5 times by pure water, dried in air at 75°C for 12 h and dried in vacuum at 75°C for 3h. The obtained 4 dried precipitates, which were identified as ferrocyanides of Fe, Co, Mn and Al by XRD, respectively. They were crushed and used for the simultaneous adsorption tests of PGMs and Mo[8],[9].

1.5 mol/L $HNO_3$ solution with 1mmol/L of nitrate compounds of Pd, Ru, Rh, Mo, Cs, Na, Fe and Gd was prepared. The simultaneous adsorption of PGMs and Mo into ferrocyanide compounds was tested by adding 20mg of each ferrocyanide and 10mL of the $HNO_3$ solution and shaking at room temperature for 16h. The change of metal concentration in the $HNO_3$ solution was measured by ICP. The experimental results are shown in Table 1. Metal ferrocyanides are suitable for the adsorption of PGMs. Especially, Al(III) ferrocyanide shows high adsorption ability for the simultaneous recovery of PGMs and Mo, compared with other ferrocyanides. A typical rare earth element (REE), Gd, was not adsorbed by ferrocyanides. PGMs and Mo can be recovered selectively from REEs.

Table 1 Adsorption tests of major 8 elements (Pd, Ru, Rh, Mo, Cs, Gd, Na and Fe)

| Adsorbent (FC: ferrocyanide) | Pd Ads[%] | Ru Ads[%] | Rh Ads[%] | Cs Ads[%] | Na Ads[%] | Fe Ads[%] | Mo Ads[%] | Gd Ads[%] | M Conc. [mg/L] |
|---|---|---|---|---|---|---|---|---|---|
| AlFC | 100 | 91.5 | 15.3 | 15.2 | 1.8 | 16.7 | 43.0 | 0.0 | 61.8 |
| MnFC | 100 | 60.8 | 6.4 | 79.2 | 6.3 | 3.1 | 3.9 | 0.3 | 69.8 |
| FeFC | 100 | 14.5 | 3.0 | 26.3 | 1.8 | -80.6 | 5.4 | 0.0 | 104 |
| CoFC | 88.6 | 1.3 | 0.0 | 0.3 | 3.6 | -12.2 | 0.0 | 0.1 | 37.2 |

### (2) Selective Adsorption of PGMs and Molybdenum from Simulated HLLW

The simultaneous adsorption of PGMs and Mo from a simulated HLLW (sHLLW) with 26 elements was tested by using AlFC. Table 2 shows the composition of the sHLLW. 0.4 g AlFC was added to 5ml sHLLW in a vial (correspond to 80 kg AlFC in 1 $m^3$ HLLW), which was sealed and shaken at room temperature for 16 hr. A small amount of the solution was sampled by a syringe with filter and the concentrations of major elements containing PGMs and Mo were measured by ICP.

Fig.2 shows the experimental results. Blue and red bars mean the concentrations of metal components before and after the adsorption test, respectively. The height difference between two bars on each component means the adsorption amount. The adsorption percentages of Mo, Ru, Rh and Pd from the sHLLW were evaluated to be 80, 70, 50 and 100%, respectively. Co-adsorbed FP elements were Cs (adsorption percent: about 40%) and Zr (about 10%). Rare earth elements (REEs) were not adsorbed. Maybe the adsorption performance of minor actinides (MAs) is similar to that of REEs. Therefore, it is not necessary to consider the adsorption of MAs in AlFC. These results suggest that AlFC adsorbs PGMs and Mo selectively from HLLW.

Table 2    Composition of simulated HLLW (26 elements)

| Element | Concentration | | | Regent |
|---|---|---|---|---|
| | [mol/L] | [mg/L] | Analysis | |
| Na | 9.8E-01 | 22530.2 | ICP-AES | NaNO₃ |
| P | 4.0E-03 | 123.9 | ICP-AES | H₃PO₄ |
| K | 1.8E-03 | 70.4 | ICP-AES | KNO₃ |
| Fe | 3.0E-02 | 1675.5 | ICP-AES | Fe(NO₃)₃·9H₂O |
| Cr | 5.9E-03 | 306.8 | ICP-AES | Cr(NO₃)₃·9H₂O |
| Ni | 9.6E-03 | 563.4 | ICP-MS | Ni(NO₃)₂·6H₂O |
| Co | 1.9E-03 | 112.0 | ICP-MS | Co(NO₃)₂·6H₂O |
| Cs | 4.1E-02 | 5448.9 | ICP-MS | CsNO₃ |
| Sr | 9.9E-03 | 867.4 | ICP-AES | Sr(NO₃)₂ |
| Ba | 2.0E-02 | 2746.0 | ICP-AES | Ba(NO₃)₂ |
| Zr | 4.9E-02 | 4469.8 | ICP-AES | ZrO(NO₃)₂·2H2O |
| Mo | 3.0E-02 | 2878.2 | ICP-AES | Na₂MoO₄·2H₂O |
| Mn | 1.9E-02 | 1043.9 | ICP-AES | Mn(NO₃)₂·6H₂O |
| Ru | 1.9E-02 | 1920.9 | ICP-AES | RuNO(NO₃)₃·2H₂O |
| Rh | 4.5E-03 | 463.1 | ICP-AES | Nitrate solution |
| Pd | 1.9E-02 | 2021.6 | ICP-AES | Nitrate solution |
| Ag | 1.1E-03 | 118.7 | ICP-MS | AgNO₃ |
| Zn | 4.0E-04 | 26.2 | ICP-MS | Zn(NO₃)₂·6H₂O |
| Te | 5.1E-03 | 650.8 | ICP-AES | H₆TeO₆ |
| Y | 8.1E-03 | 720.2 | ICP-AES | Y(NO₃)₃·6H₂O |
| La | 2.0E-02 | 2778.0 | ICP-AES | La(NO₃)₃·6H₂O |
| Ce | 4.0E-02 | 5604.0 | ICP-AES | Ce(NO₃)₃·6H₂O |
| Pr | 2.0E-02 | 2818.0 | ICP-MS | Pr(NO₃)₃·6H₂O |
| Nd | 5.9E-02 | 8507.8 | ICP-AES | Nd(NO₃)₃·6H₂O |
| Sm | 9.0E-03 | 1353.6 | ICP-MS | Sm(NO₃)₃·6H₂O |
| Gd | 4.0E-02 | 6292.0 | ICP-AES | Gd(NO₃)₃·6H₂O |
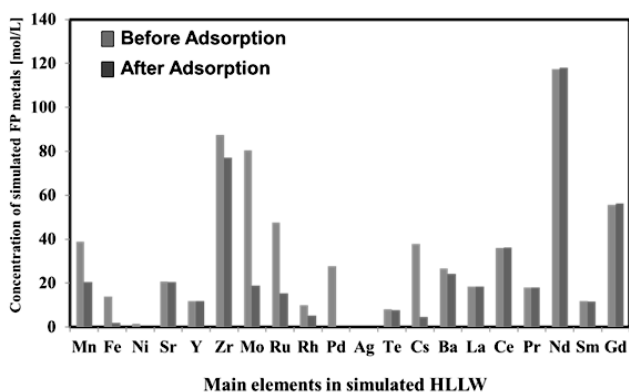


Fig.2 Adsorption of simulated HLLW (26 elements)
into AlFC

## 2.3. Separation of PGMs and Molybdenum by Solvent 」 Extraction

In the former section, we confirmed that AlFC adsorbs PGMs and Mo selectively from HLLW.   As shown in Fig.1, AlFC adsorbing PGMs and Mo is decomposed thermally in air. The residue is washed by water or diluted $HNO_3$ and PGMs and Mo are leached almost completely to the washing solutions. PGMs and Mo in the leachate are separated mutually by solvent extraction technique.

The practical separation of Mo has already been studied by a typical acidic phosphorus compound, D2EHPA (di-2-ethylheylphosphorus acid). Morita et al. tested the extraction separation of Mo from Zr, Y, Pd and Nd and succeeded the separation of Mo and Zr from other metals[10]. In this study, a new extraction process using MTTDGA (*N,N'*-dimethyl-

*N,N'*-ditolylthiodiglycolamide) and EHTAA (Tris(*N,N*-di-2-ethylhexylethylamine)amine) was proposed for the separation of PGMs in $HNO_3$ solution. Fig.3 shows the chemical structures of used extractants [11].
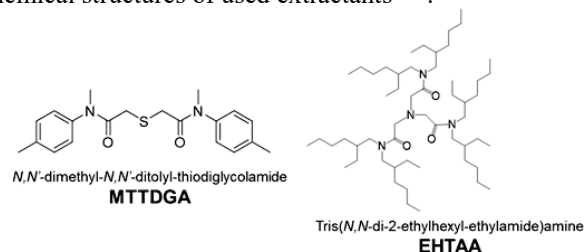


Fig.3    Chemical structures of used extractants

Table 3 Composition of simulated feed solution

| Element | Concentration (mM) |
|---|---|
| Al | 0.1 |
| Na | 2.8 |
| K | 0.12 |
| Pd | 0.24 |
| Rh | 0.03 |
| Ru | 0.2 |

As shown in Fig.1, PGMs and Mo are recovered simultaneously from HLLW by the adsorption process using AlFC and the feed solution to the extraction process are prepared by the thermal decomposition process of AlFC and the washing process of decomposed residue using diluted $HNO_3$ solution. From the results of fundamental experiments, the composition of the feed solution was decided as shown in Table 3. We prepared the simulated feed solution containing Pd(II), Ru(III), Rh(III), Al(III), Na(I) and K(I). Pd, Rh, Al, Na and K were added as metal nitrate. Ru was added as Ru(III) nitrosyl nitrate which is a typical chemical form in HLLW.

Extraction of PGMs from the simulated feed solution was conducted in batch experiments. Firstly, the $HNO_3$ concentration in the simulated feed solution was adjusted to 1 M. MTTDGA was diluted by toluene and the concentration of MTTDGA in toluene was adjusted to 5 mM. Fig.4a shows the results of extraction tests. It is clear that MTTDGA can extract Pd(II) quantitatively within one hour, while all the other elements were not extracted. Only Pd(II) is extracted by MTTDGA under the condition of low $HNO_3$ concentration. Next, the $HNO_3$ concentration in the simulated feed solution was increased to 8M. The results of extraction tests were shown in Fig.4b. 20% of Rh(III) and Ru(III) as well as Pd(II) was extracted by MTTDGA. The simultaneous extraction of Rh(III) and Ru(III) by MTTDGA is possible under the condition of high $HNO_3$ concentration. Furthermore, the extraction using mixed extractants of MTTDGA and EHTAA was tested. As shown in Fig.4c, the use of a mixed extractants of MTTDGA and EHTAA resulted in significant improvement of Rh(III) and Ru(III) extraction, giving ~90% extraction of Rh(III) in 24 hours and 35% extraction of Ru(III) in the same time. Al, K and Na were not extracted into organic phase in any of the

studied cases.



(a) 1M HNO₃, MTTDGA     (b) 8M HNO₃ , MTTDGA

(c) 8M HNO₃ , MTTDGA+EHTAA
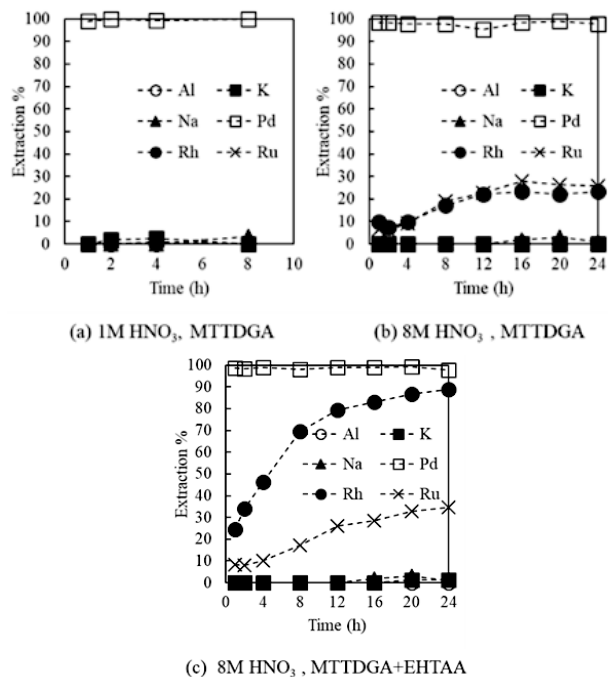
Fig.4 Extraction percentage of Al, K, Na Pd(II), Ru(III) and
Rh(III) withMTTDGA and MTTDGA+EHTAA as
a function of time.

From the results of extraction experiments, a separation flow of Pd(II), Rh(III) and Ru(III) was proposed. As shown in Fig.5, Pd(II) is selectively extracted over Rh(III) and Ru(III) with MTTDGA under the $HNO_3$ concentration condition of 1 M. The concentration of $HNO_3$ in the raffinate solution from the Pd(II) extraction step is adjusted to 8 M. Then, the co-extraction of Rh(III) and Ru(III) is promoted by use of a mixture of MTTDGA and EHTAA. Pd in HLLW has a long-lived isotope, Pd-107 (t1/2= 6.5 million year). Therefore, the separated Pd is disposed of as low-level waste or can be used industrially as catalyst by shielding β ray from Pd-107. On the other hand, Ru and Rh have no long-lived nuclide. After the storage for 70 y, these metals can be reused industrially.
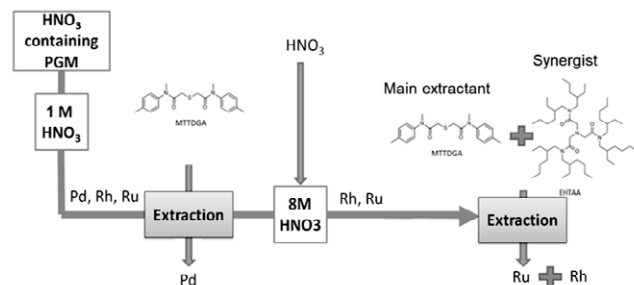


Fig.5    Separation flow for selective separation of Pd,
Rh and Ru

### 2.4. *Effect of Introduction of Simultaneous Adsorption System of PGMs and Mo on Final Disposal.*

From the adsorption performance of AlFC (Fig.2), the

mass balance of separation system of PGMs and Mo from HLLW was calculated. It is known that a part of Mo in HLLW is precipitated by the formation of zirconium molybdate hydrate ($ZrMoO_2(OH)_2 2H_2O$) and a half of PGMs is not dissolved in nitric acid. It was assumed that 20% of Mo and 50% of PGMs was remained in insoluble residue formed in a PUREX reprocessing plant. The insoluble residue is transferred directly to the glass melter. Fig.6 shows the calculation results. These results suggest that both Mo and PGMs remained in the dissolved $HNO_3$ solution can be removed completely under the conditions that 80 kg of AlFC is added in $1m^3$ of HLLW.

From the results of the mass balance calculation, we discuss the effect of the introduction of the simultaneous adsorption process of PGMs and Mo on the production of vitrified objects. We assumed $UO_2$ fuel with the burn-up of 45 GWd/T in PWR. The decay chain was calculated by ORIGEN-ARP. The conditions of fuel reprocessing were as follows,

- Recovery of U and Pu : 99.6%, 99.5%
- Release of gaseous and volatile elements : 100%
- Release of others : 0% (FP and MA are remained in HLLW)

For the stable disposal of vitrified objects, we assumed the vitrification conditions as follows,

- Heating of vitrified object < 2.3kW / glass rod
- MoO₃ content < 1.5wt%loric restriction
- PGMs (Ru+Rh+Pd)content < 1.5wt%
- Na₂O content : 10wt%

Table 4 shows the relation between the cooling time of spent fuel and the waste loading in vitrified objects. In this table, the effects of the introduction of simultaneous adsorption system of PGMs and Mo was compared. See the case of no adsorption system. A factor restricting the production of vitrified objects is heat generation of vitrified objects at the cooling time of 4 years and changes to Mo content when the cooling time becomes longer. Then, the waste loading is restricted to 21-22wt%. On the other hand, in the case of the introduction of the adsorption process, the waste loading can increase with increasing the adsorption percentages of Mo and PGMs. As shown in Fig6, 50% of PGMs and 80% of Mo can be removed from HLLW under the condition that 80kg AlFC is added in $1m^3$ HLLW. Therefore, the waste loading can be enhanced from 22wt% to 35wt% by the introduction of the simultaneous adsorption system of PGMs and Mo. The amount of HLLW charged in vitrified object is represented as the weight percentage of metal oxides derived from HLLW. As 10wt% of Na₂O is contained with HLLW in vitrified object, the practical amount of metal oxides from HLLW is evaluated to be 12wt% at the waste loading of 22wt% and 25wt% at that of 35wt%. This means that twice amount of HLLW can be treated in the vitrification process by increasing the waste loading from 22wt% to 35wt%. Therefore, the number of produced vitrified objects can be reduced to a half of that without the simultaneous adsorption system of Mo and PGMs. However, due to increasing the contents of Cs and Sr with increasing the waste loading, the heat quantity of

vitrified objects exceeds a restriction factor for the heat generation from vitrified objects, 0.35 kW/glass rod. If 90% of Sr and Cs are separated from HLLW, the vitrified objects with the waste loading of 35wt% can be finally disposed of after the cooling period of 40 y.
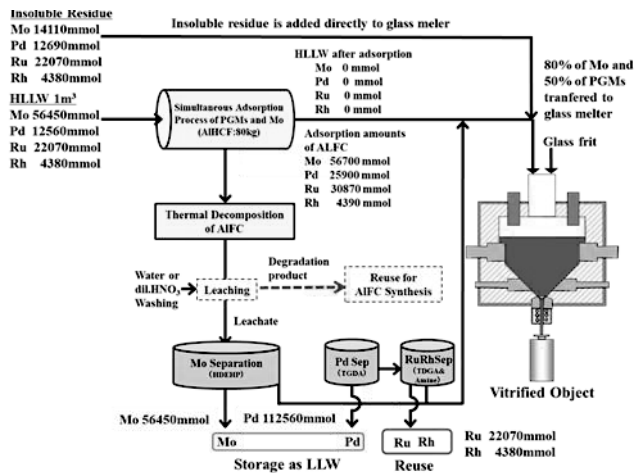


Fig. 6 Mass balance of simultaneous adsorption system of PGMs and Mo.20% of Mo and 50% of PGMs were assumed to be recovered in insoluble residue

Table 4 Relation between cooling period of spent fuel and waste loading of vitrified objects

| Cooling period of HLLW [yr] | No adsorption of Mo and PGM | | Adsorption of Mo and PGM | | | |
|---|---|---|---|---|---|---|
| | Waste Content [wt%] | Limiting Factor | Mo [%] | PGMs [%] | Waste Content [wt%] | Multiplication factor Waste Content [-] |
| 4 | 21.0 | Heating | - | - | - | - |
| 10 | 22.0 | Mo content >1.5 wt% | 46.1 | 32.0 | 30.0 | 1.67 |
| 20 | 22.1 | | 58.8 | 48.1 | 35.4 | 2.10 |
| 30 | 22.1 | | 66.2 | 57.4 | 40.4 | 2.51 |

## 2.5. Conclusions

(1) A new simultaneous adsorption system of PGMs and Mo from HLLW was proposed for the quality improvement and volume reduction of vitrified object. The use of aluminum ferrocyanide (AlFC) is valid for the selective adsorption of PGMs and Mo from HLLW.

(2) The separation of PGMs and Mo from the $HNO_3$ solution obtained by the thermal decomposition of AlFC adsorbing PGMs and Mo and the acid leaching of the decomposed residue was accomplished by the combination of two extraction processes, the extraction process of Mo with D2EHPA and extraction processes of PGMs with MTTDGA and EHTAA.

(3) 80% of Mo and 50% of PGMs can be separated from HLLW by the introduction of simultaneous adsorption system of PGMs and Mo under the condition that 80kg of AlFC is added in 1 m³ HLLW. As a result, the content of metal oxides derived from HLLW in vitrified object can be increased from 22wt% to 35wt%. The number of vitrified objects is reduced to a half of that without the simultaneous adsorption process of Mo and PGMs. If 90% of Sr and Cs are separated from HLLW, the vitrified objects with the waste loading of 35wt% can be finally disposed of after the cooling period of 40 y.

**Reference**

1. Research Papers on Fuel Reprocessing Technology and Minor Actinide Separation. For example, *ACS Symp. Ser.* **933**:261-273 (2008); *Progress in Nuclear Energy* **50(2)** 466-469 (2008); *J. Nucl. Sci. Technol.* **41(11)** 1122-112 (2012); *Chem.Lett.*, **44(12)** 1626-1636 (2015); *Progress in Nuclear Science and Technology*, **5** 56-60 (2018); *Dalton Transactions* **47(30)** 10063-10070 (2018); *Chemistry Letters* **47(6)** 732-735 (2018); *Solvent Extraction Research and Development, Japan*, **28(1)**, 69-77 (2021) etc.

2. Research Papers on Fukushima Reconstruction and Revitalization. For example, *Chemistry Letters* **45(3)** 256-258 (2016); *Journal of Hazardous Materials* **326** 47-53 (2017); *Chemistry Letters* **46(9)** 1350-1352 (2017); *Environmental Science & Technology*, **51(23)** 13886-13894 (2017); *Chemical Engineering Journal* **333** 392-401 (2018); *Journal of Hazardous Materials*, **387**, 5 April 2020, 121677; *Water Research*, **177**, 15 June 2020, 115804; *Journal of Nuclear Science and Technology*, **58(4)**, 399-404 (2021) etc.

3. Research Papers on Nuclear Fuel Cycle in the Era of Carbon Neutrality. For example, *RSC Advances,* **11**, 20701-20707 (2021); *IOP Conf. Ser.: Mater. Sci. Eng.* 835 012001 (2020); *Chemistry Letters*, **49(1)** 83-86 (2020); *Separation Science and Technology*, **54(12)**, 1970-1976 (2019); *Solvent Extraction Research and Development, Japan*, **26(2)**, 43-49 (2019); *Journal of Nuclear Science and Technology*, **55(10)**, 1130-1140 (2018); *AIP Advances* **8(4)** 045221-045221 (2018); *Journal of Applied Physics* **119**, 235102 (2016); *EPJ Nuclear Sci. Technol.* **2**, 44 (2016) etc.

4. M. Motohashi, R.Shindo, K.Shinzawa, M.Uryu, T.Sannomiya, O.Hashimoto, *Donen Giho*, **84**, 35-39 (1992).

5. O. Pinet, J.L.Dussossoy, C. David and C. Fillet, *J. Nucl. Mat.,* **377**, 307-312 (2008).

6. R.J. Short, R.J. Hand, and N.C. Hyatt, 2002 MRS Fall Meeting & Exhibit Symposium II Scientific Basis for Nuclear Waste Management XXVI, vol. 757, p. 141

7. I. L. Pegg, H. Gan, K. S. Matlack, Y. Endo, T. Fukui, A. Ohashi, I. Joseph and B. W. Bowan, II, WM-2010 Conference, Paper No.10107, Phoenix (2010).

8. H.Mimura, *Journal of Ion Exchange*, **21**, 2-19 (2010).

9. H. Mimura, J. Lehto and R. Harjula, *J.Nucl.Sci.Technol.,* **34**, 582-587 (1997).

10. Y. Morita, I. Yamagishi, Y. Tsubata, K. Matsumura, K. Sakurai and T. Iijima, JAEA-Research 2012-031.

11. T. Ito, S-Y. Kim, Y. Xu, K. Hitomi, K. Ishii, R. Nagaishi and T. Kimura, *Separation Science and Technology*, **48**, 2616-2625 (2013).

# III. Research Reports

# III. 1      Criticality Safety Study for Fukushima Daiichi NPS Decommissioning and Breed-and-Burn Fast Reactor Study

## Toru Obara

Criticality safety studies for Fukushima Daiichi Nuclear Power Station Decommissioning have been performed. They are the fundamental studies for the dose evaluation in criticality accidents and to estimate possibility of criticality when the fuel debris particles are falling into water. Study on CANDLE burning reactor has performed also as an innovative nuclear reactor design study.

## 1. Calculation of Transient Parameters of the Integral Kinetic Model with Delayed Neutrons for Space-dependent Kinetic Analysis of Coupled Reactors [1]

This study introduces new methodologies for integrating fission reactions induced by delayed neutrons into the Multi-Region Integral Kinetic (MIK) code by using a Monte Carlo neutron transport calculation. First, it was confirmed that it is feasible to solve the Integral Kinetic Model (IKM) with delayed neutrons by the forward Euler discretization method in terms of the number of time steps. This can be done with the help of the law of radioactive decay to reflect the delay in the emission of delayed neutrons in the discretized IKM. Second, a new Monte Carlo–based methodology was introduced for calculating the cumulative distribution functions of secondary fission induced by prompt and delayed neutrons. These functions are necessary for the discretized IKM. A new MIK code that has the capability of calculating the fission reaction rates for delayed neutrons is currently under development. Based on the preliminary verification results, future studies will verify the discretized IKM with delayed neutrons using kinetic analyses and compare them to experimental results for prompt and delayed supercritical transients in diverse reactor configurations.

## 2. Characteristics of reactivity change as fuel debris falls in water [2]

In the study, the characteristics of reactivity change due to fuel debris falling into water was investigated. The impact of each parameter on criticality was evaluated using a basic parametric survey. The results clearly indicated that when a large number of fuel debris pieces suddenly sediment in water, the reactivity increases rapidly. It suggested that this situation must be avoided to prevent criticality accidents during fuel debris retrieval operations. On the other hand, when fuel debris pieces gradually sediment, falling from a low height onto a floor with high friction, the sedimentation shape can easily condense to a significant height. In such cases, the criticality risk might become large once the sedimentation process is complete.

## 3. Supercritical Transient Analysis for Ramp Reactivity Insertion Using Multiregion Integral Kinetics Code [3]

To proceed with the decommissioning of the Fukushima Daiichi Nuclear Power Station, analyses of unexpected fuel debris criticality accidents are needed. Supercritical transient analyses have been conducted for fuel debris using the Multiregion Integral Kinetic (MIK) code, which can take the space dependence of fuel debris into account. In those analyses, reactivity is assumed as stepwise insertion because the MIK code does not include delayed neutron effects, which might be negligible. However, reactivity insertion may not always be stepwise. Therefore, it is important to clarify an applicable range of the MIK code for nonstepwise insertion, such as ramp reactivity insertion. To show that kinetics codes without delayed neutron effects could be applied for a supercritical transient induced by ramp reactivity insertion, an analysis using the point reactor kinetics model was introduced as a pre-analysis to clarify this range in the case of ramp reactivity insertion in terms of the contribution of delayed neutrons. It is successfully demonstrated a supercritical transient analysis for ramp reactivity insertion using the MIK code is feasible.

## 4. Optimization of reactor size in the small sodium-cooled CANDLE burning reactor [4]

In this study, a sodium-cooled CANDLE burning reactor was optimized to minimize the reactor's size while maintaining its power. This study proved that with better heat-removal features of sodium coolant, it was feasible to reduce fuel pin pitch from 1.08 cm to 1.02 cm from a thermal hydraulics standpoint. Changing the radial reflectors from sodium to lead-based materials reduced the radius of the critical core and reflector 15.7%, from 187.4 cm to 158.0 cm. With these optimizations, a small sodium-cooled CANDLE burning reactor was designed with a core and reflector radius comparable to those of other small sodium fast-reactor concepts. The core height of the CANDLE burning reactor could be optimized by shortening the spent fuel region of the core.

## Reference
1. Hiroki Takezawa, Delgersaikhan Tuya, Toru Obara; *Nuclear Science and Engineering*, Vol. **195**, pp. 1236-1246 (2021).
2. Takeshi Muramoto, Jun Nishiyama, Toru Obara; *Progress in Nuclear Energy*, Vol. 139, 103857 (2021).
3. Kodai Fukuda, Jun Nishiyama, Toru Obara; *Nuclear Science and Engineering*, Vol. **195**, pp.453-463 (2021).
4. Hoang Hai Nguyen, Jun Nishiyama, Toru Obara; *Annals of Nuclear Energy*, Vol. **153**, 108040 (2021).

# III. 2 Metallurgy for zero-carbon iron/steelmaking process and energy systems

Yoshinao Kobayashi

## 1. Introduction

Toward realization of Zero Carbon society, it is essential to establish the material creation process with carbon neutral loop. We are targeting the utilization of recycled steel, which is the base material for construction, transportation and energy supply, to suppress inevitable $CO_2$ emission in iron oxide reduction process and realize the Zero Carbon steelmaking process to lead the materials circulating society.

## 2. Zero-carbon ironmaking process

In the conventional ironmaking process, blast furnace has been centered upon as the most efficient molten metal production process that our race has ever devised. During this process, iron oxide in iron ore is reduced by carbon in cokes inevitably produces $CO_2$ fully exhausted to the environment. Direct iron ore smelting reduction process[1] also emits $CO_2$ produced molten iron oxide reduction process originated from the usage of coal with impurities such as phosphorus and sulfur, the same goes for blast furnace process. To solve these problems, direct steelmaking by CO gas blowing reduction is newly proposed, under the scheme of GXI(Green transformation initiative) [2], which has been launched on the platform of Laboratory for Zero-Carbon Energy. In this proposed process, CO gas blowing from the bottom of furnace reduces iron oxide dissolved in the molten slag to finally produce $CO_2$. Emitted $CO_2$ gas which can be reduced by electrolyzation using zero-carbon energy to revert back to CO, which can be used as reducing gas again for bottom blowing. In this loop, emission of $CO_2$ gas is virtually zero, where, carbon is circulating as if playing a quasi-catalytic role continuously producing metallic iron. Differently from conventional ironmaking process starting from coal, impurity is not included in principle because recycled CO does not contain any other element, possibly resulting in steelmaking process without refining.
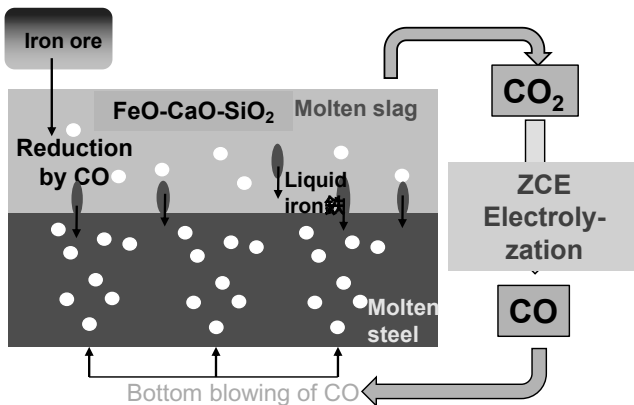
## 3. Steel scrap recycling process

The accumulated amount of steel once having come on to the market is increasing in the world including that still in service as well as that beyond end-of-life. Rotary flow returning back from this accumulation to crude steel production as iron resource would be important factor to reduce $CO_2$ emission, essentially because steel scrap has been already reduced to metal, with no need of iron oxide reduction process inherently accompanying $CO_2$ emission. Steel scrap usually contain nobler element than iron such as copper, bringing about characteristic problem of copper embrittlement which is crucial in viewpoint of processability. To avoid this problem originated from copper, many types of countermeasure has been taken up and tried for application. Among them, copper sulphide precipitation has been paid growing attention to suppress the above problem by stabilizing copper as solid phase separated from matrix, which may weaken the factor for formation of copper enriched liquid phase induced by preferential oxidation of iron [3]. Experimental study was implemented to mainly investigate the critical cooling rate for the precipitation of copper sulphide in our laboratory. On the basis of the observational results on cross section of the as-cast or heat treated sample with variation in experimental condition, several tens kelvin per second would be probable value for the critical cooling rate[4]. Enlargement of usage of steel scrap for crude steel production should be important issue in viewpoint of hybridization of iron-steelmaking process.
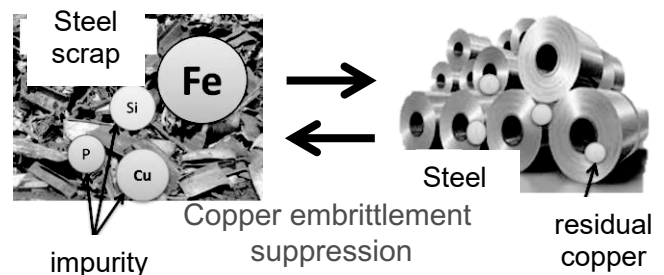
Fig.2 Condensation loop of copper in steel scrap

## Reference

1.  T. Kitagawa: Tetsu-to-Hagané, Vol.88(2002), p.432
2.  http://www.gxi.iir.titech.ac.jp/index.php#gxi
3.  Z. Liu, Y. Kobayashi, K. Nagai, Jian Yang and M. Kuwabara: ISIJ International, 46, 744-753 (2006)
4.  Y. Kobayashi:; The 183rd ISIJ Meeting Mar. 2022.

Fig.1 Conceptual cross section of ZC ironmaking process

# III. 3  Estimation of reactor vessel failure by metallic interaction in Fukushima Daiichi Nuclear Power Plant accident

Ayumi Itoh, Shintaro Yasui, Yoshinao Kobayashi

## 1. Introduction

In March 2011, Units 1–3 of the Fukushima Daiichi Nuclear Power Plant (1F NPP) were involved in a severe accident that resulted from the Great East Japan earthquake and the subsequent tsunami. On the basis of muon tomography and primary containment vessel (PCV) investigations, the damage to the core was summarized as follows: 1) in Unit 1, most of the fuel assemblies shifted from the original position and moved out of the reactor pressure vessel (RPV) [1]; 2) in Unit 2, some fuel assemblies remained around the periphery of the core region; most of the damaged core materials were present in the lower head, with some debris being discharged out of the RPV [2] and 3) in Unit 3, most of the fuel assemblies were lost from the core region; some damaged core materials were present in the lower head and a certain amount of debris was discharged out of the RPV [3]. The images obtained from the PCV inspection of Unit 2 show that the partially unmolten upper tie plate of the fuel assembly fell on the pedestal floor. In addition, in Unit 3, partially unmolten control guide tubes were found among the accumulated debris on the pedestal floor. These observations indicate the presence of a hole in the RPV wall that let these tubes fall through, and the discharging materials were liquid–solid mixtures that were not completely liquefied.

In this study, the RPV failure scenario caused by the interaction of the metallic materials formed when the molten fuel and the stainless steel react under the "dry-core" condition was proposed. First, the mechanism of uranium transport from the molten fuel to the stainless steel and the method for estimating the RPV failure timing were introduced. The scenario was applied to the progression of core degradation of the 1F NPP Units 1–3, and the RPV failure timings were estimated in comparison with the values obtained from the pressure response of the plants. Finally, features to improve the accuracy of the estimation were proposed.

## 2. RESULTS AND DISCUSSIONS

Figure 1-3 show the measured RPV pressure data (green circles) with the calculated RPV failure time. In the case of Unit 1, the cooling function was completely lost immediately after the tsunami owing to the station blackout. Thereafter, the water in the RPV evaporated with a discharge of steam to the suppression pool (S/C) and/or dry-well (D/W), resulting in a decrease in the water level, exposure of fuel to the gas phase, temperature escalation of core materials triggering chemical reactions, core melt, and relocation. The international benchmarking project [4] after the incident also confirmed this accident progression.

As the measured RPV pressure was approximately 1 MPa at t = 11.2 h (t is an elapsed time since the earthquake occurred) after the earthquake occurred, the lower head of the RPV is considered to have already ruptured at this moment. Because there are only two measurement points until the RPV failure, it is impossible to estimate the onset of dry-out from the measured data. In this study, the timing of large slumping estimated by TEPCO [4] was applied as the dry-out time, i.e., 3/11 22:00 (t = 7.0 h). Substituting the decay heat of 10.26 MW for Unit 1 (68 tonU) [7] into Eq. (1), the liquefaction of U-contaminated stainless steel is initiated at 3/12 0:45 (t = 10.0 h), and the RPV failure timing was calculated as 3/12 2:25 (t = 11.7 h).

In the case of Unit 2, the cooling function (reactor core isolation cooling, RCIC) was operational in the first 74 h, and core melting was prevented. According to the comprehensive estimation analysis in ref. [2], the core melt progression was likely to be initiated by the decompression boiling at 3/14 18:00, as shown in Figure 4. Based on the analytical evaluation of steam and hydrogen generation to reproduce the pressure transient, it is estimated that the core melt progression could occur during three peaks from 3/14 21:00 (t = 75.4 h) to 3/15 2:00 (t = 83.2 h). Each pressure peak may have been caused by steam generation at the slumping of the core materials and hydrogen generation by the Zr-steam reaction. Thereafter, the pressure level was maintained at a certain level and began to decrease slightly around 3/14 4:00 (t = 85.4), which may be the onset of dry-out. After a while, the pressure drops at 3/15 11:00 (t = 92.2 h), which indicates that the RPV failure occurred before this time. Substituting the decay heat of 7 MW (94 tonU) [7] for Unit 2 into Eq. (1), the liquefaction of U-contaminated stainless steel is initiated at 3/15 9:53 (t = 91.1 h), and the instant of RPV failure was calculated as 3/15 11:33 (t = 92.8 h).

In the case of Unit 3, the plant did not lose complete DC power on the arrival of the tsunami, and the cooling functions (RCIC and HPCI, high-pressure cooling injection) were maintained in the first two days to prevent the core melt progression. The core melt progression is considered to have been initiated at approximately 3/13 9:10 (t = 42.3 h), triggered by the depressurization, as shown in Figure 5. In addition to the benchmarking studies, several numerical studies for Unit 3 have been conducted by different research groups using different codes [5,8,9]. These studies have reproduced some of the signatures in the RPV/PCV pressure data, but the uncertainty of water injection makes it difficult to provide a single interpretation. In this study, the interpretation of the measured pressure data by Li et al. was used to determine the key events. The RPV pressure was 0.351 MPa at 3/13 20:05 (t = 53.3 h) and it decreased to approximately 0.2 MPa at 3/13 23:00 (t = 56.2 h). The

pressures of D/W and S/C also show a gradual decrease in the same interval, which suggests that the RPV pressure also tends to decrease, although the measured data were unavailable. This pressure decrease indicates that the steam generation in the RPV was reduced because dry-out occurred during this period. Hence, the instant when the D/W and S/C pressures start decreasing, i.e., 3/13 21:00 (t = 54.2 h), was taken as the onset of dry-out in this study. Substituting the decay heat of 12.85 MW (93 tonU)[14] for Unit 3 into Eq. (1), the liquefaction of U-contaminated stainless steel was initiated at 3/14 1:37 (t = 58.9 h), and the RPV failure was calculated as 3/14 3:18 (t = 60.5 h). From the measured data, it is difficult to specify the RPV failure timing, and it might be reasonable to say that the RPV failure occurred from approximately 3/13 23:00 (t = 56.2 h) to 3/14 3:00 (t = 60.2 h), in which the pressure data showed a minimum value and increased again.
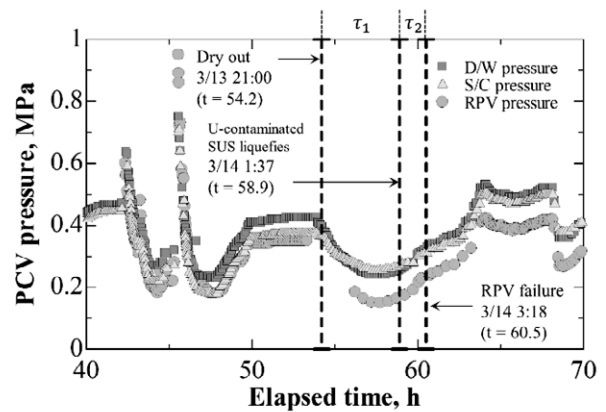


Fig. 3 Measured RPV pressure data of Unit 3 (green circles) with calculated timings of U-containing SUS liquefaction and RPV failure.
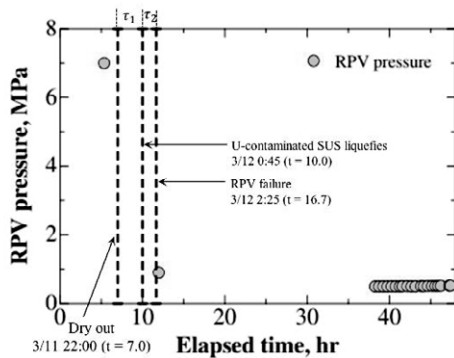


Fig. 1 Measured RPV pressure data of Unit 1 (green circles) with calculated timings of U-containing SUS liquefaction and RPV failure.
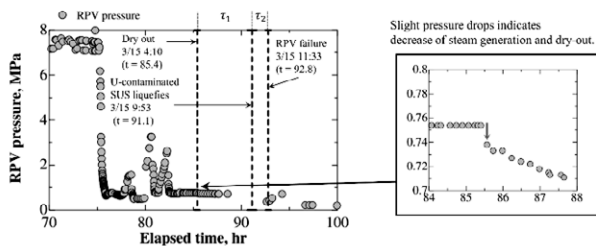


Fig. 2 Measured RPV pressure data of Unit 2 (green circles) with calculated timings of U-containing SUS liquefaction and RPV failure.

**Reference**
[1] Fujii H, Hara K, Hayashi K, et al. Investigation of the Unit-1 nuclear reactor of Fukushima Daiichi by cosmic muon radiography. Prog Theor Exp Phys. 2020;1–14.
[2] Yamashita T, Sato I, Honda T, et al. Comprehensive Analysis and Evaluation of Fukushima Daiichi Nuclear Power Station Unit 2. Nucl Technol. 2020;206:1517–1537.
[3] TEPCO. Locating Fuel Debris inside the Unit 3 Reactor Using a Muon Measurement Technology at Fukushima Daiichi Nuclear Power Station [Internet]. 2017 [cited 2021 Feb 6]. Available from: https://www.tepco.co.jp/en/nu/fukushima-np/handouts/2017/images/handouts_170928_01-e.pdf.
[4] OECD/NEA. Benchmark Study of the Accident at the Fukushima Daiichi Nuclear Power Plant (BSAF Project), Phase I Summary Report, NEA/CSNI/R. 2015.
[5] TEPCO : Progress Reports on the Investigation and Examination of Unconfirmed and Unresolved Issues [Internet]. [cited 2021 May 3]. Available from: https://www.tepco.co.jp/en/decommision/accident/unsolved-e.html.
[6] Li X, Sato I, Yamaji A, et al. Sensitivity analysis of core slumping and debris quenching behavior of Fukushima Daiichi Unit-3 accident. Ann Nucl Energy. 2021;150:107819.
[7] IAE. Information Portal for the Fukushima Daiichi Accident Analysis and Decommissioning Activities [Internet]. [cited 2021 Jan 25]. Available from: https://fdada.info/.
[8] Pellegrini M, Suzuki H, Mizouchi H, et al. Early phase accident progression analysis of Fukushima Daiichi unit 3 by the SAMPSON code. Nucl Technol. 2014;186:241–254.
[9] Fernandez-Moguel L, Rydl A, Lind T. Updated analysis of Fukushima unit 3 with MELCOR 2.1. Part 1: Thermal-hydraulic analysis. Ann Nucl Energy. 2019;123:59–77.

# III. 4 Unique polarization switching system in $\kappa$-Al$_2$O$_3$-type ferroelectrics

Shintaro Yasui

## 1. INTRODUCTION

Perovskite type structured ferroelectric materials such as BaTiO$_3$ and Pb(Zr,Ti)O$_3$ and related compounds have been used for memory, sensor, and various applications since they are found around 70 years ago. Since Perovskite-type ferroelectrics are found, they have been used until now because of their superior ferroelectric and piezoelectric properties.

To evolve forward from this situation, we would like to suggest novel ferroelectric/ferrimagnetic ferroelectric which has $\kappa$-Al$_2$O$_3$-type crystal structure classified as polar $Pna2_1$ space group(fig. 1(a)). This structure consists of the corundum-type and spinel-type staking layers along c-axis. The corundum and spinel layers consist of only oxygen-octahedra, and mixture of oxygen-octahedra and oxygen-tetrahedra, respectively. The spontaneous polarization direction is c-axis. It is note that coordination recombination from octahedra to tetrahedra (6 to 4) and tetrahedra to octahedra (4 to 6) in spinel layer is occurred during polarization switching. At the same time, corundum layer moves right and left alternately along in-plane a-axis which is like shear motion. This polarization switching system is optimized by the first principal calculation. However, almost all of the materials with $\kappa$-Al$_2$O$_3$-type crystal structure are metastable phase, which is difficult to prepare conventional technique in chemical equilibrium. Here, we succeeded to prepare this structure's materials by physical vapor deposition technique. We would like to introduce the ferroelectricity of this material's family.[1-9]

## 2. RESULTS AND DISCUSSIONS

Theoretically determined activation energies and polarization switching mechanisms of x-AFO were obtained based on ab initio calculations performed on $\kappa$-Al$_2$O$_3$ and $\varepsilon$-Fe$_2$O$_3$. One possible mechanism of polarization switching of $\kappa$-Al$_2$O$_3$ type x-AFO is via an intermediate non-polar centrosymmetric state. Earlier, Stoeffler et al. calculated the activation energy and net polarization of isostructural GaFeO$_3$ by considering a Pnna space group as the intermediate state. However, the reported activation energy for the polarization switching was 0.5 eV, which is much larger than that seen in conventional ferroelectric compounds (e.g. BaTiO$_3$-0.02 eV, PbTiO$_3$-0.03 eV). Xu et al. suggested an alternative centrosymmetric space group, $Pbcn$, which gave a much lower activation energy for polarization in $\varepsilon$-Fe$_2$O$_3$. Hence, we considered the $Pbcn$ space group as the non-polar polarized structure for our calculations. Fig. 1(a–e) show the schematic of transition from a negatively polarized structure to a centrosymmetric structure, and then to a positively polarized structure. The calculation yielded

activation energies for polarization switching of 0.088 and 0.155 eV/f.u. for $\varepsilon$-Fe$_2$O$_3$ and $\kappa$-Al$_2$O$_3$, respectively. We can expect the activation energies for the intermediate x-AFO structures also to be of a similar order. These values are fairly small and acceptable, compared to the high value previously reported for GaFeO$_3$. During the polarization reversal process, the polarization switches from $-Ps$ to $+Ps$, while smoothly passing through zero (Fig. 1(e and h)). Viewing the structure along the b-axis clearly explains the polarization switching mechanism (Fig. 1(f–j)). Close-packed oxygen layers in corundum layers keep their octahedral shape during the switching. However, oxygen above and below the corundum layers shifts along the a-axis, in opposite directions relative to each other. This shearing motion of oxygen layers induces a coordination switching of cation Fe1 and Al1 sites. An originally tetrahedral(octahedral) Al1(Al2) site turns into an octahedral(tetrahedral) Al2(Al1) site after the polarization switching. This mechanism is quite different from conventional ferroelectric oxides, where cations and anions move in opposite directions in a linear manner (Slater mode). By using Berry's phase approach, the polarization of Al$_2$O$_3$ and $\varepsilon$-Fe$_2$O$_3$ was calculated to be about 26 $\mu$C/cm$^2$ and 21 $\mu$C/cm$^2$, respectively. Since there is no structure change in the substituted x-AFO series, their theoretical polarization values will also lie in between 21 and 26 $\mu$C/cm$^2$. While this value of polarization is comparable to theoretical values reported for other isostructural compounds like GaFeO$_3$ and $\varepsilon$-Fe$_2$O$_3$, it is about two orders of magnitude larger than that observed experimentally. Similar ambiguity is observed in GaFeO$_3$ based films as well, and the exact reason for this is not yet known. We speculate that the multi-domain structure of the thin film obstructs complete polarization reversal, as there is in-plane shearing of oxygen layers involved. Hence, the actual polarization is considerably less than that predicted.
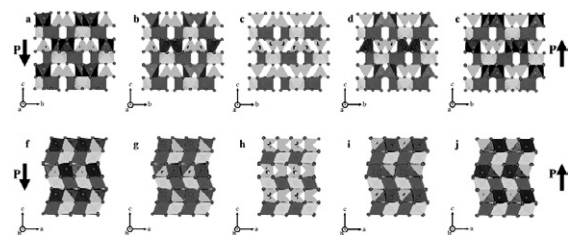


Fig. 1 Illustration of structural changes upon polarization reversal. (a–e) Structure viewed along the a-axis, and (f–j) structure viewed along the b-axis. The 3 octahedral sites are indicated in purple (Fe1), brown (Fe2) and blue (Al1), and the tetrahedral site is indicated in green (Al1). The intermediate pentahedral site is indicated in red.

[1] Y. Hamasaki *et al*., Appl. Phys. Lett., 104, 082906 (2014).
[2] Y. Hamasaki *et al*., Cry. Growth. Des., 16, 5214 (2016).
[3] Y. Hamasaki *et al*., Appl. Phys. Lett., 109, 162901 (2016).
[4] Y. Hamasaki *et al*., J. Appl. Phys., 122, 015301 (2017).
[5] T. Katayama *et al*., Appl. Phys. Lett., 110, 212905 (2017).
[6] T. Katayama *et al.*, Adv. Funct. Mater., 28, 1704789 (2018).
[7] S. Yasui *et al*, J. Ceram. Soc. Jpn., 127, 474 (2019).
[8] B. Rao *et al.*, J. Mater. Chem. C, 8, 706-714 (2020).
[9] B. Rao *et al*., ACS Appl. Electro. Mater., 2, 1065-1073 (2020).

# III. 5   Cross-disciplinary research on nuclear power systems to reduce the environmental impact of waste disposal

Hidekazu Asano, Chi Young Han, Masahiko Nakase, Hiroshi Sagara, Kenji Takeshita

## 1. Introduction

Radioactive waste management is indispensable in the use of nuclear energy. The amount and properties of waste to be disposed of depend on the power generation and subsequent fuel cycle conditions. At the same time, it affects repository size and long-term radiation safety after the repository closure. Research on radionuclide partitioning and transmutation technology is underway to reduce the volume and toxicity of radioactive waste. In order to take realistic and effective measures to reduce the burden of waste disposal, it is necessary to conduct process evaluations from a cross-sectoral perspective, from power generation to waste disposal, and indicators to evaluate their effects [1].

The authors are overlooking the entire nuclear power system, and on the premise of introducing a simplified MA separation process of 70-90% MA (Am) separation, a four-year nuclear power system research project has been started from FY2019 on the environmental impact of waste disposal, evaluation of the entire fuel cycle, engineering feasibility of separation technology, and advancement of the fast reactor combustion model with consideration for separated nuclides. The concept of this research and the results up to the second year have been introduced in previous reports [2,3]. This paper introduces the progress made in the third year and the tasks for the final year's research.

## 2. Research progress

### 2.1 Study on the environmental impact of radioactive waste disposal

*(1) Evaluation of environmental impact and introduction of environmental index for geological disposal.*

Table 1 shows the classification of environmental impact assessment indicators for waste disposal in this study. An inventory of vitrified waste derived from $UO_2$ and MOX fuels was obtained, and the waste occupied area in the repository based on the heat generation capacity, exposure dose based on nuclide migration from the repository, and exposure dose due to a human intrusion scenario (boring core observation) were calculated. Based on these results, combinations of nuclear fuel cycle conditions assuming to introduce simplified MA separation of 70% and 90%, which leads to the reduction of the environmental burden were proposed.

It was also shown that the three indicators of the amount of waste(repository area), dynamic and static radiation effects are relative and quantitative comparisons of the degree of load reduction in waste disposal, from the viewpoint of cross-sectoral perspective under various combinations of nuclear fuel cycle conditions[4,5] .Table 2

shows an example of the environmental impact assessment results for vitrified waste derived from $UO_2$ fuel.

Table 1 Classification of environmental load assessment indices

| Evaluation items | | Phenomenon | Evaluation method | | Unit |
|---|---|---|---|---|---|
| Environmental Load | Amount of waste | Heat generation | Waste-occupied area at the repository | | m²/waste package |
| | Radiation effect | Nuclide migration | Dynamic | Exposure dose | Sv/y |
| | | Presence of Nuclides | Static | Potential Radiotoxicity | Sv or Sv/y |
| Contribution | Power generation | Power generation corresponding to the generation of vitrified waste | | | TWh |
| Environmental impact | | Environmental load/Contribution | | | |

Table 2 Environmental impact assessment for disposal of $UO_2$ derived vitrified waste

| Condition | NFC Condition | | | | | Environmental Load/Criteria | | |
|---|---|---|---|---|---|---|---|---|
| | | | | | | | Disposal System | |
| | | | | | | Amount of waste | Radiation effect | |
| | Fuel B.U. (GWd/tHM) | SF cooling period (y) | MA separation ratio (wt%) | Vitrification/Vitrified waste | | Waste occupied area/repository (m2/TWh) | Radiation dose | |
| | | | | Waste loading (wt%) | Generated Amount (No./TWh) | | Nuclide migration ($\mu$Sv/y/TWh) $\times 10^7$ | Human intrusion (mSv/y) (aft. 300y) |
| 1 | 45 | 15 | 0 | 20.8 | 3.43 | 152 | 4.1 | 29 |
| 2 | | | 70 | 25.0 | 2.41 | 107 | 4.1 | 13 |
| 3 | | | 90 | 25.0 | 2.39 | 106 | 4.1 | 5 |
| 4 | | | 99.5 | 25.0 | 2.39 | 106 | 4.1 | 1 |
| 5 | | | 99.9 | 25.0 | 2.39 | 106 | 4.1 | 1 |

*(2) Evaluation of fuel cycle quantities for waste disposal load by using the Nuclear Fuel Cycle Simulation System (NFCSS) open simulation code.*

A new Excel program has been developed that enables the evaluation of nuclear fuel cycle parameters under various treatment and disposal conditions, such as spent fuel reprocessing, nuclide separation, and geological disposal, as well as the decay heat and radiotoxicity of high-level radioactive waste, This was implemented as an functional expansion of various quantity evaluation in the back-end area of the nuclear fuel cycle to the Nuclear Fuel Cycle Simulation System (NFCSS) code published by the International Atomic Energy Agency (IAEA) [6]. As a result, it was confirmed that the ORIGEN2.2-UPJ code calculation and the benchmark match with an error of less than 0.5% (RMSE: Root Mean Square Error). In addition, based on the evaluation results obtained, methods for improving the function of the calculation code were investigated in order to evaluate the fuel cycle parameters and the load of radioactive waste on the premise of introducing a new reactor.

*2.2 Engineering design study of simplified MA separation technology.*

*(1) Validation of americium (Am) separation mechanism*

Published literatures and reports were investigated and evaluated for MA extraction equilibrium and extraction rate data necessary for MA separation process evaluation. Verification of the flow sheet of the mixer-settler single-stage extraction process, scale of the MA separation process, and required engineering requirements were examined. Based on these results, engineering considerations such as that the separation factor may fluctuate due to the influence of extraction speed in the case of simplified MA separation were identified.

*(2) Presentation of a feasible Am separation process.*

A process simulation was performed using the PARC-MA code for the MA/RE mutual separation process of the "SELECT process"[7], which is the MA separation process developed by the Japan Atomic Energy Agency. At 99.9% Am recovery, 40 mixer-settler stages are required for both extraction and washing stages, but under the condition of 70% Am recovery for simplified MA separation, it is expected that MA purity of 50% can be obtained with 6 extraction stages. As a result, the feasibility of constructing a realistic and rational MA separation process was shown by comparing the supply conditions of MA products and the Am recovery rate to the transmutation system.

*(3) Development of an advanced fast reactor (FR) burn-up calculation model.*

As a comprehensive fast reactor core burn-up calculation under various preconditions, the effects of changes in the TRU composition of new fuels on the core characteristics and waste properties, and the effects of accompaniment of rare earth elements on the core characteristics in transitional period were evaluated. In addition, the improvement of the core burn-up model (alternative model) for the fast reactor, which can derive the same result by the usual core burn-up calculation by inputting the nuclear fuel composition and operating conditions. And development and verification of the fast reactor core burn-up calculation tool was continued.

## 3. Future plan

In this study, the overall nuclear fuel cycle in nuclear power utilization is viewed, and the selection of the combination of various conditions that are effective in reducing the volume and toxicity of radioactive waste is examined on the premise of the introduction of simplified MA separation. To this end, it is necessary to establish cross-sectoral evaluation methods and to select technology options that reduce the environmental impact of waste disposal. In the final year of the research (FY2022), after clearly defining the simplified MA separation technology, we plan to summarize the research from the two perspectives of methodology and feasibility of the technology.

## References

1. S. Ssato, et al., Technical options of radioactive waste management for the second half of the 21st Century, in consideration of Pu utilization and less environmentally impacted geological disposal, 3O11-16, Proc. 2018 Spring Meeting, Atomic Energy Society of Japan, Tokyo, Japan (2011) [in Japanese].

2. H. Asano, et al., Cross-disciplinary nuclear system research for load reduction of radioactive waste management, Vol.5 , Bull. Lab. Adv. Nucl. Energy, 2020, Institute of Innovative Research, Tokyo Institute of Technology, ISSN 2432-8375

3. H. Asano,et. al., Study on Advanced nuclear energy system based on the environmental impact of radioactive waste disposal, Vol.6 , Bull. Lab. Adv. Nucl. Energy, 2021, Institute of Innovative Research, Tokyo Institute of Technology, ISSN 2432-8375

4. H. Asano, et.al., Study on advanced nuclear energy system based on the environmental impact of radioactive waste disposal - An integrated cross- disciplinary approach to diversifying nuclear fuel cycle conditions –, Proc International Conference on Radioactive Waste Management: Solution for a Sustainable Future, IAEA-CN294, IAEA Headquarters, Vienna, Austria, 1-5 Nov., 2021

5. R. Hamada, Environmental impact of radioactive waste disposal in advanced nuclear energy systems - Radiation impact evaluation of nuclide migration and human intrusion for geological disposal considering nuclear fuel cycle conditions –, Proc International Conference on Radioactive Waste Management: Solution for a Sustainable Future, IAEA-CN294, IAEA Headquarters, Vienna, Austria, 1-5 Nov., 2021

6. Nuclear Fuel Cycle Simulation System: Improvements and Applications, IAEA-TECDOC-1864,IAEA,2019

7. Y. BAN, et al., Minor actinides separation by N,N,N',N',N'',N''-Hexaoctyl Nitrilotriacetamide (HONTA) using mixer-settler extractors in a hot cell, Solvent Extraction and Ion Exchange, 37 7, 489 – 499,2019

# III. 6　　　　　Study on assessment of inherent safety of a molten salt fast reactor

## Hiroyasu Mochizuki

## 1. Introduction

Although the degree of safety may vary slightly depending on the design of Molten Salt Reactors (MSRs), one of objectives of the research is to summarize the inherent safety characteristics of a Molten Chloride Salt Fast Reactor (MCSFR) illustrated in **Fig. 1**. In an MCSFR, liquid fuel flows out from the core and circulates inside the equipment installed in the reactor vessel. The liquid fuel expands in volume as its temperature increases, resulting in a lower fuel density and lower reactivity. Therefore, neutronics and thermal-hydraulics coupling model should be used to analyze the reactor behavior. The analysis code used must be validated in advance because the calculation method differs from the method used to investigate the behavior of conventional nuclear reactors. The author proposed a neutronics and thermal-hydraulics coupling method [1] using the FLUENT code and the RELAP5-3D code. In this method, the FLUENT code with a user defined function (UDF) incorporated the point-kinetics model is applied to the core simulation and the RELAP5-3D code is applied to the outside of the core to analyze the transient behavior. However, since FLUENT requires boundary conditions at the core inlet, a neutronics and thermal-hydraulics coupling analysis with RELAP5-3D is required once. The method using FLUENT is characterized by the fact that it is not necessary to solve the simultaneous differential equations relating the point kinetics because the discretization is devised after making a prompt jump approximation, and the solution can be obtained explicitly. As a result, this method enables a transient calculation with a large time step of approximately 0.01 s for the neutronics and the thermal-hydraulics.   This method was validated with data measured at the Molten Salt Reactor Experiment (MSRE) operated by Oakridge National Laboratory (ORNL).
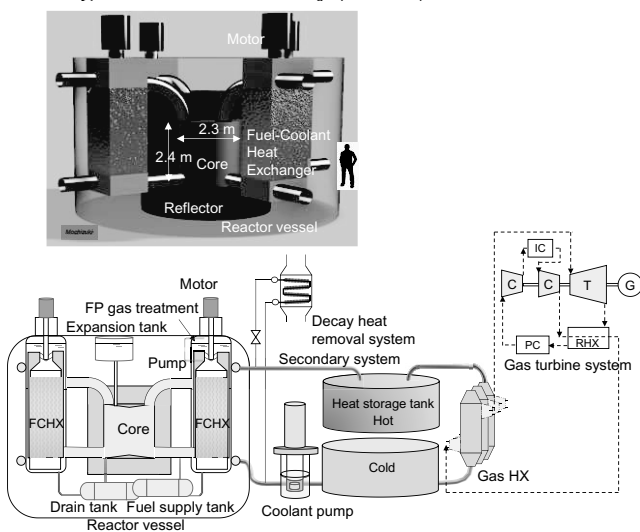


Fig. 1　Outline of the system and core region of MCSFR.

## 2. Validation of the neutronics model incorporated in FLUENT [2]

The delayed neutron point-kinetics equations have the same form as the fixed fuel case. However, the decay constants of delayed neutron precursors change as fuel flows out and back out of the core. The changes in the core transit time and the exterior loop transit time are calculated using the flow rate in the combined UDF which incorporates the neutronics parameters. The kinetic parameter change due to the flow rate change is updated in every time step based on the theory mentioned above. Tests of starting and tripping the fuel pump under zero-power conditions were conducted at the MSRE, and negative and positive reactivity were applied, respectively. Reactivities in these cases were compensated for by control rods to keep the criticality. Since the movement of the control rods was controlled by the controller, the assumed proportional-integral-derivative (PID) control logic is also incorporated into the UDF for analyses. The calculated result is illustrated in **Fig. 2.** These transients have been analyzed by many researchers up to now, and it can be seen that the neutron kinetic equations used in all studies are correctly incorporated into the codes. In the transient analysis when the pump is started, some results where the calculation trends do not match the behavior of the measurement result are due to the setting of the control circuit. The FLUENT code simulated the measurement results in good agreement. The neutronics model used in the present study is considered to have been validated by these calculations.
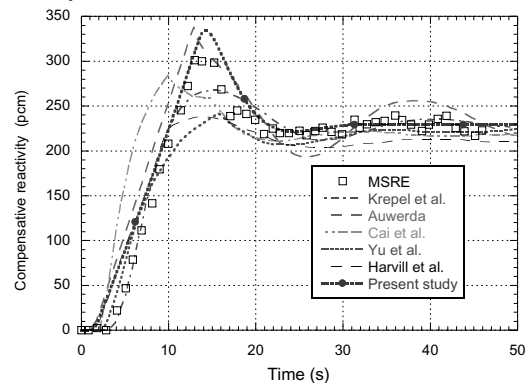


Fig. 2　Evolution of compensative reactivity by pump startup computed by FLUENT.

## 3. Validation of the neutronics and thermalhydraulics coupling model of RELAP5-3D [3]

In the case of the system code RELAP5-3D, the built-in equations are for static fuels. Therefore, it is necessary to analyze the experimental results of the molten salt reactor and confirm the performance of the code. If the analysis result is not good because the built-in equations are incomplete for MSR, it is necessary to reflect the reactor power analysis result of FLUENT to RELAP5-3D all the

time and dedicate it to the analysis of the external loop. Therefore, the neutronics and thermal-hydraulics coupling model of RELAP5-3D has been validated using MSRE data.
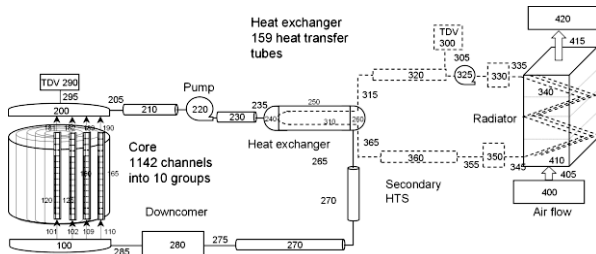


Fig. 3    Nodalization scheme of MSRE for the RELAP5-3D code.
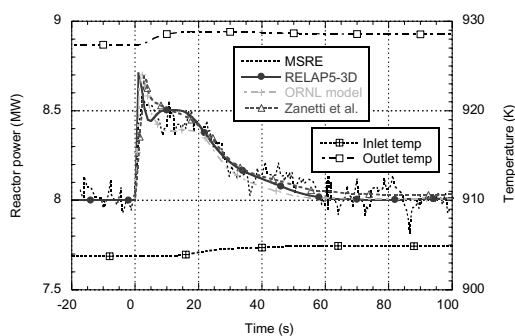


Fig. 4 Comparison between the measured reactor power evolution and the calculated result with RELAP5-3D when the 13 pcm step reactivity is applied to the MSRE operating at 8 MW reactor power.

Reactivity insertion tests were conducted at 1, 5, and 8 MW reactor power using MSRE. **Figure 3** illustrates the nodalization scheme of MSRE to validate the neutronics and thermal-hydraulics model implemented in the RELAP5-3D code. Since the event used for verification is related to the increase in reactor power due to the insertion of reactivity and the transport of the increased temperature, it is necessary to model the entire system. The kinetic parameters of MSRE are used in ORNL reports. The effect of mooving precursors is considered through the input data at the initial. **Figure 4** compares the MSRE response and the RELAP 5-3D analysis results when a reactivity of 13 pcm is applied at 8 MW reactor power together with the calculation result by Zanneti et al. who used a Monte-Carlo code. As illustrated in this figure, the calculated power transient is almost the same as the test result and the calculated result by Zanneti et al. The complex peaks of reactor power are caused by the applied reactivity and the negative reactivity feedback. Negative reactivity is caused by an increase in the core temperature and an increase in temperature that arrives at the core again via the heat exchanger. The calculation model of RELAP5-3D in terms of neutronics and thermal-hydraulics coupling is considered validated through the calculations mentioned above. It is also shown that the point-kinetics model works appropriately to simulate the MSRE transient.

**4. Design of heat exchanger**

The author created a CFD model of the experimental setup that measured heat transfer coefficients and pressure loss coefficients of a zigzag flow pass various flow conditions with super-critical carbon dioxide. After investigating the turbulence model of the FLUENT code, the measured data were simulated with high accuracy. In addition, the analysis model was also validated using the loss coefficient data of a straight smooth pipe.

From this experimental result, the zigzag flow path has good heat transfer, but results in large pressure loss. Therefore, the author proposed to make channels of the heat exchanger with a sinusoidal curve that can be manufactured by press working, instead of the expensive etching used in the previous experiment. The heat transfer coefficient of the sinusoidal channel is almost the same as that of the zigzag, and the pressure loss coefficient can be halved.

Based on the results of the FLUENT analysis, the actual heat exchanger system was evaluated and the heat transfer coefficient obtained from the analysis was applied to the RELAP5-3D system code to evaluate the actual heat exchanger system.

In a normal plate-type heat exchanger, each plate is sandwiched using a packing to prevent leakage. Since the proposed heat exchanger handles liquid nuclear fuel, it is necessary to be welded by diffusion welding after pressing a steel plate with a thickness of 0.5 mm to form 100 channels, stack the required number of sheets to form a single component. 6,000 pairs of heat transfer channels are formed by stacking 120 sheets with 0.5 mm flat plates in between. As a result, the heat exchanger can remove 125 MW of heat when the heat transfer length is approximately 4 m.

**5. Conclusion**

Validation of CFD code and system code used for safety analysis has completed. Also, the design of the heat exchanger that transfers the heat generated in the reactor to the secondary cooling system has been completed. These studies set the stage for evaluating the safety of molten salt fast reactors.

**References**
1. Hiroyasu Mochizuki: Neutronics and thermal-hydraulics coupling analysis using the FLUENT code and RELAP5-3D code for a molten salt fast reactor; *Nuclear Engineering and Design*, **368** (2020), 110793.
2. Hiroyasu Mochizuki: Verification of neutronics and thermal-hydraulics coupling method for FLUENT code using the MSRE pump startup, trip data; *Nuclear Engineering and Design,* **378** (2021), 111191.
3. Hiroyasu Mochizuki: Validation of neutronics and thermal-hydraulics coupling model of the RELAP5-3D code using the MSRE reactivity insertion tests; *Nuclear Engineering and Design*, **389**, (2022), 111669.
4. Hiroyasu Mochizuki, Study of thermal-hydraulics of a sinusoidal layered heat exchanger for MSR, *Nuclear Engineering and Design,* **396**, (2022), 111900.

# III. 7        Measurement of Electron Temperature and Density by Emission Spectroscopy of Ar-N₂ Atmospheric-Pressure Non-Equilibrium Plasma

Hiroshi Akatsuka, Atsushi Nezu

## 1. Introduction

Atmospheric non-equilibrium plasmas are currently expected to have a wide range of applications. Examples include surface treatment of materials, promotion of vegetable growth, and blood coagulation against trauma. On the other hand, there are only a limited number of reports on the measurement of "electron temperature $T_e$" and "electron density $N_e$", which are the most necessary data for radical density simulations and indispensable for controlling radical density with high precision. In particular, in view of the above industrial applications, it is desired to measure the atmospheric-pressure non-equilibrium plasmas mixed with reactive gases. Therefore, in this study, the electron temperature and electron density of Ar/N₂ mixed atmospheric non-equilibrium plasma are conducted by the spectral analysis of the continuum radiation of emission due to electron-atom bremsstrahlung with optical emission spectroscopy (OES) measurement.

## 2. Experimental device

In the present experiment, the discharge device shown in Fig. 1 (manufactured by Ecodesign Co., Ltd.) was applied [1]. The device consists of electrodes, inner glass tubes that cover each of them, an outer glass tube that serves as the gas flow path, a high-voltage power supply that uses a switching element and a neon transformer, an optical fiber introduction tube, and a support plate. A pulse voltage with a maximum secondary voltage value of 9 kVp-p is applied between the two electrodes at a frequency of 20 kHz. The inside of the glass tubes covering both electrodes are filled with deionized water for cooling, between which a gap of 1 mm is provided to create the atmospheric-pressure non-equilibrium plasma as a streamer-like dielectric barrier discharge.

## 3. Analytical method
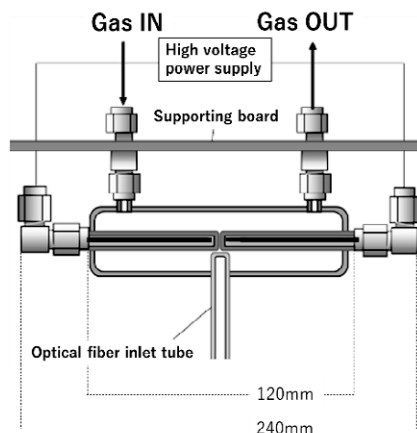


Fig. 1 Schematic diagram of discharge device.
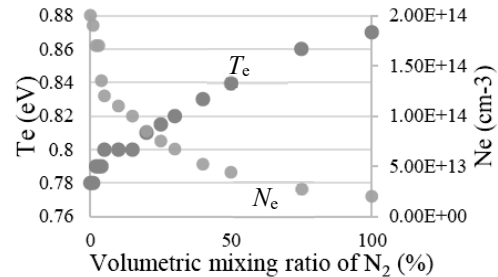


Fig. 2 Results of OES measurement.

This time, the technique used for the measurement of electron temperature and electron density is the continuum spectrum analysis [2]. This is a method to find the electron temperature and density by fitting the obtained spectrum with theoretical equations assuming that electron-atom bremsstrahlung is dominant in the plasma. In this method, the electron energy distribution function (EEDF) is essential, and the Druyvesteynian EEDF is selected based on the conclusion of previous research [1].

## 4. Results and Discussion

The results are shown in Fig.2, which indicates that the electron temperature ranges from 0.78 to 0.87 eV, while the electron density ranges from $2.0 \times 10^{13}$ to $2.0 \times 10^{14}$ cm$^{-3}$. In addition, it can be confirmed that the electron temperature increases almost monotonically and the electron density monotonously decreases as the N₂ mixture ratio increases. It is considered that the reason for this behavior is attributed to be the energy gap between the metastable state and the ionized state of Ar and N₂, respectively, and the difference in the excitation lifetime of the metastable states [3].

It was also examined how the discharge current characteristics change by adjusting the frequency of the applied voltage. As the frequency of the supply voltage was increased, the frequency of the current pulses generated by the atmospheric-pressure discharge also increased. It was also found that when the frequency exceeded around 55 kHz, the discharge suddenly became more intense and the current pulses became seven times larger, which is found to be attributed to the ion lifetime [4].

**References**
[1] H. Onishi, F. Yamazaki, Y. Hakozaki, M. Takemura, A. Nezu and H. Akatsuka, Jpn. J. Appl. Phys., **60**, 026002 (2021).
[2] T. van der Gaag, H. Onishi and H. Akatsuka, Phys. Plasmas, **28**, 033511 (2021).
[3] R. Ishizuka, A. Nezu, and H. Akatsuka, Extended Abstracts of the 82nd JSAP Autumn Meeting 2021, 10a-S301-3, the Japan Society of Applied Physics, 07-003 (2021).
[4] M. Takemura, A. Nezu, and H. Akatsuka, Proc. 2022 Annual Meeting IEE Jpn. 1-047, p. 64, (2022)

# III. 8    Low-Pressure Non-Equilibrium Plasma Measurement by Optical Emission Spectroscopy and Line Spectrum Analysis

Hiroshi Akatsuka, Atsushi Nezu

## 1. Introduction

In any kind of experimental plasma research, its measurement becomes necessary. Particularly, the plasmas require measurement when they are applied in industries for the process efficiency. Historically, low-pressure gas discharge plasmas have been widely applied in electronical engineering, such as dry etching processes, deposition of thin films, or surface modification. To understand plasma parameters like electron temperature $T_e$ and density $N_e$, non-intrusive measurement methods are desired, one of which is the optical emission spectroscopy (OES) measurement.

## 2. Line Spectrum Analysis for Low-pressure Plasmas

For this purpose, however, the interpretation of the observed spectra is not so simple, because the low-pressure discharge plasmas are generally in the state of non-equilibrium. The excited-state population must be analyzed based on excitation kinetic networks described with the elementary processes involved, where the collisional-radiative (CR) model works very well.

There are several methods to determine $T_e$ and $N_e$. The method of "extraction of dominant elementary processes" should be examined, where the population balance of the essential excited states is described with rate equations. When the appropriate model is constructed for population balance, the rate equations contain the number densities of the excited states, which can be examined with the OES measurement. After their substitution, the equations can be solved to obtain $T_e$ and $N_e$ [1].

Another method is now proposed, where the CR model is more directly applied. This is to minimize the summation of the square-root deviation between the excited-state densities observed by the OES and those calculated with the CR model. However, to do this, the essential excited states must be found for the comparison between the experiments and the CR-model calculations. That is, the levels, whose number density changes most sensitively with the variation of $T_e$ and $N_e$ within the conditions considered, must be selected within a practical number to be observed. Here, the proposed method applies a trust region method as a data driven science [2].

## 3. Methodology, Results and Discussion

The optical emission lines used for diagnosis were selected based on the developed algorithm, which is as follows. First, the dependence of $N_i/g_i$ on ($T_e$, $x$, $N_e$) was examined for the range "I" expected for the plasma to be observed, where $N_i$ and $g_i$ are the number density and the statistical weight of the $i$-th excited level, and $x$ is a parameter to determine the electron energy distribution function in the exponential factor [2]. The algorithm
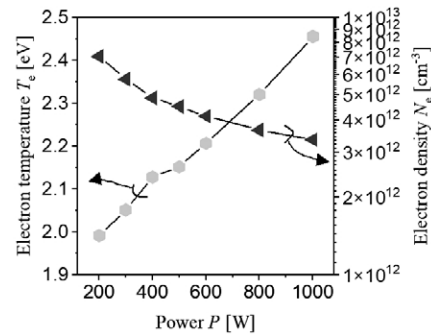


Fig. 1 The dependence of $T_e$ and $N_e$ on microwave discharge power [3].

generated the objective function for the fitting as follows:

$$f_1(T_e, x, N_e) = \sum_{i \in I} \left[ \frac{N_{i\_calc}(T_e, x, N_e)/g_i}{N_{i\_obs}/g_i} - 1 \right]^2, \quad (1)$$

where $N_{i\_calc}(T_e, x, N_e)/g_i$ is the reduced number density calculated with the CR model, and $N_{i\_obs}/g_i$ is that obtained with the OES measurement. In this study, it is found that the combination of $i$ = 4p[1/2]$_1$, 4p'[3/2]$_1$, 4p[1/2]$_0$, and 4p'[1/2]$_0$ was estimated to be the best levels for diagnosis for the condition of ICP argon plasma with its discharge pressure of 1 Pa.

The diagnostic results of $T_e$ and $N_e$ by the proposed method is shown in Fig. 1 [3]. It is considered that the dependence of $T_e$ on the discharge power is well traced, which monotonically increases with increasing power. Meanwhile, $T_e$ was found to decrease monotonically with increasing power. One of the possible reasons is the RF discharge mode has changed closer to CCP than to ICP [3].

Application of this methodology should be expanded for other discharge parameter range, and moderate-pressure microwave discharge [4] and atmospheric-pressure non-equilibrium plasma [5] are also now being confirmed for the feasibility [6].

## References

1. H. Akatsuka. ADV. PHYS. X, **4**, 1592707 (2019).
2. Y. Yamashita, T. Akiba, T. Iwanaga, H. Yamaoka, S. Date, and H. Akatsuka, Jpn. J. Appl. Phys. **60**, 046003 (2021).
3. Y. Yamashita, T. Akiba, T. Iwanaga, S. Date, H. Yamaoka, and H. Akatsuka, IEEE Trans. Plasma Sci. **50**, 1875 – 1889 (2022).
4. Y. Yamashita, T. Akiba, T. Iwanaga, S. Date, H. Yamaoka, and H. Akatsuka, Proc. 42 Int. Symp. Dry Process (DPS), pp. 57-58 (2021).
5. Y. Yamashita, T. Akiba, T. Iwanaga, H. Yamaoka, S. Date, and H. Akatsuka, Extended Abstracts of the 68th JSAP Spring Meeting 2021, 18p-Z17-1, 07-043 (2021).
6. H. Akatsuka, Proc. 12th Asia-Pacific International Symposium on the Basics and Applications of Plasma Technology (APSPT-12), Plenary Lecture 2, pp. 16-17 (2021).

# III. 9        Progress of Neutron Nuclear Data Measurements

Tatsuya Katabuchi, Yu Kodama, Hideto Nakano, Yaoki Saito

## 1. Neutron capture cross section measurements using a neutron beam filter system at J-PARC

A neutron filtering system was implemented at the ANNRI beamline to bypass the double pulse structure of the neutron beam [1]. Silicon and iron were chosen as filter materials. Both Si and Fe filters provide sharp well-defined energy neutron peaks. Three neutron filter assemblies consisting of 20 cm of Fe, 20 cm of Si and 30 cm of Si were tested in ANNRI by means of capture experiments and transmission experiments. The incident neutron spectra through the filtering system were measure by TOF method. In addition, the experimental results were accurately reproduced by Monte Carlo simulations with the PHITS code. Finally, the $^{197}$Au neutron capture cross-section was measured using the filtering system. The experimental results of the cross section agree with the evaluated data from JENDL-4.0 within uncertainties.

The recent development of intense pulsed neutron facilities employing spallation neutron sources has allowed for the measurement of neutron-induced reactions, namely neutron capture, using small amounts of sample. The ANNRI beamline in MLF experimental facility of J-PARC provides one of the most intense neutron beams currently available and was thoroughly designed in order to measure neutron-induced reactions with high accuracy. However, the J-PARC accelerator is operated in a double-bunch mode in which two proton bunches are injected into the spallation target with a time difference of 600 ns. Events detected with a specific TOF have two different energies as they could have been originated from each of the two different proton pulses. In order to bypass the doublet structure of the neutron beam, a neutron filtering system was designed, built and tested in the present work.

Fe and Si filters were designed. The filters consisted of stacked cylinders. Each cylinder has a diameter of 10 cm and a thickness of 5 cm. The filters were introduced upstream of Experimental Area 1 of ANNRI. For Fe, the total thickness was 20 cm. In the case of the Si filter, the two configurations, 20 and 30 cm in thickness, were tested.

Measurements with the NaI(Tl) spectrometer of the ANNRI beamline were employed to obtain the time distribution of the filtered neutron beam. The energy dependence of the incident neutron beam was determined by measuring the 478-keV γ-rays from the $^{10}$B(n, αγ)$^7$Li reaction using a boron sample with calculations with the PHITS simulation code. Transmission measurements were also carried out to assess the performance of the filtered assemblies. Li-glass scintillation detectors were employed in the measurements.

The neutron capture cross sections of $^{237}$Np, $^{243}$Am and $^{241}$Am were measured using the neutron beam filter system of ANNRI at J-PARC [2,3]. The pulse-height weighting technique was employed to derive the neutron capture yield. Measurements of gold samples were also made as standard measurements. The absolute values of the capture cross sections were determined from the JENDL-4.0 evaluated cross section of $^{197}$Au(n,γ)$^{198}$Au..

## 2. Development of a neutron beam monitor with a thin plastic scintillator for nuclear data measurement using spallation neutron source

Spallation neutron sources have extended nuclear data measurement into new frontiers. An intense neutron beam from a spallation neutron source enables nuclear data measurement of radioactive samples and small cross-section reactions. However, traditional neutron detectors are not suitable to measuring an intense neutron beam from a spallation neutron source due to its high counting rate. In the present work, a new neutron detector to monitor a neutron beam from a spallation neutron source was developed [4].

Figure 1 shows a schematic diagram of the present neutron detector. The detector consists of an aluminum foil with a thin 6Li layer, a thin plastic scintillator and a photomultiplier tube. Triton and alpha particles emitted from the $^6$Li(n,t)$^4$He reaction are detected with the plastic scintillator. The thin $^6$Li layer gives an enough small detection efficiency, allowing the detector to be used to measure a high-intensity neutron beam without paralysis.
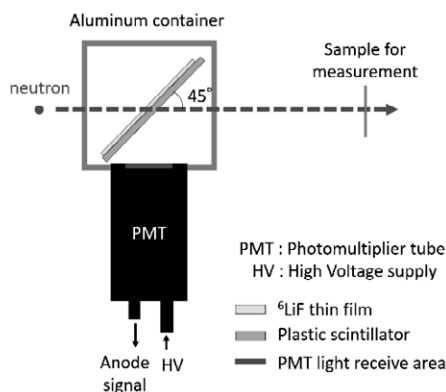


Fig. 1 Schematic diagram of the neutron detector.

The neutron detector system was tested with a neutron beam from the spallation neutron source of J-PARC. Experiments were carried out at the ANNRI beamline of MLF. The detector system was placed at a neutron flight length of 28.6 m from the neutron source. Neutron energy was measured with the TOF method

Measurements were made for both $^6$LiF and $^{nat}$LiF

deposited Al foils. The counting rate with the enriched 6LiF foil is much higher than that with the $^{nat}$LiF foil because of the 6Li abundance difference. The neutron TOF spectrum was successfully measured from 3.5 meV to 275 keV without significant count loss or detector paralysis. The statistical uncertainty reached 0.7% at neutron energies around 6 meV. To verify the applicability of the present detector system, the energy dependence of the neutron spectrum was compared with a previous measurement. The neutron energy spectrum was in good agreement with a different method. Thus, it is concluded that this detector system can be used to monitor an intense neutron beam for nuclear data measurement.

**Reference**
1. G. Rovira et al., Nuclear Instruments and Methods in Physics Research Section A, Vol. 1003, p. 165318 (2021).
2. Y. Kodama et al., Journal of Nuclear Science and Technology, Vol. 58, No. 11, pp. 1159-1164 (2021).
3. G. Rovira et al., Journal of Nuclear Science and Technology, (to be published).
   4. H. Nakano et al., Journal of Nuclear Science and Technology, (2022).

# III. 10        Ultrasonic Velocity Profile Measurement in Sub-Cooled Boiling Bubbly Flow

## Hiroshige Kikura, Naruki Shoji, Hideharu Takahashi

### 1. Introduction

In Boiling Water Reactor (BWR), two-phase bubbly flow occurs in sub-cooled boiling region of the reactor core. The velocity distribution of the bubbly flow; bubble, and liquid phases is a mainly crucial parameter that affects heat transfer enhancement and the phase distribution, which strongly influences the safety aspect. Hence, investigation of this parameter on the experimental apparatus is necessary to be clarified accurately.

The Ultrasonic Velocity Profiling (UVP) method is proposed in this study. It is a non-invasive measurement, needless of transparency and bubble-overlapping problem is minimized. This technique can obtain the velocity profile of liquid by means of ultrasonic reflection. The Doppler frequency obtained from moving particle dispersed in the liquid (liquid tracer) along measurement path can be used to calculate the liquid velocity profile.

In the bubbly flow, Wongsaroj et al. proposed the single ultrasonic gas-liquid two-phase separation (SUTS). This method can measure the velocity distribution of gas bubbles and liquid in bubbly flow separately. In this paper, the SUTS is applied to the sub-cooled boiling flow condition.

### 2. Method

Wongsaroj et al. developed SUTS that separate the gas and liquid phase velocity distribution with UVP method in this study. The SUTS utilizes the Doppler signal amplitude difference between liquid phase (small particles) and gas phase. The signal amplitude depends on the acoustic impedance, and it is different about $10^6$ times between particle and gas. Therefore, the liquid phase and gas phase can be separated by setting the threshold to the Doppler signal amplitude. Namely, each velocity is separated like the following equation.

$$v_g(x) = \frac{cf_D}{2f_c} \ \text{if} \ a(x) > threshold$$
$$v_l(x) = \frac{cf_D}{2f_c} \ \text{if} \ a(x) \le threshold \tag{1}$$

where, $v_g$ and $v_l$ are gas and liquid velocity, $c$ is the sound velocity, $f_D$ is the Doppler frequency, $f_c$ is the ultrasonic frequency, and $a$ is the Doppler signal amplitude, respectively.

### 3. Experiment

To confirm the ability of SUTS on the bubbly flow in sub-cooled boiling conditions, in this experiment, the SUTS was applied to measure the velocity profile of the liquid flow in elevated temperature and bubbly flow in sub-cooled boiling condition, respectively. The experimental measurement was executed on the vertical pipe flow apparatus, as shown in Figure 1(a). The tap water worked as a liquid phase was dispersed with 80 μm nylon particles. The measurement test section was located on a vertical pipe made up of polycarbonate with an inner diameter (D) of 50 mm. The water was circulated from the bottom tank to the top tank by the pump. The water flow rate was measured by the orifice flow meter. A heating rod utilized to make the vapor bubble was inserted into the main pipe upstream of the test section (6D between the test section and heating rod end). Also, the water was preheated by the heating coil immersed in the bottom tank. The temperature controller controlled the heated temperature produced by the heater. Figure 2 shows the measurement result in the sub-cooled boiling flow. The blue circle indicates the liquid phase, and red circle means the bubble velocity distribution, respectively. Each phase was measured separately by using SUTS.



(b) Image

(a) Experimental setup

(c) Bubble diameter distribution
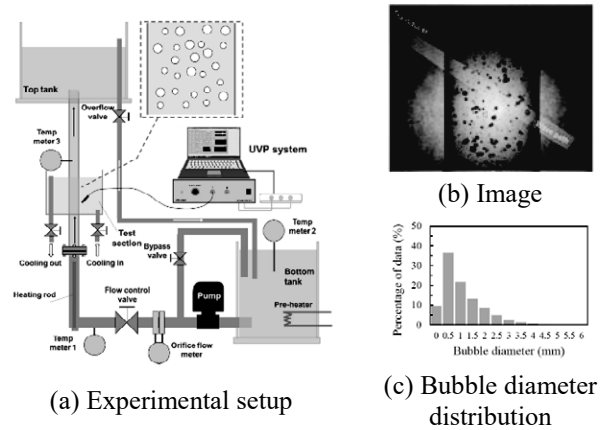
Fig. 1 Experimental setup and the flow conditions
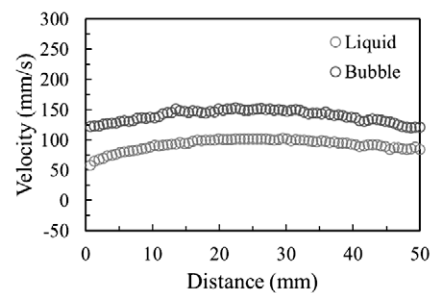


Fig. 2 Liquid and bubble velocity profiles with SUTS

### 4. Conclusion

The UVP with SUTS was applied to sub-cooled boiling flow. The measurement applicability was demonstrated experimentally in vertical pipe flow apparatus, and the validity of the method to sub-cooled boiling flow was suggested.

### Reference

[1] W. Wongsaroj et al.; 13th International Symposium on Ultrasonic Doppler Methods for Fluid Mechanics and Fluid Engineering (ISUD 2021), June 13-15, Online, (2021).

# III. 11     Development of Three-Dimensional Ultrasonic Velocity Profiler for Leakage Investigation

Hiroshige Kikura, Naruki Shoji, Hideharu Takahashi

## 1. Introduction

On March 11th, 2011, the severe accident of the Fukushima Dai-ichi nuclear power plant (1F NPP) was happened by the earth quack and the massive tsunami in Tohoku area, Japan. And then, fuel debris was generated in the primary containment vessels (PCVs) of units 1, 2, and 3, respectively. Recently, optical inspections have been conducted for the decommissioning of the 1F NPP. However, these inspections have not yet unveiled completely the leakage location of contaminated water due to the dark and high-radiation environment. To investigate the information of leakage, such as location and flowrate, we have proposed to detect the location by capturing the water flow generated by a leak and have developed a flow measurement system focusing on the ultrasonic velocity profiling method (UVP). Ultrasonic measurement is considered as a promising non-optical inspection method. Ultrasonic sound can be used in opaque liquids and ultrasonic transducers are generally suited to high radiation levels. On the other hand, the original UVP is a single velocity component measurement, and three-dimensional measurements are needed to capture the flow in the complex structure within the PCV. The purpose of this study is development of the 3-D flow vector measurement system. In this paper, the developed vector UVP system is introduced, and applied to a simulated leakage flow to confirm the validity of 1F investigation.

## 2. Measurement System

To realize the three-dimensional velocity vector profile measurement, the measurement instruments was developed. The overview of developed instruments is shown in figure 1. The measurement system consisted of four-transducer array, laboratory made ultrasonic pulser/receiver circuits, and signal processing personal computer. The pulser/receiver included the ultrasound drive circuits, echo signal amplifiers, filters, and A/D converters (50 MS/s). The signal processing was performed in the computer based on the UVP signal processing, with the programming software LabVIEW 2019 (National Instruments). We named the measurement system as 3-D vector UVP.
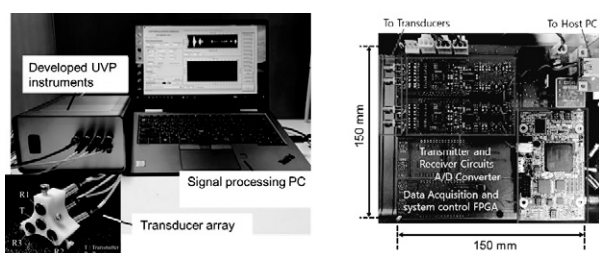
## 3. Experiment

To confirm the validity of the developed 3-D vector UVP system in detecting the leakage point, the flow velocity vector distribution measurement was conducted for the simulated leakage flow. The experimental apparatus of this experiment is shown in figure 2(a). Water was stored in a water tank and circulated at a constant flow rate by a magnet pump through a simulated leakage hole (19 mm diameter) on the bottom of the tank to simulate water leakage. The developed 3-D vector UVP system can measure three velocity components on the ultrasonic propagation axis, and by moving the measurement line, a wide range of spatial velocity vector distribution can be obtained. In this experiment, the transducer array was mounted on the rotation system of a waterproof servo motor, and the measurement line scanning in the YZ plane was performed. In addition, the servo motor and transducer array were mounted on a 1-axis stage and scanning in the X-axis direction was also performed. The result of 3-D flow mapping is shown in figure 2(b). The measured vectors were directed to the simulated leakage hole, and the flow velocities were increased around the hole. Therefore, it was suggested the developed system is effectiveness for the leakage detection.
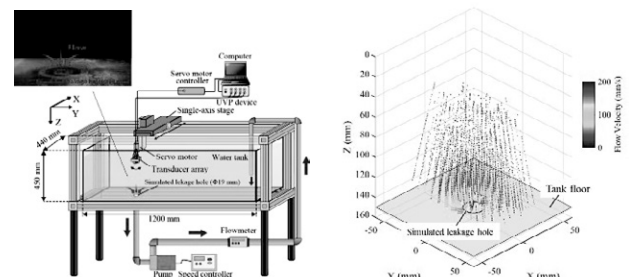


(a) Experimental apparatus     (b) 3-D flow mapping
Fig. 2 Experimental apparatus of simulated leakage flow measurement and result of 3-D flow mapping.

## 4. Conclusion

The 3-D vector UVP system was developed for the leakage detection in PCVs, and the validity was confirmed with the simulated leakage flow measurement. In future, the scale upping of the system will be considered.

## Reference

[1]  N. Shoji, et al.; 13th International Symposium on Ultrasonic Doppler Methods for Fluid Mechanics and Fluid Engineering (ISUD 2021), June 13-15, Online, (2021).

[2]  N. Shoji, et al.; 11th International Conference on Advances in Fluid Dynamics with emphasis on Multiphase and Complex Flow (AFM/MPF 2021), July 6-8, Online, (2021).

(a) Measurement Instruments     (b) Developed circuits
Fig. 1 The develped 3-D vector UVP system

# III. 12 Microscopic Hydrodynamic Bubble Behavior in Suppression Pool During Wet/Well Venting

Hiroshige Kikura, Hideo Nagasaka, Naruki Shoji, Hideharu Takahashi

## 1. Introduction

In the existing pool scrubbing codes, the Fission product (FP) aerosol transport model and the bubble hydrodynamic model are combined to evaluate the efficiency of the pool scrubbing effect. In the codes, Decontamination Factor (DF) used for pool scrubbing efficiency evaluation is obtained from FP aerosol removal mechanisms, which depend on the bubble diameter and bubble rising velocity. This research demonstrates the necessity of introducing Sauter Mean Diameter (SMD) as representative bubble diameter in the existing codes for analyzing pool scrubbing effects, since SMD is defined as the ratio of the total volume of the bubbles that is proportional to the amount of FP inside the bubble and the total surface area of the bubbles that governs mass transfer of FP particles. The bubble behavior of the rising bubbles prior to wet/well venting (constant pressure condition) and during wet/well venting (depressurization conditions) (Fig. 1) was observed and evaluated under the prototypical severe accident conditions of temperature, non-condensable gas content, submergence, downcomer diameter and pressure.

## 2. Experimental result validation

Experimentally collected SMD database was validated by using directly measured DF reported in the reference. The DF was estimated based on not only the SMD and corresponding rising bubble velocity, but also average values of bubble diameter and bubble rising velocity. The tendencies of DF showed a good agreement with total DF presented in the reference. On the contrary, order of DF based on average values was extremely larger than measured DF and were widely scattered. Thus, based on the present experimental results, SMD is more appropriate for single bubble model in pool scrubbing codes and is strongly suggested to adopt in the future updates of the pool scrubbing codes.

## 3. Pool scrubbing effect deterioration under depressurization

Reflecting to the conditions in Fukushima Daiichi severe accident and the FPs release to the environment after W/W ventings, experimental data of bubble size and bubble rising velocity were collected under depressurization and were used for evaluation of depressurization effect on bubble parameters and evaluation of pool scrubbing deterioration under depressurization condition. It was clarified that DF degrades to 1/100 under depressurization without steam condensation compared with the condition under constant pressure with steam condensation (Fig. 2).

Adopting W/W venting as severe accident management, it is important to consider that since the steam condensation is the dominant retention mechanism, it would be advisable to assure that while conducting W/W venting, the large vent under higher W/W pressure and the resultant higher suppression pool temperature in which rapid depressurization occurs, should be avoided since steam condensation does not occur during depressurization. Hence, FPs release to the environments could be is significantly reduced applying small venting combined with drywell spray compared with large venting, since the amount of FP in S/P is reduced and the discharge flow to the environment is smaller.

## 4. Conclusion

Based on the present experimental results, SMD is much more appropriate than arithmetic mean bubble diameter for single bubble model in pool scrubbing codes and is strongly suggested to adopt in the future updates of the pool scrubbing codes. Moreover, experimental data collected under depressurization were used for evaluation of depressurization condition effect on bubble parameters and evaluation of pool scrubbing deterioration under depressurization condition.
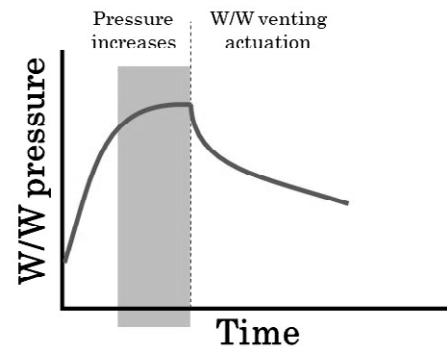


Fig. 1 Pressure transient during the severe accident progression
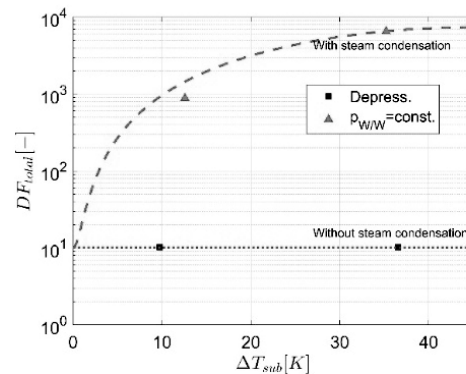


Fig. 2 DF comparison between constant pressure and depressurization condition

## Reference

1. Y. Iijima, et al.: The 5th Visualization Workshop, Online Conference, February 24, (2021).

# III. 13        Study on Gas Thermal Fluid Measurement Technique with Tunable Diode Laser Absorption Spectroscopy

Hideharu Takahashi, Naruki Shoji, Hiroshige Kikura

## 1. Introduction

The severe accident of Fukushima Dai-ichi nuclear power plant was happened caused by the hydrogen explosion. To prevent such the accident, understanding of thermal hydraulics phenomena, such as temperature, concentration, and velocity of the air-steam-hydrogen gas mixture in the primary containment vessel (PCV), is important. Recently, computational fluid dynamics (CFD) codes have been developed and used for the evaluation of thermal hydraulics phenomena in the PCVs. To validate and verify the CFD code, some experiments were conducted in the simulated PCV apparatus with air-steam-helium (instead of the hydrogen) mixture gas. However, these experiments have not been obtained sufficient results of steam temperature and concentration measurements due to low spatio-temporal resolution and inversive measurement. Therefore, steam temperature and concentration distribution measurement methods are required with high spatio-temporal resolution and non-inversive measurement. In this study, we focused on the tunable diode laser absorption spectroscopy (TDLAS) as the temperature and concentration measurement method. To apply the TDLAS to steam flow condition, the experimental apparatus and measurement system were constructed, and the laser absorption spectrum was obtained in various steam temperature conditions.

## 2. Method

The TDLAS is a measurement technique for obtaining absorption spectrum in a certain wavelength range by high-speed wavelength sweeping using a tunable laser diode. The laser absorption can be described with following equation, and depends on the target number density (concentration) of molecules and temperature.

$$A = -\log_{10}\{I(\lambda)/I_0(\lambda)\}$$
$$= \sum_i \left( n_i L \sum_j S_{i,j}(T) G_{vi,j} \right) \qquad (1)$$

where, $n_i$ is the number density (concentration) of molecules at energy level $i$, $L$ is the optical path length, $S_{i,j}(T)$ is the absorption line intensity at the transition from energy level $i$ to $j$, $T$ is the temperature of gas molecules, and $G_{vi,j}$ is the broadening function of absorption. The TDLAS utilizes the laser absorption dependence of the gas concentration and temperature to measure these parameters.

Figure 1 shows the measurement setup and experimental apparatus for steam temperature measurement with TDLAS system. The measurement system consists of the laser diodes with the wavelength band of 1579 nm and 1343 nm, right detector, respectively. The laser beam was transmitted to the vessel filled with superheated vaper. In this time, laser wavelength was swept in short time, and the laser absorption spectrum was obtained by the detector.
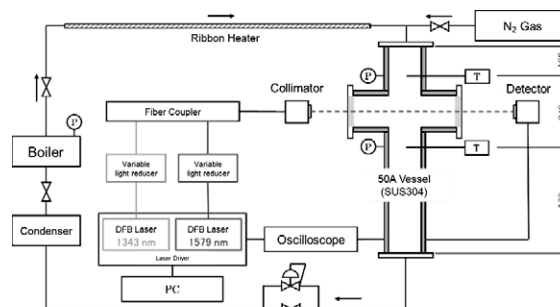


Fig. 1 Schematic diagram of the steam temperature measurement experiment with TDLAS system.

## 3. Results and Discussion

The measured laser absorption spectrum is shown in figure 2. The signals were measured for a certain period, and absorption spectrums were calculated using the time-averaged signals of the background and transmitted light of the various temperature steam and fitted by the gaussian distribution function. In figure 2, the absorption level was increased with increasing temperature. Namely, it is possible to detect the steam temperature on the laser path by drawing a calibration curve against the absorption level.
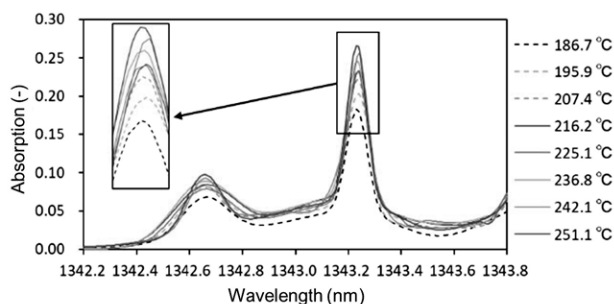


Fig.2 Temperature dependence of the laser absorption spectrum in the steam condition.

## 4. Conclusion

The TDLAS system was constructed to measure gas concentration and temperature simultaneously, and it was applied to the steam gas temperature measurement. In future, multi-path system will be constructed, and the spatial distribution measurement is considered.

## Reference

[1] M. Muto, N. Shoji et al.; 2021 JSME Annual Conference on Experimental Mechanics, August 25-27 (2021).

[2] M. Muto, N. Shoji et al.; AESJ Kanto-Koetsu Branch 15th Student Research Presentation Conference, March 1 (2022).

# III. 14    Study on material compatibility in liquid metal based fusion reactors operating at elevated temperature

## Masatoshi KONDO

### 1. Background and purpose

Fusion reactors can generate clean electricity. Therefore, several potential designs are being studied and proposed in the world. In a fusion reactor, the fusion reaction of two nuclear atoms releases massive amounts of energy. This energy is captured and converted to heat in a breeding blanket (BB), typically a liquid lithium alloy, surrounding the reactor core. This heat is then used to run a turbine and generate electricity. The BB also has an important function of fusion fuel breeding, which creates a closed fuel cycle for the sustainable operation of the reactors without fuel depletion.

The operation of BB at extremely high temperature over 1100 K serves the attractive function to produce hydrogen from water, which is a promising technology to realize a carbon-neutral society. This is possible because the BB heats up to over 1100 K by absorbing the energy from the fusion reaction. At such elevated temperatures, chemical compatibility of structural materials with liquid Li alloy in the BB is one of the important issue to be addressed, since this issue compromise the safety and stability of the reactors. It is, thus, necessary to find structural materials that are chemically compatible with the BB material at these high temperatures.

One type of BB currently being explored is the liquid metal BB. A promising candidate for such BBs is liquid lithium lead alloy (LiPb). A silicon carbide (SiC) material and FeCrAl alloys are candidate structural materials which can chemically compatible with liquid LiPb at very high temperatures. But information on this compatibility is quite limited beyond 973 K.

The purpose of the present study is to make clear the corrosion resistance of CVD-SiC and FeCrAl alloys in liquid LiPb at 873 K, 1023 K and 1173 K. Liquid LiPb was newly synthesized by melting and mixing of Pb and Li under a vacuum condition by the use of apparatus which was newly developed. The corrosion tests were performed in static LiPb up to 1173 K, and the surfaces and cross-sections of the post-exposure specimens were microscopically and chemically characterized. We have demonstrated compatibility at much higher temperatures.

### 2. Results and discussions

High-purity LiPb was synthesized by melting and mixing granules of Li and Pb in an apparatus which was newly designed and constructed as shown in Fig. 1. The LiPb synthesis was performed at 623 K under vacuum conditions. Rectangular specimens of CVD-SiC and two variants of the FeCrAl alloy—with and without pre-oxidation treatment to form an $\alpha$-Al$_2$O$_3$ surface layer—were installed in this liquid LiPb for 250 hours for corrosion testing.

The surface of CVD-SiC chemically reacted with Fe, Cr, Ni and O dissolved in liquid LiPb, and formed complex oxide on the surfaces as shown in Fig.2. The matrix was invaded by the oxide formation. The specimens revealed mass gain due to the oxide formation. The oxide formation was promoted at higher temperature. The corrosion of 316L crucible in liquid LiPb supplied metal impurities which contributed the oxide formation. The oxide formed as it invaded the SiC matrix.

The FeCrAl alloys (i.e., APMT and NF12) without preoxidation treatment formed the oxide layer of $\gamma$-LiAlO$_2$ on their surface in liquid LiPb. The $\gamma$-LiAlO$_2$ layer had a porous structure. The thickness of the $\gamma$-LiAlO$_2$ layer formed at 873 K was approximately 3-5 µm, though that at 1173 K was approximately 10 µm. The Li enrichment at the interface between the oxide layer and the substrate was detected by STEM-EELS observation. The mass changes of the specimens in the tests were much smaller than that of 316L austenitic steel at the same conditions. The $\gamma$-LiAlO$_2$ layer functioned as an anti-corrosion layer in the current short-term tests.

$\alpha$-Al$_2$O$_3$ layer was formed on the specimens of the FeCrAl alloys by the pre-oxidation treatment in air at 1273 K for 10 hours. The layer revealed the corrosion resistance in liquid LiPb at 873K, though the outer most part of the layer reacted with Li of liquid LiPb. Li penetrated along the grain boundaries of the oxide layer. $\alpha$-Al$_2$O$_3$ layer reacted with Li of liquid LiPb, and chemically transformed to $\gamma$-LiAlO$_2$ in the test at 1023 K and 1173 K. $\alpha$-LiAlO$_2$ coexisted with $\gamma$-LiAlO$_2$ at 1023K. The density of $\gamma$-LiAlO$_2$ was smaller than that of $\alpha$-Al$_2$O$_3.$ Therefore, the chemical transformation induced the crack occurrence due to the internal stress, which was caused by the volume expansion of the oxide layer. The layer of $\gamma$-LiAlO$_2$ was formed on the specimen surface, which had a porous structure. The pre-oxidation treatment was not effective to suppress the corrosion in liquid LiPb at the elevated temperatures above 1023 K.

These research findings are published in Corrosion Science[1]. The insights from these findings are expected to prove useful when designing and choosing new structural materials for nuclear fusion reactors, which could pave the way for a greener economy.

**Reference**

1. M. Kondo, S. Hatakeyama, N. Oono and T. Nozawa, Corrosion-resistant materials for liquid LiPb fusion blanket in elevated temperature operation, Corros. Sci., Volume 197, 1 April 2022, 110070.
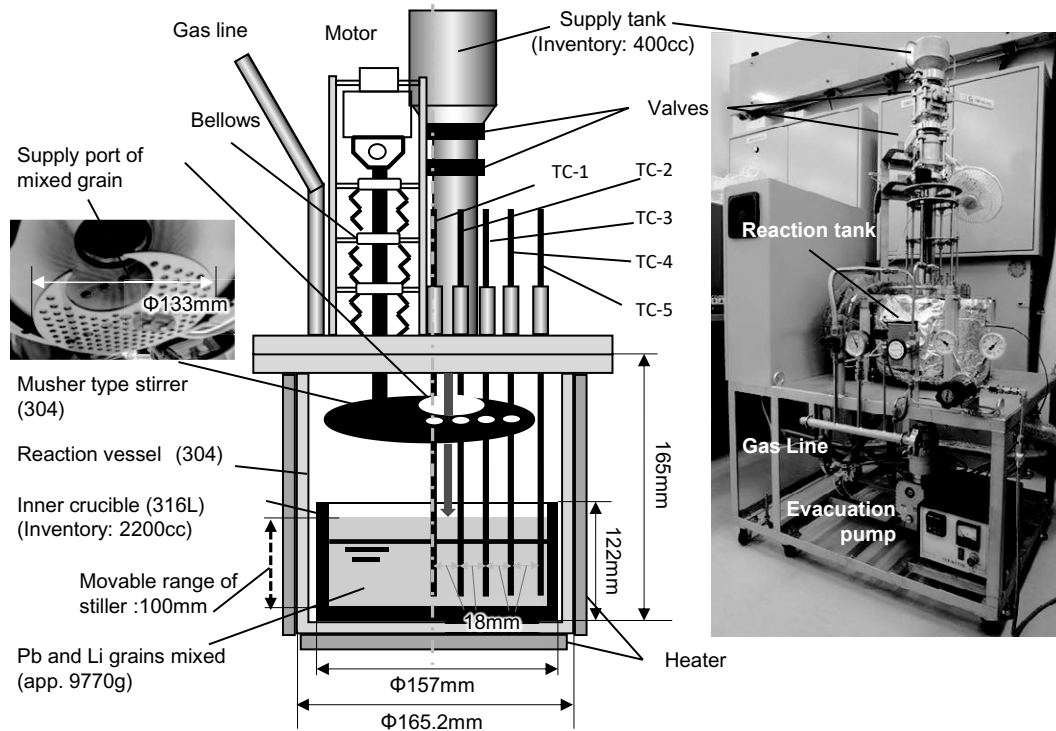
Fig.1 Synthesis apparatus of high-purity LiPb alloy[1]
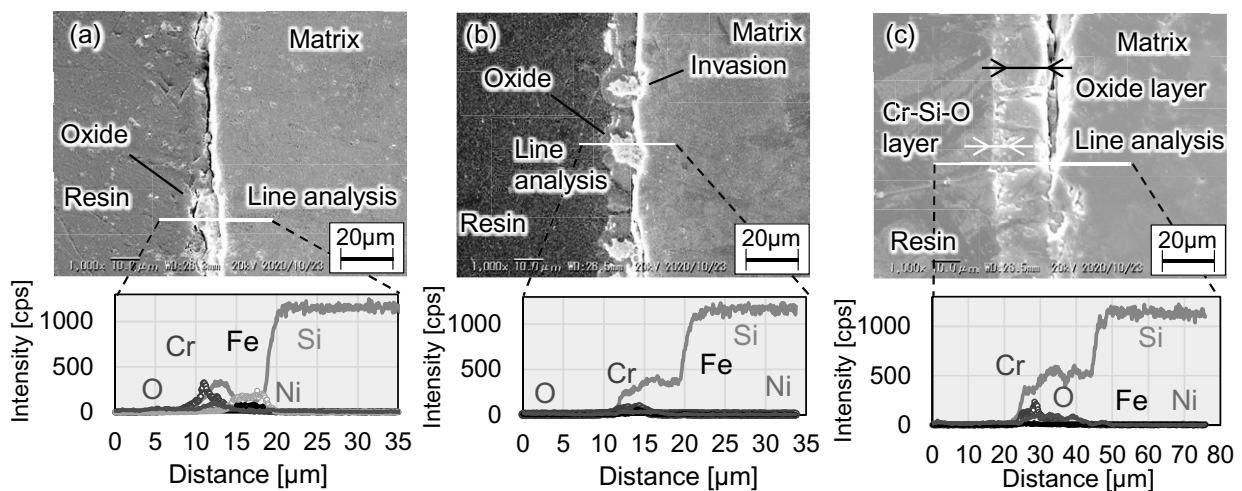


Fig. 2 SEM/EDX cross-sectional analysis on surface of SiC specimens after exposure to LiPb at (a) 873 K, (b) 1023 K and (c) 1173 K [1]

# III. 15 Effects of $U_3Si_2$ fuel and minor actinide doping on fundamental neutronics, nuclear safety, and security of small and medium PWRs in comparison to conventional $UO_2$ fuel

Natsumi Mitsuboshi, Hiroshi Sagara

## 1. Introduction

Small modular reactors (SMRs) have attracted significant research interest owing to their various applications. The scale of SMRs can be adjusted according to the site. To realize the flexibility of SMRs, introduction of a graded approach in their regulation based on nuclear safety and security features is essential. The effects of $U_3Si_2$ fuel and minor actinide (MA) doping on the fundamental neutronics, nuclear safety, and security of small and medium pressurized water reactors (SMPWRs) were evaluated in comparison to the case where $UO_2$ fuel was employed.

## 2. Results

The effects of the $U_3Si_2$ fuel and MA-doped on the fundamental neutronics, nuclear safety, and security of the SMPWR were evaluated by comparing it with the $UO_2$ fuel. The fundamental neutronics proved that the maximum burn-up days of the $U_3Si_2$ fuel was longer than that of the UO2 fuel, and the difference in the penalty for the initial reactivity of the 28,29,30Si and $^{16}O$ was only 0.3 %Δk, despite their large difference in thermal neutron capture cross-sections. Furthermore, owing to the large neutron capture cross-sections of the $^{237}Np$ and $^{241}Am$, the initial reactivity and burn-up reactivity change of the MA-doped fuel reduced, and the effects of the burnable poison were confirmed(**Fig.1**).

The evaluation of the impacts of the geometrical core size revealed that the initial U enrichment, which was required to satisfy the assumed one-batch two-year operating cycle of the $U_3Si_2$ fuel, could be reduced by ∼ 0.4 wt% compared to that of the $UO_2$ fuel because of the higher fissile isotope density of the $U_3Si_2$ fuel.

The fuel temperature coefficient of the $U_3Si_2$ fuel and the MAdoped $U_3Si_2$ fuel were negative, and the moderator reactivity coefficient of the $U_3Si_2$ fuel was more negative than that of the $UO_2$ fuel. Additionally, the moderator reactivity coefficient of the MA doped fuel was more negative than that of the non-doped fuel. The temperature gradient inside the $U_3Si_2$ fuel was smaller than that in the UO2 fuel owing to the higher thermal conductivity during the cycle. The temperature in the fuel center of the $U_3Si_2$ fuel was more than 300 K lower than that of the $UO_2$ fuel, and the temperature in the fuel center of the $U_3Si_2$ fuel was 900 K lower than the melting points(**Fig.2**).

Attractiveness was evaluated for non-state actors aiming for nuclear explosive device manufacturing. The attractiveness of fresh and spent $U_3Si_2$ fuel was equivalent to that of the fresh and spent $UO_2$ fuel in the processing phase, although the complexity of Pu separation in the spent $U_3Si_2$ fuel was higher than that in the $UO_2$ fuel. Using 0.5 wt% MA doping, the decay heat of the separated Pu from the spent fuel was enhanced to degrade by one level in the utilization phase. In conclusion, the present study demonstrated that the $U_3Si_2$ fuel and the MA-doped $U_3Si_2$ fuel are superior to the $UO_2$ fuel in fundamental neutronics, safety, and security features.
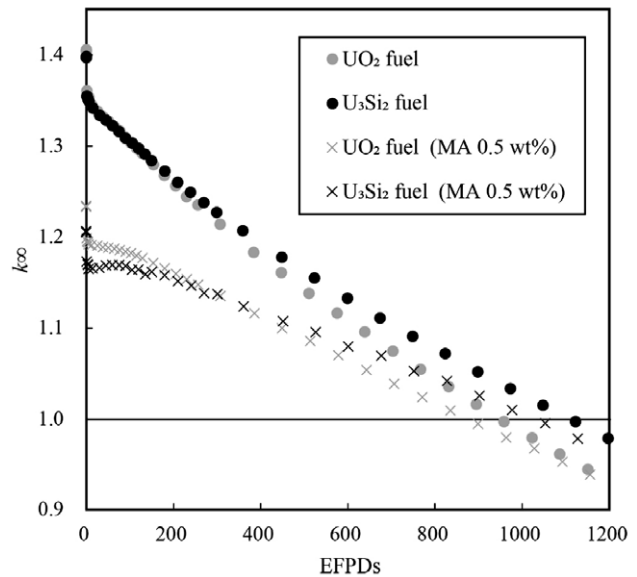


Fig. 1 $k_\infty$ as a function of Effective Full Power Days.
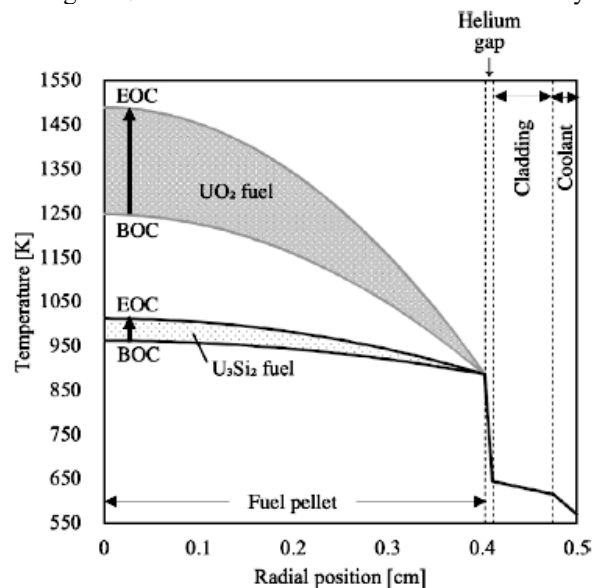


Fig. 2 Temperature distribution in fuels

## Reference

1. N. Mitsuboshi, H. Sagara, Annals, Nuclear Energy, Vol. 153, 108078, 2021.

# III. 16    Application of photofission reaction to identify high-enriched uranium by bremsstrahlung photons

Kim Wei Chin, Hiroshi Sagara, Chi Young Han

## 1. Introduction

The applicability of the photofission reaction ratio (PFRR) method to identify high-enriched uranium is studied by switching the photon source from the Gaussian spectrum to a bremsstrahlung spectrum. The combination of 6 and 11 MeV Gaussian photon energy was used in previous study for applying PFRR method because the photofission cross sections between $^{235}U$ and $^{238}U$ at these two energies differ significantly. A parametric study was conducted with the incident electron energy 7.0 MeV and the result showed that these electrons generate similar photofission reactions as that of 6.0 MeV Gaussian photons, while 13.5 MeV electrons is found to give even better results for PFRR considering the measurement noise contributed by multiple neutron emission, (γ, 2n) reaction. Bremsstrahlung photons were injected into a 1 mm thick uranium metal target with varying uranium enrichment. The PFRR increases linearly with uranium enrichment, and is found to provide a higher sensitivity than the Gaussian photons owing to higher total photofission reactions.

## 2. Results

After switching the photon source from the Gaussian spectrum, as in a previous study, to a more practical bremsstrahlung spectrum, a positive linear relationship between PFRR and uranium enrichment was confirmed, thus validating the principle of PFRR methodology. To achieve a similar photofission reaction rate of 6 and 11 MeV of Gaussian photons, a parametric study of incident electron energies was conducted. Based on the photofission reaction peak criteria as well as the measurement noise due to the (γ, 2n) reaction, 7.0 and 13.5 MeV were chosen as incident electron energies. Higher sensitivity is exhibited by bremsstrahlung photons than Gaussian photons owing to higher total photofission reaction rate associated with the former (Fig. 1, 2).

The correlations between uranium enrichment and PFRR by bremsstrahlung source as well as bremsstrahlung source considering (γ, 2n) reaction noise are represented by %EU = 32.953PFRR - 184.02 and %EU = 38.032PFRR - 228.02, respectively. Despite the existence of (γ, 2n) reaction noise, HEU can be identified with an uncertainty range of 20–30% for 20%EU(Fig. 3). However, there might be false alarms by 10%EU because uranium uncertainty ranges from 10 to 21%EU. For future tasks, the size of the uranium target, where multiple scatterings occur within the target, and filtering of low-energy photons from the tantalum converter target by a hydrogen-based moderator will be considered.

Future experimental planning for validation of the PFRR principle will be conducted.
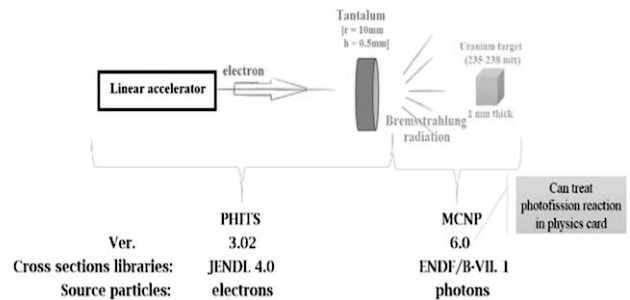


Fig. 1 Simulation setup overview
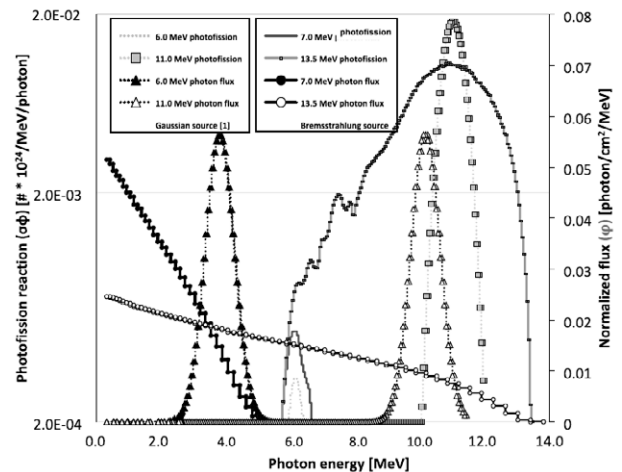


Fig. 2 Selected flux energies spectra and photofission reaction comparing with Gaussian source.
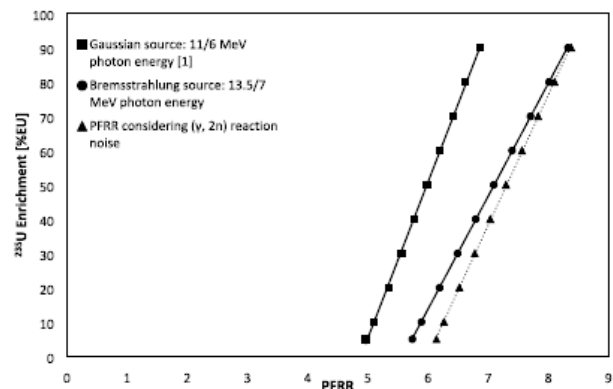


Fig. 3 Sensitivity of PFRR to uranium enrichment comparing to Gaussian source.

## Reference

1. Kim Wei Chin, Hiroshi Sagara, Chi Young Han, Annals, Nuclear Energy, Vol. 158, 108295, 2021.

# III. 17      Development of a Long-Life High-Charged Carbon Ion Source for Next Generation Heavy Ion Cancer Therapy Machines

## Yuji INOUE, Jun HASEGAWA

### 1. Introduction

Heavy ion cancer therapy is a type of radiation cancer treatment using carbon ions. Energetic heavy ions locally deposit their kinetic energy just before they stop in the target, so they can damage cancer cells deep in the human body more effectively compared to conventional radiotherapy using X-rays, etc. However, because of the high construction cost of the heavy ion accelerator system, the spread of heavy ion cancer therapy to developing countries is still on the way.

At present accelerator facilities for heavy ion cancer therapy, $C^{4+}$ ions are usually generated by conventional plasma ion sources. After accelerated to several MeV/u by linear accelerators, $C^{4+}$ ions are converted to $C^{6+}$ by a carbon thin film stripper and then injected to a synchrotron. To reduce the size and cost of the heavy ion cancer therapy machine, a novel accelerator system based on induction synchrotron have recently proposed, in which a laser ion source is used to supply highly-stripped carbon ions ($C^{5+}$ and $C^{6+}$) directly to the synchrotron. Thus, the injector such as RF linear accelerators is not necessary in this accelerator system, leading to the reduction of the size and cost of the heavy ion cancer therapy facility.

On the other hand, when a solid target in the laser ion source is repeatedly irradiated by a laser to produce source plasma, damage accumulates on the target surface, which makes it difficult to reuse the target for succeeding plasma generation. Thus, one needs to replace the target on a regular basis, which limits the continuous operation time of the laser ion source *i.e.* the accelerator system. To solve this problem, we propose to adopt a cryogenic target instead of the solid target for laser ion sources. In this scheme, a thin solid layer consisting of gas molecules is formed by sublimation on a metal cylinder cooled with liquid nitrogen and plasma is generated by irradiating it with a pulsed laser. The solid layer is locally removed after laser irradiation, but is reformed by sublimation of continuously supplied gas molecules.

The purpose of this study is to develop a new laser ion source using a cryogenic target and to demonstrate that it can operate stably without a limit on the lifetime of the target. Here we report results of preliminary experiments using a sublimated carbon dioxide ($CO_2$) target.

### 2. Experimental Setup

Figure 1 shows the experimental equipment developed in this study. The equipment is composed of a plasma generation chamber, an ion flux measurement chamber, and an electrostatic energy analyzer. These chambers are evaluated to ~$10^{-4}$ Pa by two sets of turbo molecular pumps.

A cylindrical cryogenic target is located in the plasma generation chamber. The structure of the target is shown in Fig. 2. The target consists of a cylindrical cryogenic cold head, a cylindrical radiation shield, and a gas supply system.

Both the cryogenic head and the shield are made of stainless steel. To protect the cold head from laser ablation, a 100-µm thick copper sheet covers the side wall of the head.

Plasma generation is performed as follows. First, the surface of the cold head is cooled to ~88 K with liquid nitrogen. Then, by feeding $CO_2$ gas through a mass flow controller into the radiation shield, a sublimation layer of $CO_2$ is gradually formed on the cold head surface. After the thickness of the sublimation layer reaches a certain value, the layer is irradiated by a frequency-doubled Nd:YAG laser through a ø5-mm aperture on the radiation shield. Finally, a dense and hot plasma produced by laser ablation is extracted through the aperture into vacuum.

Because the sublimation layer is locally removed by laser ablation, the cold head is rotated horizontally by precise motorized stages to avoid the overlap of laser spots on the target. In the present experiment, the pulse energy of the laser was set to 90 mJ. The laser spot size on the target has a diameter of 0.3 mm. Thus, the laser power density on the target surface was ~$10^9$ W/cm$^2$.

In the plasma ion flux measurement section, a Faraday cup with an entrance aperture of 5 mm was installed 850 mm away from the laser irradiation surface of the cryogenic
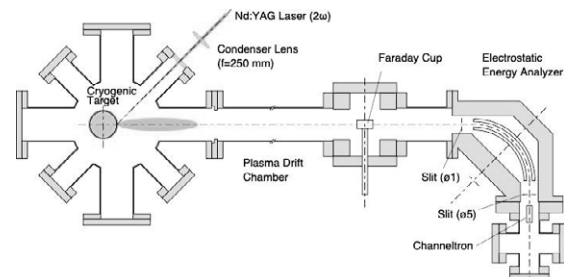


Fig. 1. An experimental equipment for the analysis of laser ablation plasma produced from a cryogenic target.
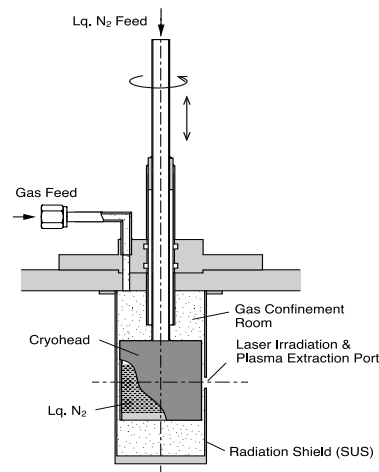


Fig. 2. The structure of the cryogenic target.

target. A bias voltage of –50 V was applied to the cup to measure the ion flux in the laser-generated plasma.

The electrostatic energy analyzer was used for the charge-state analysis of the plasma ions. The analyzer consists of two cylindrical deflection electrodes, entrance and exit slits, and a channel electron multiplier (CEM) detector. Under a specific deflection voltage, only ions with a specific charge-to-mass ratio and a specific kinetic energy can be detected. From ion signal data obtained with various deflection voltages, we reconstruct flux waveforms of ions having a specific mass-to-charge ratio.

## 3. Results and Discussion

Figure 3 shows plasma ion flux waveforms observed by the Faraday cup when the same position on the cryogenic target was repeatedly irradiated by the laser. As shown in the figure, there is a big difference between the waveform obtained by the first laser shot and those obtained by succeeding laser shots. The first shot waveform has a larger and sharper peak than the other waveforms. Also, the average kinetic energy of the ions composing the first-shot waveform seems to be considerably larger than the others. This result implies that the plasma ion flux produced by the first laser shot is mainly composed of light ions such as carbon and oxygen ions, while the plasma ion fluxes from subsequent laser shots are composed of heavy ions such as copper ions. Therefore, it is natural to assume that almost all of the solid $CO_2$ layer in the laser spot was lost by the first laser shot, meaning that the cryogenic target must be changed after each laser shot.

To investigate conditions for stable plasma generation from the cryogenic target, the peak value of plasma ion flux was measured by the Faraday cup as a function of the target feed distance. Here, the target feed distance is defined as the distance between the irradiation positions of two successive laser shots on the target. The peak current increased with increasing feed distance and reached almost constant value with feed distances more than ~0.3 mm. When the feed distance was smaller than 0.2 mm, the laser ablation of the sublimation layer was significantly disturbed by the local destruction of the solid $CO_2$ layer caused by the previous
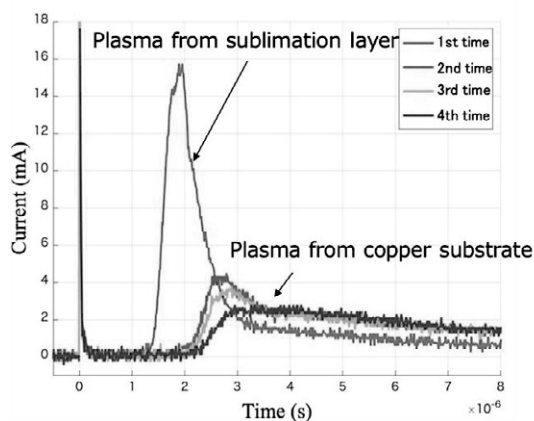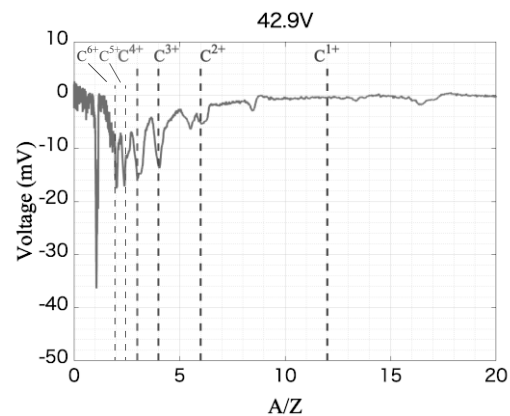
Fig. 4. An ion signal from the CEM detector with a deflection voltage of 42.9 V.

laser shot, leading to a large reduction in peak ion flux. On the other hand, when the target feed distance set to 0.3 mm or more, we could avoid the overlap of the laser spots on the target and achieve stable plasma generation from the sublimation layer.

Figure 4 shows a typical signal waveform from the CEM detector in the electrostatic energy analyzer when the deflection voltage was 42.9 V. Note that the values on the horizontal axis in the figure were converted from time to mass-to-charge ratio of detected ions. This result confirms that $C^+ \sim C^{6+}$ ions were successfully generated from the sublimated solid $CO_2$ layer.

The solid $CO_2$ layer formed on the cold head by sublimation was transparent to visible light. Because the frequency-doubled Nd:YAG laser ($\lambda$=532 nm) was used for laser ablation of the cryogenic target in this study, it is important to optimize incident laser optics so as to cause the laser ablation stably on the solid $CO_2$ layer surface. Results of the ion flux measurement under various focal point positions showed that changes in focal position over a distance of a few millimeters significantly changed the available plasma ion flux. This is probably due to the difference in whether the laser ablation initiates on the surface of the solid $CO_2$ layer or at the interface between the solid layer and the copper base plate.

## 4. Conclusions

We proposed and developed a novel laser ion source using a cryogenic target to meet the demand for long-time supply of highly stripped carbon ions at next generation heavy-ion cancer therapy machines. In the preliminary experiments presented here, we succeeded in generating a sublimated solid $CO_2$ layer on a cold head cooled with liquid nitrogen. Although the solid layer formed on the cold head was locally removed by a single laser irradiation, it was found that the damage was limited to the laser spot area. By setting the target feed distance to the diameter of the laser spot or more, we successfully demonstrated stable plasma generation from the solid $CO_2$ layer. We clarified that carbon ions with charge states of 1+ to 6+ were produced and supplied by the developed laser ion source.

Fig. 3. Plasma ion flux waveforms obtained by repeatedly irradiating the same position of the cryogenic target with the laser.

# III. 18   Evaluation of Thermal Shock Fracture Behavior of B₄C/CNT Composites using High-Frequency Induction-Heating Furnace

Ryosuke Maki, Jelena Maletaskic, Anna Gubarevich, Katsumi Yoshida

## 1. Introduction

Boron carbide ($B_4C$) has excellent properties such as high melting point, good chemical and thermal stability, light weight and extremely large neutron absorption cross-section, and $B_4C$ pellets have been used as neutron absorbers in the control rods for fast reactors. The control rod plays a major role in power control of fast reactors. However, thermal stress and the cracking of $B_4C$ pellets due to swelling and helium bubbles occurred during neutron irradiation have been one of the practical problems, and they result in extensive mechanical interactions between pellets and cladding tubes. For extension of lifetime of the control rods and the improvement of the safety of fast reactors, it is essential to enhance the thermal and mechanical properties of $B_4C$ pellets. To enhance the thermal and mechanical properties of $B_4C$ ceramics, carbon nanotubes (CNT) are considered to be attractive as reinforcements of ceramics because of their high thermal conductivity and high tensile strength. $B_4C$/CNT composites demonstrated good mechanical properties such as high strength and fracture toughness [1]. In this study, $B_4C$/CNT composites were fabricated, and the effect of the CNT-orientation in the $B_4C$/CNT composites on their thermal properties was evaluated. Fracture-resistance parameter by thermal stress, $R'$, was calculated based on the thermal and mechanical properties of the obtained $B_4C$/CNT composites. Moreover, the thermal shock fracture resistance of $B_4C$/CNT composites and $B_4C$ pellets used in JOYO experimental fast reactor was evaluated by thermal shock test using a high-frequency induction-heating furnace.

## 2. Experimental Procedures

### 2.1. Sample Preparation

$B_4C$, $\alpha$-$Al_2O_3$ and CNT (multi-walled CNT) were used as starting materials. Details of the fabrication process of $B_4C$/CNT composites by hot-pressing were described in ref.2. The hot-pressed samples were cut perpendicular and parallel to the axis of hot-pressing direction because the CNTs in the $B_4C$/CNT composites are dispersed in two dimensionally random, which tend to array perpendicular to the hot-pressing direction. The sample cut perpendicular to the hot-pressing direction is named as Composite A and sample cut parallel is named as Composite B as shown in Fig. 1. In comparison, the thermal properties and thermal shock fracture resistance of the $B_4C$ pellet prepared for the fast reactor, JOYO, was also evaluated.

### 2.2. Evaluations

The constitution phases of Composite A and Composite B were analyzed by X-ray diffraction. To determine their
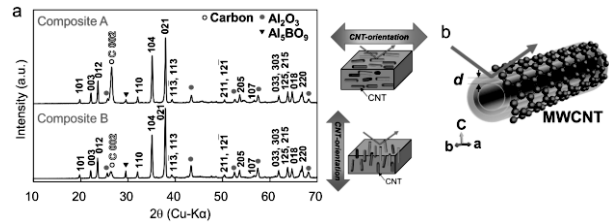


Fig. 1 (a) Schematic image of cutting and measurement direction for $B_4C$/CNT composites. (b) SEM image of CNTs array perpendicular to the hot-pressing direction is shown inset.

thermal conductivity, thermal diffusivity coefficient and specific heat capacity were measured from RT to 1000°C by a laser flash method and a differential scanning calorimetry, respectively. The thermal conductivity, $\kappa$, was calculated using a following equation (1);

$$\kappa = C_p \cdot \alpha \cdot \rho \tag{1}$$

where $C_p$ is the specific heat capacity, $\alpha$ the thermal diffusivity and $\rho$ the bulk density. The bending strength was measured by 3-point bending test. The elastic modulus and Poisson's ratio were measured by ultrasonic pulse-echo technique. The coefficient of thermal expansion (CTE) was evaluated by dilatometry. The thermal diffusivity coefficient, elastic modulus and Poisson's ratio of $B_4C$/CNT composites were measured in different directions, parallel and perpendicular to the longitudinal axis of CNTs dispersed in two dimensionally random. Fracture-resistance parameter by thermal stress, $R'$, was calculated based on the following equation (2) reported by Hasselman;

$$R' = \frac{\sigma_f \kappa (1-\nu)}{E\alpha} \tag{2}$$

where $\sigma_f$ is the fracture strength, $\nu$ the Poisson's ratio and $E$ the elastic modulus. This parameter corresponds to the resistance for crack initiation under thermal stress. Thermal shock test was performed using a high-frequency induction-heating furnace. The samples were heating up to 600°C in Ar flow. After heating the samples for 30 min, they were quenched immediately from the furnace into water. This heating and quenching was repeated for the same specimen several times. Microstructural observation was carried out for each thermal-shock-tested sample to observe the cracking behavior under thermal stress with an optical and scanning electron microscope.

## 3. Results and Discussion

XRD revealed that the hot-pressed $B_4C$/CNT composites consisted mainly of $B_4C$ phase, but some minor phases such as carbon, $Al_5BO_9$ and $Al_2O_3$, were also confirmed. Peak intensity of the carbon reflections in Composite A was much higher than that from Composite B, and this difference is

Table 1    Thermal and mechanical properties of B$_4$C (JOYO)
and B$_4$C/CNT composites.

| Sample | $\sigma_f$ (MPa) | $E$ (GPa) | $\nu$ | $\kappa$ (W/m·K) | CTE ($10^{-6}$/K) (at 40-600°C) | $R'$ (KW/m) |
|---|---|---|---|---|---|---|
| B$_4$C (JOYO) | 435 | 400 | 0.34 | 28.0 | 5.0 | 4.0 |
| Composite A | 400 | 372 | 0.34 | 29.8 | 5.1 | 4.1 |
| Composite B |  | 382 | 0.37 | 32.4 |  | 4.2 |

likely due to the CNT-orientation in these composites.

The thermal conductivity of B$_4$C (JOYO) was 28 W/m·K at RT, but decreased to 11 W/m·K at 1000°C. B$_4$C/CNT composites had higher thermal conductivities than that of B$_4$C (JOYO) at entire temperature range. The thermal conductivity of Composite B had the highest value, 32 W/m·K at RT. The thermal properties of B$_4$C/CNT composites depended on the CNT-orientation, and the highest value was obtained for the direction of the composite parallel to CNTs-orientation.

Thermal and mechanical properties and calculated fracture-resistance parameter by thermal stress of B$_4$C (JOYO) and B$_4$C/CNT composites are summarized in Table 1. As for the fracture strength and CTE of B$_4$C (JOYO), the reported value (435 MPa, as the bending strength and $5.0 \times 10^{-6}$ K$^{-1}$ as the CTE) were used. For B$_4$C/CNT composites, the fracture strength, 400 MPa, and CTE, $5.1 \times 10^{-6}$ K$^{-1}$, measured in this study were used to calculate $R'$ for both of Composite A and Composite B, since it was difficult to prepare the samples by hot-pressing to evaluate these properties in perpendicular to the axis of CNT-orientation. The elastic modulus of B$_4$C/CNT composites were slightly lower than that of B$_4$C (JOYO), and there was a difference of elastic modulus and Poisson's ratio between the Composite A and Composite B likely due to the CNT-orientation. It is reported that elastic modulus of longitudinal axis of CNT is probably much higher than that along the radial direction. The CTE was almost unchanged by CNT addition. As a result, B$_4$C/CNT composites exhibited higher $R'$ value than that of B$_4$C (JOYO) because of lower elastic modulus and higher thermal conductivity. However, CNT addition did not significantly enhance the thermal shock fracture resistance parameter $R'$. The critical temperature ($\Delta T_{max}$) for fracture induced by thermal stress was estimated based on the following equation (3) reported by Hasselman, and the calculated critical temperature for each sample were given as ~160°C.

$$\Delta T_{max} = \frac{\sigma_f (1 - \nu)}{E \alpha} \qquad (3)$$

To estimate the $R'$ of the composites, thermal shock test using a high-frequency induction-heating furnace was carried out. In order to evaluate the cracking behavior of each sample, the thermal shock test was performed at temperature difference of $\Delta T =$ ~600°C, which is higher temperature than the calculated critical temperature, to quickly evaluate the cracking behavior. In the case of the B$_4$C pellet (JOYO) after 9th thermal shock test, the cracks and chipping were clearly observed. Cracks in B$_4$C pellet (JOYO) were induced in the 2nd thermal shock test, and
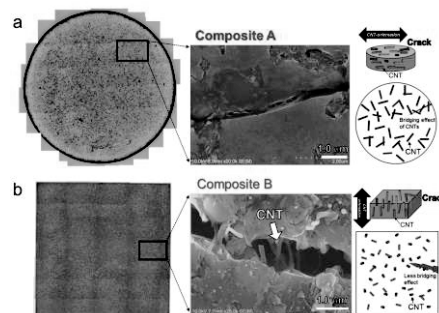


Fig. 2    Microstructure in the B$_4$C/CNT composites after 9$^{th}$ thermal shock test at $\Delta T =$ ~600°C.

crack propagation and chipping continually occurred by repeating the cycle. On the other hand, B$_4$C/CNT composites had an advantage in the resistance of crack propagation under thermal shock (Fig. 2). Cracks were introduced in 2nd thermal shock test as well as B$_4$C pellet (JOYO), but crack propagation was suppressed by bridging effect of CNTs even after 9th cycle. The CNT seems to be orientated parallel to the plane direction in Composite A. The enhancement of thermal shock damage resistance was clearly confirmed in the Composite B as well, but the crack size was bit larger than that of Composite A. This is attributed to the CNT-orientation axis, which is perpendicular to the plane direction in Composite B. Although the calculated $R'$ was almost the same between B$_4$C (JOYO) and B$_4$C/CNT composites, improvement of the thermal shock damage resistance of the B$_4$C composites by CNT addition was evident from the thermal shock test.

## 4. Conclusion

We prepared the B$_4$C/CNT composites with 5vol% Al$_2$O$_3$ additive, and evaluated their thermal and mechanical properties. Addition of CNT effectively enhanced the thermal conductivity of B$_4$C ceramics from 28.0 to 32.4 W/m·K at RT, leading to better thermal-shock-resistance parameter. Thermal shock test demonstrated that the crack propagation was suppressed by bridging effect of CNT even after 9th thermal shock test of water-quenching with $\Delta T = 600°$C. Although the calculated thermal shock fracture resistance parameter $R'$ of the B$_4$C/CNT composites were almost the same with B$_4$C (JOYO), improvement of the thermal shock damage resistance of the B$_4$C composites by CNT addition was evident from thermal shock experiments.

## Reference

1.   T. Kobayashi et al.: Journal of Nuclear Materials, Vol. 440, pp.524–529 (2013).
2.   Ryosuke S.S. Maki et al.: Materials Today; Proceedings, Vol. 16, Part 1, pp.137-143 (2019).

# III. 19 Study for nuclear fission and its applications

Chikako Ishizuka, Satoshi Chiba

## 1. Introduction

Chiba laboratory mainly studies nuclear data. Nuclear data is evaluated or measured physics quantity such as nuclear reaction cross sections, nuclear reaction rates, energies, the amounts of something which is produced by nuclear reactions. These information has been applied to nuclear reactor designs, shielding and radiation protection calculations, criticality safety, nuclear weapons, nuclear physics research, medical radiotherapy, radioisotope therapy etc. Thus, nuclear data is the most basic information when we use nuclear reactions. Among those nuclear data, data about nuclear fissions is the most essential for nuclear energy systems because we convert nuclear energy released by nuclear fission into electric power in nuclear power plant.

To run the power plant safely, there are abundant measurements on neutron-induced $^{235}$U fissions, while the experimental information on the other actinides is very limited. Added to such a fact, the complete understanding of the nuclear fission phenomenon is still challenging even now, though more than eighty years has passed after nuclear fission was discovered. In Chiba laboratory, we have studies nuclear data from very basic to its application. Recently, we have focused on the uncertainty in nuclear data and its influence on the nuclear transmutation rate, neutron deep penetrations [1] etc as shown in Fig.1. In this report, we introduce some topics we studied in 2021 fiscal year.
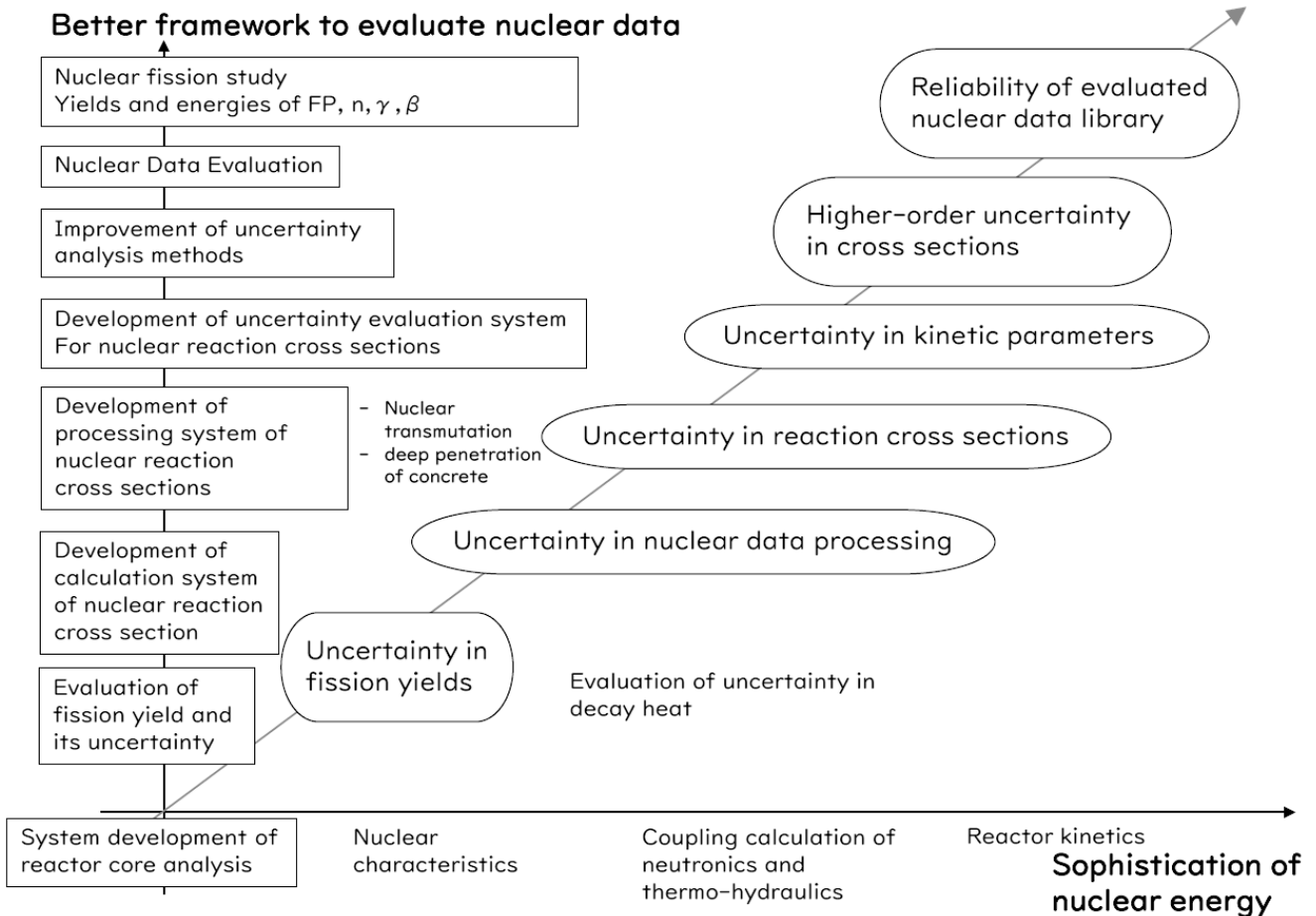


Fig. 1 Various uncertainties and their relating topics studied in Chiba laboratory.

## 2. Fission mechanism and basic fission observables

### 2.1. Fission yields and delayed neutrons

In the nuclear reactors, uranium absorbs one neutron and becomes a metastable state called a compound nucleus. Then it splits into two pieces. Major actinides such as uranium and plutonium become a pair of fission fragments, one light nucleus and one heavy nucleus. That is called asymmetric fission when nuclear fission derived by low energy neutrons or gammas. On the other hand, some minor actinides favors to split into the same size nuclei (so called symmetric fission). Chiba laboratory has tried to understand which nucleus tends to be asymmetric/symmetric fission and why those nuclei do so applying machine learning techniques to our calculation results based on our four-dimensional Langevin model which can predict both fission fragment yields and their total kinetic energies at the same time for actinides. We have also investigated the delayed neutrons and gammas emitted from fission fragments based on the Langevin model and the statistical decay model.

### 2.2. Fission barrier heights

Fission barrier heights (inner/outer barrier height) are one of representative observables which characterize nuclear fission. As the other fission observables, we need to supplement such information by theoretical studies. However, the existing nuclear model cannot reproduce those heights with enough precision. Then we study the fission barrier height of actinides using relativistic [2] and non-relativistic mean field approaches. In our study [2], pairing rotation can consistently explain various observable such as inner fission barrier, binding energy, and pairing momentum inertia simultaneously.

Another challenging aspect of this topic is nuclear interaction for fissions. There is no nuclear interaction used in non-relativistic/relativistic mean field models proposed for nuclear fission. Then we have developed a specific interaction for nuclear fission in both models.

## 3. Study for nuclear data applications

### 3.1. Fundamental Study for Heavy Particle Therapy

Heavy particle therapy using $^{12}$C can treat cancers more efficiently than X-rays and proton beams. However, the simulation scheme has not been established for expected nuclear reactions used in the therapy. Then, we simulate the $^{12}$C induced reaction performed at HIMAC and compare our results using the Anti-symmetrized Molecular Dynamics (AMD) with the measured data. The AMD can describe nuclear reactions at expected energy range in the therapy. Added to that, $^{12}$C has an alpha cluster structure which is difficult to treat in other nuclear models. At present, there is no simulation scheme for the heavy particle therapy using the AMD. We have performed the AMD calculations with various nuclear interaction models for improvement of the simulation accuracy of the therapy.

### 3.2. Influence of Nuclear Data Uncertainty on Concrete Deep Penetration Calculations

We developed the total Monte Carlo method to calculate the uncertainty in cross sections including correlations between all different reactions and the perturbations in angular distributions of secondary neutrons. In our previous study [1] shows that the correlation between total cross section and angular distribution of elastic scattering affects uncertainty of the calculated neutron dose when we assume a spherical concrete system with a point neutron source at its center.

Based on the above result, we study the influence of such uncertainty in the benchmark problem of bare, highly enriched uranium sphere (Godiva). Then we found that the correlation between total cross section and forward elastic scattering of $^{235}$U data does not affect the critical benchmark calculation. In $^{235}$U, those correlation is weak, while Si in the concrete wall shows strong positive correlations. We have evaluated the influence of the above uncertainty in the other system where the strong correlations between the total cross section and the forward elastic scattering cross section, such as Si case, is expected.

## Reference

1. N. Yamano et al., Journal of Nuclear Science and Technology, Vol. 59, Issue 5, pp. 641-646 (2022).
2. T. Kouno et al., Progress of Theoretical and Experimental Physics, Vol. 2022, Issue 2, 023D02, pp.1-13 (2022).

# III. 20     The effect of High LET irradiation to the cell division in pluripotent stem cells

Mikio Shimada

## 1. Introduction

Centrosomes are organelles consisting of two centrioles and pericentriolar material. Centrosomes function as microtubule organizing center during mitosis and duplicate only once during each cell division providing 2 centrosomes, which form a bipolar mitotic spindle. Improper duplication of centrosomes results in supernumerary centrosomes and forms multipolar spindles, leading to cell death through mitotic catastrophe. It has been reported that a small fraction of excess centrosome containing cells can survive and form polyploidy cells, which are associated with tumorigenesis and tumor progression. Indeed, over-duplicated centrosomes have been observed in several tissue tumors.

High linear energy transfer (LET) radiation including heavy ion bean and photon beam effectively generates massive and complicated DNA damage called cluster DNA damage in cell nucleus. Cluster DNA damage is difficult to repair and needs time to repair. Delay of DNA repair leads to expansion of cell cycle checkpoint time resulting in dissociation of centrosome duplication cycle and excess centrosomes duplication. Indeed, high LET radiation (carbon beam) exposure increased centrosome overduplication.

Pluripotent stem cells including embryonic stem cells and induced pluripotent stem cells harbor multipotency to differentiate all organs. iPSCs showed hypersensitivity and cell death after ionizing radiation exposure. These data suggest that iPS cells show different response to the radiation exposure compared with somatic cells.

In this study, to investigate the effect of high LET irradiation to the pluripotent stem cells, we used human iPSCs and carbon beam as high LET irradiation.

## 2. Materials and Methods

### 2.1. Carbon beam exposure

Carbon beam exposure experiments were performed at National Institute of Radiological Sciences, National Institute for Quantum Science and Technology in Chiba.

### 2.2. Immunostaining

After radiation exposure, cells were incubated at indicated time. And then, cells were fixed with 4% para-formaldehyde for 10 min at room temperature and permeabilized with 0.5 % Triton X/PBS-T for 5 min at 4℃. Cells were stained with γ-tubulin and α-tubulin antibodies for 4 h at 4℃. And then, cells were reacted with secondary antibodies for 1h at 4℃. Cells were mounted by mounting medium and dry up. Cells were observed by fluorescence microscopy.
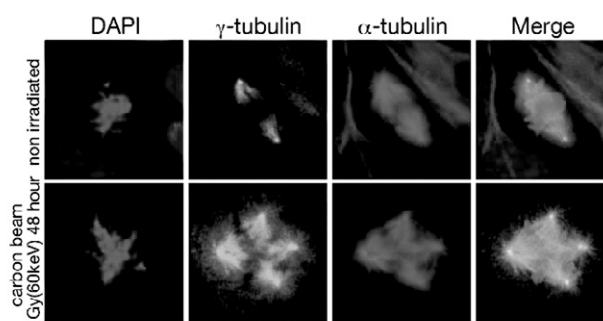


Fig. 1 Multipolar cell division after carbon beam exposure in human iPS cells

Immunostaining of γ-tubulin and microtubule marker α-tubulin in human iPSCs after non treated or carbon beam exposure treatment.

## 3. Results and Discussion

### 2.1. Carbon beam exposure in human iPS cells

To investigate the effect of high LET irradiation to the stem cells, carbon beam at 1Gy were exposed to the human iPSCs. Since previous reports showed increasing peak of centrosome overduplication is 48-72 h after IR exposure, cells were incubated for 48 h. And then, cells were stained with centrosome marker, γ-tubulin and microtube marker α-tubulin. Carbon beam exposure increased centrosome overduplication and multipolar cell division in human iPSCs. In the future plan, I will address the molecular mechanism in high LET irradiation dependent centrosome overduplication and multipolar cell division.

## Acknowledgment

# III. 21 Research project of hybrid waste solidification of various wastes generated by the Fukushima Daiichi Nuclear Power Plant Accident

Masahiko Nakase, Miki Harigai, Shinta Watanabe, Tomofumi Sakuragi, Ryo Hamada, Hidekazu Asano, Ryosuke Maki, Hidetoshi Kikunaga, Toru Kobayashi

Fukushima Daiichi Nuclear Power Station (1F) accident generates a large amount of waste, and decommissioning project is ongoing. The most complex objects fuel debris will be retrieved, and further characterization will be done shortly. One of the imminent problems should be the disposal of wastes generated by the treatment process of contaminated water, such as slurry wastes, spent zeolite absorbents, etc. Current studies mainly focus on synthesizing stable waste forms and characterization. Repository design, disposal scenarios, and safety assessments are needed to dispose of such wastes, but only a few studies are currently seen. Each conventional disposal concept, such as geological, intermediate, and shallow land disposal, requires a deep understanding of each waste, including long-term chemical stability, leaching property, and radiation resistance. Also, the waste composition and characteristics can change as time passes. Due to such uncertainty, we propose a hybrid waste solidification concept, as shown in Fig.1. The hybrid waste consists of primary waste, which itself stably confines, and a second matrix which is well-characterized metal or ceramics. The mixture of this primary waste and matrix material proceeded to stabilization and compression by Hot Isostatic Pressing (HIP) or Spark Plasma Sintering (SPS) depending on the waste form's content and the disposal requirement (Fig. 2). By utilizing zircalloy as a matrix whose corrosion behavior in various conditions is well studied, prediction of long-term behavior becomes possible. This concept can also be applied to coarse particles such as fuel debris, and the metals such as stainless-steel SUS) generated in the decommissioning of nuclear power plants may be reused for the fabrication of hybrid waste form. In this study, the mixture of various primary wastes such as A LPS sediment waste and its phosphate waste form studied elsewhere, AREVA sediment wastes, and Ag zeolite loaded with I, AgI was tested with many matrix materials. HIP and SPS techniques were explored to stabilize such wastes. Through this project, we find the optimum matrix material and condition of hybrid waste fabrication through experiments and chemical calculations from many viewpoints. These activities lead to the design of the disposal scenario and a safety assessment. The overview and progress of our 3-year-project began in FY2021, and some of the recent results will be shown, as well as to show the outline of this project to promote the 1F decontamination activity.
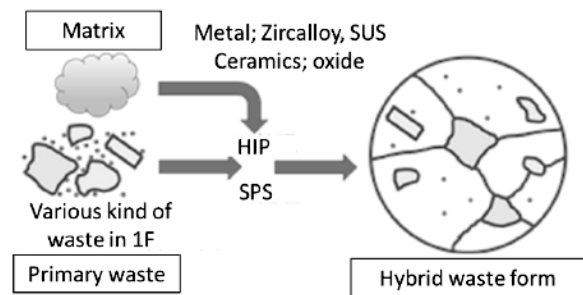


Fig.1 Concept of hybrid waste solidification.
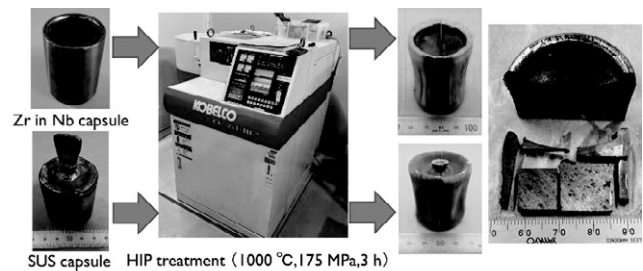


Fig.2 Hybrid waste manufactured by HIP.

**References**
(1) M.Nakase et al., Research project of hybrid waste solidification of various wastes generated by Fukushima Daiichi Nuclear Power Plant Accident; an overview, Proc FDR2022, 2022
(2) R.Maki et al., Effective/rapid immobilization of radionuclides from Fukushima decommissioning by spark plasma sintering process, Proc FDR2022, 2022
(3) T.Sakuragi et al., Composite waste form for immobilization of radionuclides from Fukushima decommissioning by powder metallurgy hot isostatic pressing, Proc FDR2022, 2022
(4) S.Kanagawa et al., Development of Stable Solidification Process of Phosphates Waste Form for ALPS Slurry Wastes, Proc FDR2022, 2022

# IV.    Co-operative Researches

## IV. Co-operative Researches

### IV.1 Co-operative Researches within Tokyo Institute of Technology

(1) Novel fiber reinforced concrete based on liquid metal technology toward resource recycling society, Masatoshi Kondo, Nobuhiro Chijiwa, Minho O (Tokyo Tech.). (Partially supported by Interdisciplinary Research Support for Scientists of Tokyo Institute of Technology).

(2) Spectroscopic Measurement of Arc-Discharge Argon Plasma Plume Injected into Water, Prof. Shinsuke Mori, Major in Chemical Science and Engineering, School of Materials and Chemical Technology.

(3) Li-ion battery thin films, Prof. Sou Yasuhara, Prof. Mitsuru Itoh

(4) Ferroelectrics, piezoelectrics and Multiferroics, Prof. Takahisa Shiraishi, Prof. Hiroshi Funakubo, Prof. Mitsuru Itoh

### IV.2 Co-operative Researches with Outside of Tokyo Institute of Technology

(1) Solid oxide electrolysis cell development for $CO_2$ reduction, JSPS Grant-in-Aid for Scientific Research (B), 2019-2022.

(2) Chemical heat pump for P2H2P, JST-MIRAI Program, Japan Sci. and Tech. Agency, 2021-2025.

(3) Solid oxide electrolysis cell for Carbon recycling, New Energy and Industrial Technology Development Organization, 2020-2022.

(4) Low-cost hydrogen permeation membrane for $CO_2$ efficient recovery, Steel Foundation for Environmental Protection Technology, 2020-2022.

(5) Challenge of novel hybrid-waste-solidification of mobile nuclei generated in Fukushima Nuclear Power Station and establishment of rational disposal concept and its safety assessment, Advanced Research and Education Program for Nuclear Decommissioning, JAEA-CLADS.

(6) Exploration of fluorine super solvent for MA extraction, Innovative Nuclear Research and Development Program, MEXT.

(7) Study on Degradation of Fuel Debris by Radiation, Chemical, and Biological Damage, Advanced Research and Education Program for Nuclear Decommissioning, MEXT.

(8) Development of apatite ceramics for stabilization of ALPS precipitation wastes, Advanced Research and Education Program for Nuclear Decommissioning, MEXT

(9) Cross-disciplinary nuclear system research for load reduction of radioactive waste management, commissioned research from Radioactive Waste Management Funding and Research Center, Innovative Nuclear Research and Development Program, MEXT

(10) Development of Subcritical Water Washing System for Cleanup and Reuse of Contaminated Soil, and Volume-reduction of Radioactive Waste, The Environment Research and Technology Development Fund, 1-1805.

(11) Study on Cs desorption from soil cay minerals by subcritical water containing metal ions, Grant-in-aid for Scientific research B, 18H03398.

(12) Volume reduction and stable solidification of recovered Cs from classified contaminated soil, JESCO

(13) Study on reprocessing and waste by the diverse condition of the nuclear fuel cycle, Subcontract from Radioactive Waste Management Funding and Research Center, Agency for Natural Resources and Energy, 2021

(14) Study on MA recovery flowsheet by extraction chromatography and in-line analysis, Subcontract from Japan Atomic Energy Agency, Agency for Natural Resources and Energy, 2021

(15) Study on the extraction separation process of minor actinide suitable for its solidification and stabilization, and index development for evaluation of the impact of MA separation on final disposal. Mitsubishi Heavy Industry, 2021

(16) Development of the recovery process of minor actinide flowsheet based on cold experiments, and its effect on final disposal (Phase 2), Mitsubishi Heavy Industry

(17) Study on trace metal separation and quantification, AGC, 2021

(18) Study on complexes formed in the adsorbent of the extraction chromatography column, JAEA, 2021

(19) Synthesis of novel phthalocyanine derivatives and effect of substituent on recognition of light actinide and chemical property, Institute for Integrated Radiation and Nuclear Science, Kyoto University, 2021

(20) Hydrothermal synthesis of Actinide-mixed oxide for fundamental study of debris, Institute for Integrated Radiation and Nuclear Science, Kyoto University, 2021

(21) Study on fuel recycling and decontamination by low-temperature hydrothermal synthesis of oxides, Institute for Materials Research, International Research Center for Nuclear Materials Science, Tohoku University, 2021

(22) Exploring the chelate ligand for Actinium and its related nuclei, Institute for Materials Research, Laboratory for alpha-Ray emitters, Tohoku University, 2021

(23) Synthesis of Uranium-Phthalocyanine complexes and measurement of electrochemical states, Institute for Materials Research, Laboratory for alpha-Ray emitters 2021

(24) Study on valence control of minor actinide and extraction by amide-type ligands, Institute for

Materials Research, International Research Center for Nuclear Materials Science, Tohoku University, 2021

(25) Development of mass-balance analysis method in nuclear back-end process and its implementation to NMB code, Joint-research of LANE with JAEA, 2021

(26) Development of extractants for Minor Actinide separation and their physical properties evaluation, Joint-research of LANE with JAEA, 2021

(27) Fretting behaviors of $Li_{2+x}TiO_{3+y}$ pebble and RAFM steel F82H under argon atmosphere, Masatoshi Kondo (Tokyo Tech.), Jae-Hwan Kim (QST), Masaru Nakamichi (QST), Masami Ando (QST), Taehyun Hwang (QST), Yutaka Sugimoto (QST). (Partially supported by QST Research Collaboration for Fusion DEMO).

(28) Chemical compatibility of F82H and 316L in liquid metal heat transfer mediums Li, Na and NaK, Masatoshi Kondo (Tokyo Tech.), Satoshi Sato (QST), Masami Ando (QST), Takashi Nozawa (QST). (Partially supported by QST Research Collaboration for Fusion DEMO)

(29) Technological development of FeCrAl-ODS alloys coexisting with liquid metal cooling system of helical fusion, Masatoshi Kondo (Tokyo Tech.), Naoko Oono (YNU), Teruya Tanaka (NIFS), Ryuta Kasada (Tohoku univ.), Hao Yu (Tohoku univ.), Masafumi Akiyoshi (OMU), Yukinori Hamaji (NIFS). (Partially supported by the NIFS Collaboration Research program (NIFS20KOBA033)).

(30) Chemical compatibility of dissimilar-metal joint in liquid breeders, Masatoshi Kondo (Tokyo Tech.), Takuya Nagasaka (NIFS). (Partially supported by the NIFS Collaboration Research program (NIFS19HDAF001)

(31) Experimental study on reduction of MHD pressure drop in liquid breeder blanket, Masatoshi Kondo (Tokyo Tech.), Naoko Oono (YNU), Teruya Tanaka (NIFS), Yoshimitsu Hishinuma (NIFS), Yukinori Hamaji (NIFS).

(32) Novel low-melting-point metal mirrors for space telescope, Masatoshi Kondo (Tokyo Tech.), Yutaka Hayano (NAOJ), Yuichi Matsuda (NAOJ).

(33) Experimental study on FeCrAl steels in PbBi coolant system of ADS, Masatoshi Kondo (Tokyo Tech.), Toshinobu Sasa (J-PARK), Shigeru Saito (J-PARK).

(34) Development of Decontamination Treatment Techniques for Dry Powder Foods by Atmospheric-Pressure Nonequilibrium DC Pulse Discharge Plasma Jet, Prof. Toshifumi Yuji and Prof. Hiroyuki Kinoshita, University of Miyazaki; Prof. Narong Mungkung, King Mongkut's University of Technology Thonburi; Prof. Sarizam Mamat, Universiti Malaysia Kelantan; Prof. Yoshifumi Suzaki, Kagawa University.

(35) Estimating Electron Temperature and Density Using Improved Collisional-Radiative Model in High-Density RF Argon Plasma, Prof. Daisuke Kuwahara, Chubu University; Prof. Shunjiro Shinohara, Tokyo University of Agriculture and Technology.

(36) Developing an Optimization Algorithm for Diagnostic Modeling of Optical Emission Spectroscopic Measurement of Non-Equilibrium Plasmas Based on the Argon Collisional-Radiative Model, Tokyo Metropolitan Industrial Technology Research Institute.

(37) Diagnostics of Electron Energy Distribution Function of Atmospheric-Pressure Plasmas with Phase-Resolved Optical Emission Spectroscopy Measurement of Continuum Spectrum, JSPS Grant-in-Aid Scientific Research (B), 19H01867, 2019-2022, Professor Kiyoyuki Yambe, Niigata University.

(38) Plasma Diagnostics Technology for Production Equipment with AI Technology, ULVAC, Inc. via "ULVAC Advanced Technology Collaborative Research Cluster".

(39) Nuclear structure, W. Horiuchi (Hokkaido University), S. Michimasa (RIKEN)

(40) Possible measurements of nuclear data using laser based neutron sources, with Takehito Hayakawa (QST)

(41) Study on prompt-neutron emission mechanism of nuclear fission based on a statistical model, with Toshihiko Kawano (LANL, USA)

(42) Development of quantitative evaluation method for charge polarization using Density functional study, with Shinichiro Ebata (Saitama Univ.)

(43) Study of nuclear reactions using AMD, with Akira Ono (Tohoku Univ.)

(44) The study on nuclei and neutron matter using finite-range three-body force, Naoyuki Itagaki (Kyoto Univ.)

(45) Fission study, Fedir Ivanyuk (Institute for Nuclear Research, Kiev, Ukraine), Mark Usang (Malaysian Nuclear Agency)

(46) Development of Long-Life Laser Ion Sources Using Cryogenic Solid Targets and Liquid Metal Targets, K. Takahashi (NUT), Jun Tamura (JAEA), K. Takayama (KEK).

(47) New Design of Ion Beam Inertial Confinement Fusion Reactor System, K. Takayama (KEK), K. Horioka (Tokyo Tech), K. Okamura (KEK), W. Jiang (NUT), T. Kikuchi (NUT), T. Sasaki (NUT), K. Takahashi (NUT), Y. Iwata (AIST), *et al*.

(48) Development of nuclear data evaluation framework for innovative reactors, MEXT Innovative Nuclear Research and Development Program.

(49) n_TOF Collaboration, CERN

(50) Study on neutron capture cross section of carbon-13. Research Collaboration between the South West Nuclear Hub, University of Bristol and Institute of Innovative Research, Tokyo Institute of Technology and The Institute for Integrated Radiation and

Nuclear Science, Kyoto University

(51) Challenge to Investigation of Fuel Debris in RPV by an Advanced Super Dragon Articulated Robot Arm, JAEA, MEXT

(52) Fundamental Research for Advancement on Ultrasonic Sensing Technology I, Tokyo Electric Power Company Holdings, Incorporated.

(53) Research on Nuclear Emergency Preparedness in Transportation of Nuclear Fuel Materials I (Study on Emergency Response System in Transportation), Nuclear Fuel Transport Co., Ltd.

(54) Fundamental Research on Multiphase Flow in Filter Vents, Chubu Electric Power Co., Inc.

(55) Fundamental Research on Multiphase Flow Measurement in Surface-based Methane Hydrate Recovery, MODEC, Inc.

(56) Fundamental Research on Mechanism of Blast Decontamination System for Small Diameter Piping, Fuji Furukawa Engineering & Construction Co.Ltd., Fuji Electric Co., Ltd., Shinto Kogio, Ltd.

(57) Development of Non-destructive Measurement System of Plant Piping Using Portable Ultrasonic Velocity Profile Dvices, MEXT.

(58) Research on Advanced Radioactive Material Removal System by Silver Zeolite, Rasa Industries, Ltd.

(59) Fundamental Research on Ultrasonic Measurment of Fused glass and Fused tin, AGC Inc.

(60) Research on Thermal-hydrodynamics for Future Light Water Reactor, Energy System and Chemical Technology Development, Nguyen Tat Thang, Duong Ngoc Hai, Vietnam Academy of Science and Technology.

(61) Research on Thermal-hydrodynamics for Future Light Water Reactor, Energy System and Chemical Technology Development, Horst-Michael Prasser, Yasushi Takeda, Swiss Federal Institute of Technology (ETH Zurich).

(62) Advanced Fluid Dynamics and Developed of Measurement Technique, Jirasak Chanwutitum, Viboon Chunkag, Chirdpong Deelertpaiboon, Natee Thong-un, Udomkiat Nontakaew, Chirdpoing Deelertpaiboon, King Mongkut's University of Technology North Bangkok.

(63) Advanced Fluid Dynamics and Developed of Measurement Technique, Weerachon Treenuson, Office of Atoms for Peace (OAP), Ministry of Science and Technology.

(64) Advanced Thermal Dynamics and Developed of Cross Linear Concentrating Solar Power(CL-CSP) Technique, Mukesh Pandey, Rajiv Gandhi Technological University

(65) Advanced Fluid Dynamics and Developed of Measurement Technique, Masahiro Kawaji, The City College of New York

(66) Development of Ultrasonic Measurement System, Bruce Drinkwater, University of Bristol.

(67) Advanced Fluid Dynamics and Developed of Measurement Techniques, Deog Hee Doh, Korea Maritime & Ocean University

(68) Advanced Fluid Dynamics and Developed of Measurement Techniques, Jae Jun Jeong, Pusan National University.

(69) Advanced Fluid Dynamics and Developed of Measurement Techniques, Xingguo Wang, Jingdezheng Ceramic Institute.

(70) Advanced Fluid Dynamics and Developed of Measurement Techniques, Won-Pil BAEK, Chul-Hwa Song, Korea Atomic Energy Research Institute (KAERI).

(71) TEPCO Decommissioning Frontier Technology Creation Collaborative Research Base, Tokyo Electronic Power Company Holdings, Inc.

(72) Uncertainty reduction of the FPs transport mechanism and debris degradation behavior and evaluation of the reactor contamination of debris state on the basis of the accident progression scenario of Fukushima Daiichi Nuclear Power Plant Unit 2 and 3, Saint Petersburg State University

(73) Development of database for debris property based on the elucidation of debris formation mechanism and verification of accident progression analysis results by synthesis of sim-debris on the basis of analytical results of materials surrounding fuel debris, Fukui Univ, Tohoku Univ, and Osaka Univ.

(74) Formation and growth mechanism of calcium sulfide in molten low carbon steel, Nippon Steel Corporation.

(75) Improvement to critical safety technology for Fukushima-Daiichi NPS decommissioning, Toru Obara, Jun Nishiyama, Tokyo Institute of Technology, Hiroki Takezawa, Tokyo City University, Georgy V. Tikhomirov, Anton Smirnov, Ivan Saldikov, Ekaterina Bogdanova, Vladislav Romanenko, National Research Nuclear University (MEPhI).

(76) Conceptual study on sodium cooled Rotational Fuel-shuffling Breed-and-Burn fast reactor with metal fuel, Toru Obara, Jun Nishiyama, Tokyo Institute of Technology, Van Khanh Hoang, Vietnam Atomic Energy Institute.

(77) Study on neutron balance features in Breed-and-Burn fast reactor, Toru Obara, Jun Nishiyama, Tokyo Institute of Technology, Odmaa Sambuu, National University of Mongolia.

(78) Astrobiology Experiments Based on MeV Ion Beams, Division of Materials Science and Chemical Engineering, Faculty of Engineering, Yokohama National University.

(79) Development of Negative Ion Sources for Tandem Accelerators, Atomic Energy Research Laboratory, Tokyo City University.

(80) Development of Low-Dose X-ray Fluorescence Analysis for Cultural Heritage Samples by Proton-Induced Monochromatic X-rays Considering Late Effects after 100-1000 years, Grant-in-Aid for Scientific Research (B), Japan Society for the

Promotion of Science.

(81) Development of a passive reactor shutdown device to prevent core damage accidents in fast reactors, MEXT Innovative Nuclear Research and Development Program in Japan, Kyushu University, University of Fukui, Tokyo City University, Japan Atomic Energy Agency.

(82) Study on Advanced Nuclear Energy System Based on the Environmental Impact of Radioactive Waste Disposal, MEXT Innovative Nuclear Research and Development Program in Japan, grant no. JPMXD02 19209423, Radioactive Waste Management Funding and Resource Center, Hokkaido University, Japan Atomic Energy Agency.

(83) Nonproliferation features of molten salt fast reactor, Texas A&M University.

(84) Easy and Advanced Non-destructive assay technique to quantify nuclear material in various type of nuclear waste forms, Japan Atomic Energy Agency.

(85) Nuclear Forensics Signatures of Spent Nuclear Fuel, Japan Atomic Energy Agency

(86) Control of Divertor Configuration by Induced Current Drive in QUEST, Tsutsui Hiroaki, Hasegawa Makoto, Masuzaki Suguru, Nakamura Kazuo, Mitarai Osamu, Iio Shunji, Idei Hiroshi, Hanada Kazuaki, WANG Jingting, Jang Sejung, Munechika Koyo

(87) Improvmement and Investigation of Tokamak Plasma Start-Up and its Breakdown by 3D-Magnetic Field Effects with Saddle Coils, Tsutsui Hiroaki, Watanabe Kiyomasa, Iio Shunji, Naito Shin, Hatakeyama shoichi, Shoji Mamoru, Munechika Koyo, Suzuki Yasuhiro, Kuwahara Daisuke, Matsuda Sinzaburo, Trilaksono Jordy, Jang Sejung, WANG Jingting, Nonaka Atsushi

(88) Li-ion battery thin films, Prof. Takashi Teranishi, Prof. Kamala Bharathi, Prof. Alex Rettie

(89) Ferroelectrics, piezoelectrics and Multiferroics, Prof. Yoshitaka Ehara, Prof. Yosuke Hamasaki, Prof. Tsukasa Katayama, Prof. Takenori Kiguchi, Dr. Jianging Yu, Prof. Nobuo Nakajima, Prof. Jun Kano,

(90) Research on Adsorbents of Siloxane Compounds for Application under Extreme Environment: Japan Aerospace Exploration Agency (JAXA).

(91) Development of CMC Bearings for Pumps for Local Torrential Rain Measures: Adaptable and Seamless Technology Transfer Program through Target-driven R&D (A-STEP), Japan Science and Technology (JST), Japan Fine Ceramics Co. Ltd., Japan Aerospace Exploration Agency (JAXA), Tokyo University of Agriculture and Technology.

(92) Sinterability of SiC Ceramics with $Al_4SiC_4$ Addition and Their Properties: National Institute for Materials Science (NIMS).

(93) Research on Formation and Characterization of Oxide Nanopowder : Vinca Institute, University of Belgrade, Serbia.

(94) Study on Low-Cost Process of SiC/SiC Composites: Japan Aerospace Exploration Agency (JAXA).

(95) Study on Neutron-Irradiation Resistance of Orientation-Controlled Ceramics: National Institute for Materials Science (NIMS).

# V.    List of Publications

## V. List of Publications

### Journals

(1) Rui Guo, Shigehiko Funayama, Seon Tae Kim, Takuya Harada, Hiroki Takasu, Yukitaka Kato: Hydration reactivity enhancement of calcium oxide based media for thermochemical energy storage; *Energy Storage*, (2021);3:e232.

(2) Yasunari Shinoda, Masakazu Takeuchi, Norikazu Dezawa, Yasuhiro Komo, Takuya Harada, Hiroki Takasu, Yukitaka Kato: Development of a $H_2$-permeable $Pd_{60}Cu_{40}$-based composite membrane using a reverse build-up method; *Int'l J Hydrogen Energy*, **46**(73), pp. 36291-36300 (2021)

(3) Hiroki Takasu, Takuya Nihei, Seon Tae Kim and Yukitaka Kato, "Additive Effect on Lithium Silicate Pellets for Thermochemical Energy Storage", *J. Chem. Eng. Japan*, **54**(5), 195–200 (2021).

(4) K. Morooka, E. Kurihara, M. Takehara, R. Takami, K. Fueda, K. Horie, M. Takehara, S. Yamasaki, T. Ohnuki, B. Grambow, G. T.W. Law, J. W.L. Ang, W. R. Bower, J. Parker, R. C. Ewing, & S. Utsunomiya: New highly radioactive particles derived from Fukushima Daiichi Reactor Unit 1: Properties and environmental impacts; *Science of The Total Environment*, Vol.773, 15 June 2021, 145639(2021).

(5) K. Kawamoto, H. Yokoo, A. Ochiai, Y. Nakano, A. Takeda, T. Oki, M.Takehara, M. Uehara, K. Fukuyama, Y. Ohara, T. Ohnuki, M. F. Hochella, S.Utsunomiya: The role of nanoscale aggregation of ferrihydrite and amorphous silica in the natural attenuation of contaminant metals at mill tailings sites; *Geochimica et Cosmochimica Acta*, Vol.298, 1 April 2021, pp.207-226(2021).

(6) Naofumi Kozai , Junya Sato, Takeshi Osugi, Iwao Shimoyama, Yurina Sekine, Fuminori Sakamoto, Toshihiko Ohnuki: Sewage sludge ash contaminated with radiocesium: Solidification with alkaline-reacted metakaolinite (geopolymer) and Portland cement; *Journal of Hazardous Materials*, Vol.416, 15 August 2021, 125965(2021).

(7) Hao Wu, Masahiko Nakase, Yusuke Inaba, Miki Harigai, Tohru Kobayashi, Tsuyoshi Yaita, Kenji Takeshita, Seong-Yun Kim: Complexation Studies of Eu(III) by a Novel Soft N and Hard O Donor Combined Ligand Including N,N,N',N'-Tetrakis(2-pyridylmethyl)-1,3-diaminoprop ane-2-amide Structure: UV-vis Titration, X-ray Crystallography, EXAFS Spectroscopy Analysis; *Solvent Extraction Research and Development, Japan*, Vol.28, No.1, pp.69-77(2021).

(8) Xiaoyan Wua, Wenjie Xie, Jie Chen, Xufeng Wang, Xiangfeng Liu, Yongliang Li, Ke Peng, Toshihiko Ohnuki, Jian Ye: Iodide ion removal from artificial iodine-containing solution using Ag-Ag2O modified Al2O3 particles prepared by electroless plating; *Journal of the Taiwan Institute of Chemical Engineers*, Vol.125, August 2021, pp.340-348(2021).

(9) Eriko Minari, Tomohiro Okamura, Masahiko Nakase, Hidekazu Asano, Kenji Takeshita: Evaluation of the technical options of radioactive waste management for utilization of MOX fuel: Thermal impact of Minor Actinide separation with geological disposal of high-level waste; *Journal of Nuclear Science and Technology*, Volume58, Issue10, pp.1123-1133(2021).

(10) Masashi Kaneko, Yuji Sasaki, Eriko Wada, Masahiko Nakase, Kenji Takeshita: Prediction of stability constants for novel chelates design in minor actinides partitioning over lanthanides using density functional theory calculation; *Chemistry Letters*, Vol.50, No.10, pp.1765-1769(2021).

(11) Chihiro Tabata, Masahiko Nakase, Miki Harigai, Kenji Shirasaki, Ayaki Sunaga, Tomoo Yamamura: Hydrofluorocarbon Diluent for CMPO Without Third Phase Formation: Extraction of Uranium(VI) and Lanthanide(III) Ions; *Separation Science and Technology*, Vol.57, Issue7, pp.1097-1110(2021).

(12) Bernd Grambow, Ayako Nitta, Atsuhiro Shibata, Yoshikazu Koma, Satoshi Utsunomiya, Ryu Takami, Kazuki Fueda, Toshihiko Ohnuki, Christophe Jegou, Hugo Laffolley, Christophe Journeau: Ten years after the NPP accident at Fukushima : review on fuel debris behavior in contact with water; *Journal of Nuclear Science and Technology*, Vol.59, Issue 1, pp.1-24 (2021).

(13) Hiroki Yokoo, Takumi Oki, Motoki Uehara, Ilma Dwi Winarni, Keiko Yamaji, Kenjin Fukuyama, Yoshiyuki Ohara, Toshihiko Ohnuki, Michael F. Hochella Jr., Satoshi Utsunomiya: Geochemistry of barium ions associated with biogenic manganese oxide nanoparticles generated by a fungus strain: Implications for radium sequestration in uranium mill tailings; *Gondwana Research*, Vol.110, October 2022, pp.270-282(2021).

(14) Tomohiro Okamura, Ryota Katano, Akito Oizumi, Kenji Nishihara, Masahiko Nakase, Hidekazu Asano, Kenji Takeshita: NMB4.0: Development of integrated nuclear fuel cycle simulator from the front to back-end; *The European Physical Journal Nuclear Science Technology*, Volume7, Article19, p13(2021).

(15) Tomoaki Kato, Naofumi Kozai, Kazuya Tanaka, Daniel I. Kaplan, Satoshi Utsunomiya, Toshihiko Ohnuki: Chemical species of iodine during sorption by activated carbon -Effects of original chemical species and fulvic acids; *Journal of Nuclear Science and Technology*, Vol.59, Issue 5, pp.580-589(2021).

(16) Yuji Sasaki, Masashi Kaneko, Masahiko Matsumiya, Masahiko Nakase, Kenji Takeshita: Mutual Separation of Ln and an Using TODGA and DTBA with High Organic Acid Concentrations; *Solvent Extraction and Ion Exchange*, Published online(2021).

(17) Eriko Minari, Tomohiro Okamura, Hidekazu Asano, Masahiko Nakase, Kenji Takeshita: Optimization of waste management for mixed oxide fuel in light-water reactors: Evaluation of the effectiveness of blending

spent uo2 and mixed oxide fuels in reprocessing; *Annals of Nuclear Energy*, Volume169, 5 April 2020, 121677(2021).

(18) Tomofumi Sakuragi, Tomohiro Okamura, Ryo Hamada, Hidekazu Asano, Eriko Minari, Masahiko Nakase, Kenji Takeshita, Toshiro Oniki, Midori Uchiyama: Optimal waste loading in high-level nuclear waste glass from high-burnup spent fuel for waste volume and geological disposal footprint reduction; *MRS Advances*, Vol.7, pp.150-154(2021).

(19) Takuhi Hara, Masahiko Nakase, Miki Harigai, Kenji Takeshita: Recovery and immobilization of cesium from aqueous solution after hydrothermal treatment using functional porous glass; *Journal of Nuclear Science and Technology*, Vol.59, Issue10, pp.1304-1313(2021).

(20) Shinta Watanabe, Yusuke Inaba, Miki Harigai, Kenji Takeshita, Jun Onoe: The uptake characteristics of Prussian-blue nanoparticles for rare metal ions for recycling of precious metals from nuclear and electronic wastes; *Scientific Reports*, 12, Article number: 5135(2021).

(21) Masatoshi Kondo, Susumu Hatakeyama, Naoko Oono, Takashi Nozawa, Corrosion-resistant materials for liquid LiPb fusion blanket in elevated temperature operation, Corrosion Science 197 (2022) 110070.

(22) Yukihiro Miyakawa, Masatoshi Kondo, Corrosion behaviors of various steels and nickel-based alloys in liquid Sn media, Nuclear Materials and Energy, Vol. 30, (2022) 101154.

(23) Tatsuhiro Hosaka, Masatoshi Kondo, Satoshi Sato, Masami Ando, Takashi Nozawa, "Chemical compatibility of F82H and 316L in liquid metal heat transfer mediums Li, Na and NaK", Journal of Nuclear Materials 561 (2022) 153546.

(24) Ryunosuke Nishio and Masatoshi Kondo, On-Line Measurement of Liquid Metal Level by Change of Static Gas Pressure, Plasma and Fusion Research, Volume 17, 2405085 (2022).

(25) Atsushi Kawarai and Masatoshi Kondo, Self-Healing Behavior of Oxide Layer in Liquid Metal, Plasma and Fusion Research, Volume 17, 2405059 (2022).

(26) Masatoshi KONDO, Bruce A. PINT, Jiheon JUN, Nick RUSSELL, Joel McDUFFEE, Masafumi AKIYOSHI, Teruya TANAKA, Naoko OONO, Junichi MIYAZAWA, Josina W GERINGER, Yutai KATOH and Yuji HATANO, Conceptual Design of HFIR Irradiation Experiment for Material Compatibility Study on Liquid Sn Divertor, Plasma and Fusion Research, Volume 16, 2405040 (2021).

(27) Tomohiro Kobayashi, Shota Ikeda, Yoshie Otake, Yujiro Ikeda, Noriyosu Hayashizaki: Completion of a new accelerator-driven compact neutron source prototype RANS-II for on-site use; *Nuclear Inst. and Methods in Physics Research*, **A 994**, 165091 (2021).

(28) Toshifumi Yuji, Kenichi Nakabayashi, Hiroyuki Kinoshita, Narong Mungkung, Yoshifumi Suzaki, Sarizam Mamat, Hiroshi Akatsuka : Development of Decontamination Treatment Techniques for Dry Powder Foods by Atmospheric-Pressure Nonequilibrium DC Pulse Discharge Plasma Jet; *Journal of Food Quality*, Vol. **2021**, 8896716 (2021).

(29) H. Horita, D. Kuwahara, H. Akatsuka, S. Shinohara: Estimating Electron Temperature and Density Using Improved Collisional-Radiative Model in High-Density RF Argon Plasma; *AIP Advances*, Vol.**11**, 075226 (2021).

(30) H. Akatsuka: Recent Trends in Fundamentals and Applications of Plasma Measurement Technology; *The 32nd Plasma Electronics Seminar, Plasma Process Fundamentals and Advanced Applied Technologies,* The Japan Society of Applied Physics, Plasma Electronics Subcommittee, pp. 19-38 (2021) [in Japanese].

(31) N. Yamano: Reconsidering of Risk Communication - Reconstruction of Nuclear Risk Communication; INSIGHTS CONCERNING THE FUKUSHIMA DAIICHI NUCLEAR ACCIDENT. Vol.3 pp. 124-132, 2021. ISBN 9784890471812, DOI: 10.15669/fukushimainsights.Vol.3.124.

(32) Y. Shinoda, N. Yamano: Survey of Tsuruga Inhabitants Concerning Radiation and Its Risks; INSIGHTS CONCERNING THE FUKUSHIMA DAIICHI NUCLEAR ACCIDENT. Vol.4 pp. 357-384, 2021. ISBN 9784890471829, DOI: 10.15669/fukushimainsights.Vol.4.357.

(33) Wataru Horiuchi, Tsunenori Inakura: Deformation effect on nuclear density profile and radius enhancement in light- and medium-mass neutron-rich nuclei; Progress of Theoretical Experimental and Physics 2021, 103D02, July 14, 2021.

(34) Md. S.R. Laskar, R. Palit, E. Ideguchi, T. Inakura, S.N. Mishra, F.S. Babra, S. Bhattacharya, D. Choudhury, Biswajit Das, B. Das, P. Dey, U. Garg, A.K. Jain, A. Kundu, D. Kumar, D. Negi, S.C. Pancholi, S. Rajbanshi, and S. Sihotra: Enhanced B(E3) strength observed in 137La; Physical Review C 104, L011301 (2021)., 22 July 2021.

(35) N. Yamano: Risk Communication on Health Effects of Low-dose Ionizing Radiation - Practice of Community-based Risk Communication; *INSIGHTS CONCERNING THE FUKUSHIMA DAIICHI NUCLEAR ACCIDENT*. Vol.**3** pp. 220-230, 2021. ISBN 9784890471812, DOI: 10.15669/fukushimainsights.Vol.3.220.

(36) Peng hong Liem, Y. Tahara, N. Takaki, D. Hartanto: Performance indices optimization of long-lived fission products transmutation in fast reactors; International Journal of Energy research, 2021; 1-12, September 2021.

(37) Kazuya Shimada, Chikako Ishizuka, Fedir Ivanyuk,

Satoshi Chiba: Dependence of total kinetic energy of fission fragments on the excitation energy of fissioning systems; *Physical Review C - Nuclear Physics, American Institute of Physics*, Vol. **104**, 054609, Nov. 2021.

(38) N. Yamano, T. Inakura, C. Ishizuka, S. Chiba: Crucial importance of correlation between cross sections and angular distributions in nuclear data of $^{28}$Si on estimation of uncertainty of neutron dose penetrating a thick concrete; *Journal of Nuclear Science and Technology*, Vol. **59**, No. 5, pp. 641-646, 2021. DOI: 10.1080/00223131.2021.1997665.

(39) Taiki Kouno, Chikako Ishizuka, Tsunenori Inakura, Satoshi Chiba: Pairing strength in the relativistic mean-field theory determined from the fission barrier heights of actinide nuclei and verified by pairing rotation and binding energies; *Progress of Theoretical and Experimental Physics, Oxford University Press*, Vol. **2022**, Issue 2, Dec. 2021.

(40) W. Horiuchi, T. Inakura, and S. Michimasa: Large enhancement of total reaction cross sections at the edge of the island of inversion in Ti, Cr, and Fe isotopes; *Physical Revirew C* **105**, 014316 (2022), 20 January 2022.

(41) Chikako Ishizuka, Kohsuke Tsubakihara, Satoshi Chiba, Yuichiro Sekiguchi, Shinya Wanajo: Semi-empirical fission model for r-process based on the recent experiments and three-dimensional Langevin approach; *The 16th International Symposium on Nuclei in the Cosmos (NIC-XVI)*, EPJ Web of Conferences, Vol. **260**, Feb. 2022.

(42) Kei Takakura, Koichi Nittoh, Haruo Miyadera, Kenichi Yoshioka, Yoshiji Karino, Eiki Hotta, Jun Hasegawa: Neutron imaging with an inertial electrostatic confinement fusion neutron source; *Applied Optics.*, Vol.**61**, 1238-1247 (2021).

(43) K. Takayama, T. Adachi, T. Kawakubo, K. Okamura, Yosuke Yuri, Jun Hasegawa, K. Horioka, T. Kikuchi, T. Sasaki, K. Takahashi: Review of the Massive Ion Inertial Fusion Driver for Future Inertial Fusion and our Understanding of Fusion Technology; *NIFS-PROC*, **121**, 25 (2021).

(44) Kazumasa Matsuda, Jun Hasegawa: One-dimensional PIC-MCC Analysis of Inertial Electrostatic Confinement Plasma; NIFS-PROC, **121**, 36 (2021).

(45) Takuma Jinai, Jun Hasegawa: Analysis of Cluster Ions Directly Generated from Laser Ablation Plasma Cooled in Ambient Helium Gas; NIFS-PROC, **121**, 48 (2021).

(46) Gerard Rovira, Atsushi Kimura, Shoji Nakamura, Shunsuke Endo, Osamu Iwamoto, Nobuyuki Iwamoto, Tatsuya Katabuchi, Kazushi Terada, Yu Kodama, Hideto Nakano, Jun-ichi Hori, Yuji Shibahara : Neutron beam filter system for fast neutron

cross-section measurement at the ANNRI beamline of MLF/J-PARC, *Nuclear Instruments and Methods in Physics Research A*, Vol. 1003, p. 165318 (2021).

(47) Yu Kodama, Tatsuya Katabuchi, Gerard Rovira, Atsushi Kimura, Shoji Nakamura, Shunsuke Endo, Nobuyuki Iwamoto, Osamu Iwamoto, Jun-ichi Hori, Yuji Shibahara, Kazushi Terada, Hideto Nakano, Yaoki Sato: Measurements of the neutron capture cross section of $^{243}$Am around 23.5 keV, *Journal of Nuclear Science and Technology*, Vol. 58, No. 11, pp. 1159-1164 (2021).

(48) Gerard Rovira, Tatsuya Katabuchi, Kenichi Tosaka, Shota Matsuura, Yu Kodama, H. Nakano, Osamu Iwamoto, Atsushi Kimura, Shoji Nakamura, Nobuyuki Iwamoto: KeV-region analysis of the neutron capture cross-section of $^{237}$Np, *Journal of Nuclear Science and Technology*, Vol. 59, No. 2, pp. 1-13, (2021).

(49) A. Gawlik-Ramięga, Tatsuya Katabuchi (64th author), n_TOF Collaboration (133 authors): Measurement of the $^{76}$Ge(n ,□) cross section at the n_TOF facility at CERN, *Physical Review C*, Vol. 104, 044610 (2021).

(50) Gerard Rovira, Atsushi Kimura, Shoji Nakamura, Shunsuke Endo, Osamu Iwamoto, Nobuyuki Iwamoto, Tatsuya Katabuchi, Yu Kodama, Hideto Nakano, Yaoki Sato, Jun-ichi Hori, Yuji Shibahara, Kazushi Terada: KeV-neutron capture cross-section measurement of $^{197}$Au with a Cr-filtered neutron beam at the ANNRI beamline of MLF/J-PARC, *Journal of Nuclear Science and Technology*, Vol. 59, No. 5 (2021).

(51) G. Tagliente, Tatsuya Katabuchi (64th author), n_TOF Collaboration (116 authors). $^{92}$Zr(n, □) and (n,tot) measurements at the GELINA and n_TOF facilities, Physical Review C, Vol. 105, 025805, Feb. 2022.

(52) H. Kikura, N. Shoji, H. Takahashi, W.Wongsaroj: Ultrasonic Measurement of Two-Dimensional Liquid Velocity Profile Using Two-Element Transducer; *Journal of Flow Control, Measurement & Visualization*, Vol.**10**,No.**1**, pp12-31(2022)

(53) N. Shoji, H. Kikura, H.Takahashi, W. Wongsaroj: Three-Dimensional Velocity Distribution Measurement Using Ultrasonic Velocity Profiler with Developed Transducer; *Journal of Flow Control, Measurement & Visualization*, Vol.**10**,No.**1**, pp32-55(2022)

(54) W. Wongsaroj, H.Takahashi, N. Thong-un, H. Kikura: Ultrasonic Measurement for Experimental Investigation of Velocity Distribution in Sub-Cooled Boiling Bubbly Flow; *International Journal of Engineering and Technology Innovation*, Vol.**12**,No.**1**,pp16-28 (2021)

(55) K. Shimada, R. Ikeda, H. Kikura, H.Takahashi: Morphological Fabrication of Rubber Cutaneous Receptors Embedded in a Stretchable Skin-Mimicking Human Tissue by the Utilization of Hybrid Fluid; *Sensors*, Vol.**21**,No.**20**, pp.1-26 (2021)

(56) D.Thanh Tung, N. Hoang Anh, R. Trewin, H. Kikura:

Uncertainty quantification of RELAP5/MOD3.3 for interfacial shear stress during small break LOCA; *Journal of Nuclear Science and Technology*, Vol.**7** No.**3**, pp1-7(2021).

(57) M.Batsaikhan, Z. Zhang, H.Takahashi, H. Kikura: Development of Measurement System for Flow and Shape using Array Ultrasonic Sensors; *Journal of Flow Control, Measurement & Visualization*, Vol.**9**, No.**3**, pp45-72 (2021).

(58) R. Ikeda, K. Shimada, H.Takahashi, H. Kikur: A Study on Piezoelectronic elements and Enargy Harvesting Technologies Utilizing Magnetic Compound Fluid Rubber and its Application; J*ournal of the Japan Society of Applied Electromagnetics and Mechanics,* Vol.**29**, No.**2**, pp421-426 (2021).

(59) V.Tran Tri, T.Narabayashi, H.Takahashi, H. Kikura: Effects of the Baffle Plate of Advanced Venturi Scrubber on Decontamination Factor of Filtered Containment Venting System; J*apanese Journal of Multiphase Flow*, Vol.**35**, Issue**2**, pp337-345 (2021).

(60) A. Itoh, S. Yasui, Y. Kobayashi: Estimation of reactor vessel failure by metallic interaction in Fukushima Daiichi Nuclear Power Plant accident.; *Journal of Nuclear Science and Technology*, Vol. 58, No.11, pp.1235-1243 (2021).

(61) Ryota Nakazawa, Kosuke Noguchi, Yoshinao Kobayashi: Thermodynamics of Oxygen in Molten Nd–Fe–B Alloy for Production of Low-Oxygen NdFe-B Magnet; Matetrials Transactions, J-STAGE, **Vol.63, No.2**, 185-189, Feb. 2022.

(62) Ryota Nakazawa, Kosuke Noguchi, Yoshinao Kobayashi: Thermodynamic Property of Oxygen in Nd–Dy–O System for Reduction of Dy Consumption in Nd–Fe–B Magnets; MATERIALS TRANSACTIONS,J-STAGE, **Vol.63, No.2**, p. 190-196, Feb. 2022.

(63) Zhi Li, Chisei Kato, Yoshinao Kobayashi: Determination of Solubility of Chromium Oxide in the CaO–SiO$_2$–Cr$_2$O$_3$ Slag System at 1873 K under Moderately Reducing Conditions; ISIJ International, j-stage, **Vol. 61, No.9**, pp 2340-2344, Sept. 2021.

(64) Li Zhi, C. Kato, Y. Kobayashi: Determination of Solubility of Chromium Oxide in the CaO–SiO$_2$–Cr$_2$O$_3$ Slag System at 1873 K under Moderately Reducing Condition; Tetsu-to-Hagané, J-STAGE, Vol.108, No.8, pp.449-454, July 2021.

(65) Taichi Abe, Masao Morishita, Ying Chen, Arkapol Saengdeejing, Kiyoshi Hashimoto, Yoshinao Kobayashi, Ikuo Ohnuma, Toshiyuki Koyama, Satoshi Hirosawa: Development of a prototype thermodynamic database for Nd-Fe-B permanent magnets; Science and Technology of Advanced Materials, June 2021.

(66) Tomoko Miyake, Munekazu Kuge, Yoshihisa Matsumoto, Mikio Shimada:α-glucosyl-rutin activates immediate early genes in human induced pluripotent stem cells; *Stem Cell Research*, Vol. **56**:102511 (2021).

(67) Hideki Matsumoto, Yoshiya Shimada, Asako J Nakamura, Noriko Usami, Mitsuaki Ojima, Shizuko Kakinuma, Mikio Shimada, Masatoshi Sunaoshi, Ryoichi Hirayama, Hiroshi Tauchi: Health effects triggered by tritium: how do we get public understanding based on scientifically supported evidence?; *Journal of Radiation Research*, Vol. **62**, No.4, pp.557-563 (2021)

(68) Anie Day D.C. Asa, Rujira Wanotayan, Mukesh Kumar Sharma, Kaima Tsukada, Mikio Shimada, Yoshihisa Matsumoto: Functional Analysis of XRCC4 Mutations in Reported Microcephaly and Growth Defect Patients in Termsof Radiosensitivity: *Journal of Radiation Research*, Vol. **62**, No.4, pp.557-389 (2021)

(69) Tomoko Miyake and Mikio Shimada (corresponding author)3D organoid culture using skin keratinocytes derived from human induced pluripotent stem cells: *Methods in Molecular Biology*, 2454, 285-295 (2021).

(70) Hisayo Tsuchiya, Mikio Shimada, Kaima Tsukada, Qingmei Meng, Junya Kobayashi, *Yoshihisa Matsumoto. Dose-rate effect; DNA double-strand break repair; Non-homologous end joining; Ku; DNA-PKcs: Journal of Radiation Research, Vol. **62**, No.2, pp.198-205 (2021).

(71) Yoshihisa Matsumoto*, Anie Day DC Asa , Chaity Modak and Mikio Shimada. DNA-dependent protein kinase catalytic subunit: the sensor for DNA double-strand breaks structurally and functionally related to Ataxia telangiectasia mutated. *Genes*, Vol. **12**, No.8, 1143 (2021).

(72) Hiroyasu Mochizuki: Verification of neutronics and thermal-hydraulics coupling method for FLUENT code using the MSRE pump startup, trip data; *Nuclear Engineering and Design,* 378 (2021), 111191.

(73) M. Yamawaki, H. Mochizuki, T. Koyama, Y. Arita, K. Mitachi, Y. Shimazu, M. Kinoshita, R. Yoshioka: Development Status of Molten Salt Reactor; *Journal of the Atomic Energy Society of Japan ATOMOΣ*, **63**, 11, (2021), 791-796.

(74) Hiroyasu Mochizuki: Validation of neutronics and thermal-hydraulics coupling model of the RELAP5-3D code using the MSRE reactivity insertion tests; *Nuclear Engineering and Design*, **389**, (2022), 111669.

(75) Hiroyasu Mochizuki, Study of thermal-hydraulics of a sinusoidal layered heat exchanger for MSR, *Nuclear Engineering and Design,* **396**, (2022), 111900.

(76) Hiroki Takezawa, Delgersaikhan Tuya, Toru Obara; Calculation of Transient Parameters of the Integral Kinetic Model with Delayed Neutrons for Space-dependent Kinetic Analysis of Coupled Reactors: *Nuclear Science and Engineering*, Vol. **195**, pp. 1236-1246 (2021).

(77) Takeshi Muramoto, Jun Nishiyama, Toru Obara; Characteristics of reactivity change as fuel debris falls in water: *Progress in Nuclear Energy*, Vol. **139**, 103857 (2021).

(78) Kodai Fukuda, Jun Nishiyama, Toru Obara; Supercritical Transient Analysis for Ramp Reactivity Insertion Using Multiregion Integral Kinetics Code: *Nuclear Science and Engineering*, Vol. **195**, pp.453-463 (2021).

(79) Hoang Hai Nguyen, Jun Nishiyama, Toru Obara; Optimization of reactor size in the small sodium-cooled CANDLE burning reactor: *Annals of Nuclear Energy*, Vol. **153**, 108040 (2021).

(80) K. Kobayashi, H. Mita, Y. Kebukawa, K. Nakagawa, T. Kaneko, Y. Obayashi, T. Sato, T. Yokoo, S. Minematsu, H. Fukuda, Y. Oguri, I. Yoda, S. Yoshida, K. Kanda, E. Imai, H. Yano, H. Hashimoto, S. Yokobori, A. Yamagishi: Space Exposure of Amino Acids and their Precursors during the Tanpopo Mission; *Astrobiology* Vol. **21**, No. 12, pp. 1479-1493 (2021).

(81) Shigeki Shiba and Hiroshi Sagara: Passive gamma emission tomography with ordered subset expectation maximization method; *Annals of Nuclear Energy*, Vol. 150, #107823, P.1-7, 2021.

(82) Kim Wei Chin, Hiroshi Sagara, Chi Young Han: Application of photofission reaction to identify high-enriched uranium by bremsstrahlung photons; Annals Nuclear Energy, Vol. 158, 108295, 2021.

(83) Natsumi Mitsuboshi, Hiroshi Sagara: Effects of U3Si2 fuel and minor actinide doping on fundamental neutronics, nuclear safety, and security of small and medium PWRs in comparison to conventional UO2 fuel; *Annals, Nuclear Energy*, Vol. 153, 108078, 2021.

(84) Shigeki Shiba and Hiroshi Sagara, "Iterative Reconstruction Algorithm Comparison Using Poisson Noise Distributed Sinogram Data in Passive Gamma Emission Tomography,"*J. Nucl. Sci. Technol.*, Vol. 58, Issue 6, Pages 659-666, 2021.

(85) Kim Wei Chin, Rei Kimura, Hiroshi Sagara, Kosuke Tanabe, On the Numerical Method for Photofission-Based Nuclear Material Isotopic Composition Estimation in Thorium-Uranium Systems, *NUCL. SCI. ENG.*, VOL. 196, No. 7, P. 852–872, (2022).

(86) S. Naito, M. Murayama, S. Hatakeyama, D. Kuwahara, Y. Suzuki, H. Tsutsui and S. Tsuji-Iio: Stabilization of vertical plasma position in the PHiX tokamak with saddle coils; *Nuclear Fusion*, Vol.**61**, No.11, 116035 (2021).

(87) Koyo MUNECHIKA, Hiroaki TSUTSUI, Shunji TSUJI-IIO: Visible Light Tomography Considering Reflection Light in a Small Tokamak Device PHiX; *Plasma and Fusion Research*, Vol. 1**6**, 2402033 (2021).

(88) Hiroshi Naganuma, Masahiko Nishijima, Hayato Adachi, Mitsuharu Uemoto, Hikari Shinya, Shintaro Yasui, Hitoshi Morioka, Akihiko Hirata, Florian Godel, Marie-Blandine Martin, Bruno Dlubak, Pierre Seneor, Kenta Amemiya: Unveiling a Chemisorbed Crystallographically Heterogeneous Graphene/L10-FePd Interface with a Robust and

(89) Ankit Singh, Shintaro Yasui, Avnish Singh Pal, Leonid A. Bendersky, Ichiro Takeuchi, R. K. Mandal, Joysurya Basu: Structure and interfaces of compositionally graded Li(Ni, Mn)$_x$O$_y$ cathodes on (111) Nb-doped SrTiO$_3$; *Philosophical Magazine*, Vol. **102**, pp. 1547-1579 (2022).

(90) Koki Kamimizutaru, Akira Nagaoka, Yusuke Shigeeda, Kensuke Nishioka, Tomohiro Higashi, Shintaro Yasui, and Kenji Yoshino: Chimney-ladder sulfide Sr9Ti8S24 as a thermoelectric material with low thermal conductivity; *J. Phys. Chem. Solids*, Vo. **163**, p.110589 (2022).

(91) Yosuke Hamasaki, Shintaro Yasui, Tsukasa Katayama, Takanori Kiguchi, Shinya Sawai, and Mitsuru Itoh: Ferroelectric and magnetic properties in $\varepsilon$-Fe$_2$O$_3$ epitaxial film; *Appl. Phys. Lett.*, Vol. **119**, p. 182904 (2021).

(92) Y. Kawahara, R. Harada, S. Maruyama, T. Koganezawa, S. Yasui, M. Itoh, and Y. Matsumoto: Epitaxial piller-matrix nano composite thin films of Bi-Ti-Fe-O and CoFe$_2$O$_4$ grown on SrTiO$_3$ (110); *J. Appl. Phys.*, Vol. **130**, pp. 084101-1-9 (2021).

(93) Yang Zhang, Hui Wang, Koki Tachiyama, Tsukasa Kaytayama, Yinghao Zhu, Si Wu, Hai-feng Li, Jinghong Fang, Qin Li, Yun Shi, Ling Wang, Zhengqian Fu, Fangfang Xu, Jianding yu, Shintaro Yasui, and Mitsutu Itoh: Single-Crystal Synthesis of $\varepsilon$-Fe$_2$O$_3$-Type Oxides Exhibiting Room- Temperature Ferrimagnetism and Ferroelectric Polarization; *Cryst. Growth Des.*, Vol. **21**, pp. 4904-4908 (2021).

(94) Sou Yasuhara, Shitnaro Yasui, Takashi Teranishi, Takuya Hoshina, Takaaki Tsurumi, and Mitsuru Itoh: A surface-supporting method for an anode material of Li$_4$Ti$_5$O$_{12}$ via an epitaxial thin film approach; *Jpn. J. Appl. Phys.*, Vol. **60**, pp. SFFB11-1-4 (2021).

(95) Sou Yasuhara, Shintaro Yasui, Takashi Teranishi, Osami Sakata, Takuya Hoshina, Takaaki Tsurumi, Yutaka Majima, and Mitsuru Itoh: Suppression Mechanisms of Solid Electrolyte Interface Formation at Triple-phase Interfaces in Thin Film Li-ion Batteries; *ACS Appl. Mater. Interfaces*, Vol. **13**, pp. 34027-34032 (2021).

(96) Tsukasa Katayama, Akira Chikamatsu, Yujun Zhang, Shintaro Yasui, Hiroki Wadati, and Tetsuya Hasegawa: Ionic Order Engineering in Double-Perovskite Cobaltite; *Chem. Mater.*, Vol. **33**, pp. 5675-5680 (2021).

(97) Vivek Paulraj, Shintaro Yasui and Kamala Bharathi Karuppanan: Excellent Electrochemical Properties, Li ion Dynamics and Room Temperature Work Function of Li$_2$MnO$_3$ Cathode Thin Films; *Nanotechnology*, Vol. **32**, pp. 385406-1-8 (2021).

(98) Ayumi Itoh, Shintaro Yasui and Yoshinao Kobayashi: Estimation of reactor vessel failure by metallic interaction in Fukushima Daiichi Nuclear Power Plant accident; *J. Nucl. Sci. Tech.*, Vol. **58**, pp. 1235-1243

(2021).

(99) Takashi Teranishi, Kaisei Kozai, Sou Yasuhara, Shintaro Yasui, Naoyuki Ishida, Kunihiro Ishida, Masanobu Nakayama, Akira Kishimoto; Ultrafast charge transfer at the electrode-electrolyte interface via an artificial dielectric layer; *J. Power Sources*, Vol. **494**, p. 229710 (2021).

(100) Hiroaki Ashizawa, Katsumi Yoshida, "Investigation of fluoride layer of yttria coatings prepared by aerosol deposition method," *Journal of the Ceramic Society of Japan*, Vol.129, No. 1, pp.46-53 (2021).

(101) Thanataon Pornphatdetaudom, Katsumi Yoshida, Toyohiko Yano, "Recovery behavior of neutron-irradiated aluminum nitride with and without containing interstitial dislocation loops," *Journal of Nuclear Materials*, Vol. 543, 152584 (2021).

(102) Takashi Akatsu, Dong Hao, Anna Gubarevich, Katsumi Yoshida: Flexural strength of alumina-strengthened porcelain with both small water absorption and small pyroplastic deformation; *Journal of the Ceramic Society of Japan*, Vol. **129**, No. 3, pp. 195-199, (2021).

(103) Shota Azuma, Tetsuo Uchikoshi, Katsumi Yoshida, Tohru S. Suzuki, "Fabrication of textured $B_4C$ ceramics with oriented tubal pores by strong magnetic field-assisted colloidal processing," *Journal of the European Ceramic Society*, Vol. 41, No. 4, pp.2366-2374 (2021).

(104) Branko Matović, Jelena Maletaškić, Tatiana Prikhna, Vladimir Urbanovich, Vladimir Girman, Maksym Lisnichuk, Bratislav Todorović, Katsumi Yoshida, Ivana Cvijović-Alagić, "Characterization of $B_4C$-SiC ceramic composites prepared by ultra-high pressure sintering," *Journal of the European Ceramic Society*, Vol. 41, No. 9, pp.4775-4760 (2021).

(105) Karthikeyan Ramachandran, Zuccarini Carmine, Katsumi Yoshida, Toru Tsunoura, Doni Daniel Jayaseelan, "Experimental investigation and mathematical modelling of water vapour corrosion of $Ti_3SiC_2$ and $Ti_2AlC$ ceramics and their mechanical behavior," Journal of the European Ceramic Society, Vol. 41, No. 9, pp.4761-4773 (2021).

**International Conference Proceedings**

(1) Shigehiko Funayama, Takahiro Furuya, Hiroki Takasu, Yukitaka Kato, Development of composite materials using calcium hydroxide and silicon-silicon carbide ceramic supports for high-temperature thermochemical energy storage, *The First Symposium on Carbon Ultimate Utilization Technologies for the Global Environment (CUUTE-1)*, 15(14-17) Dec., 2021, Nara.

(2) Yasunari Shinoda, Masakazu Takeuchi, Hiroki Takasu, Yukitaka Kato, Development of Metal Composite Hydrogen Permeable Membrane by Reverse Build-up Method, *The First Symposium on Carbon Ultimate Utilization Technologies for the Global Environment (CUUTE-1)*, 15(14-17) Dec., 2021, Nara.

(3) Saki Yoshida, Junko Kaneko, Hiroki Takasu, Yukitaka Kato, Evaluation of chemical heat pump performance of magnesium chloride and ammonia system, *The First Symposium on Carbon Ultimate Utilization Technologies for the Global Environment (CUUTE-1)*, 15(14-17) Dec., 2021, Nara

(4) Sho Kuzukami, Yuko Maruyama, Shuzo Tominaga, Hiroki Takasu, Yukitaka Kato, Electrolysis performance of a metal supported-solid oxide electrolysis cell for low-carbon iron making process, *The First Symposium on Carbon Ultimate Utilization Technologies for the Global Environment (CUUTE-1)*, 15(14-17) Dec., 2021, Nara

(5) Rui Guo, Shigehiko Funayama, Hiroki Takasu, Yukitaka Kato, Study on composite material in thermochemical energy storage system for iron and steel making industry, *The First Symposium on Carbon Ultimate Utilization Technologies for the Global Environment (CUUTE-1)*, 15(14-17) Dec., 2021, Nara.

(6) Y. Kato, [Plenary Lecture] "Renaissance of Thermal Energy Storage for Carbon Neutral Society", *the Second Asian Conference on Thermal Sciences(2nd ACTS)*, Oct. 4(3-7), 2021, Online.

(7) S. Funayama, T. Harada, H. Takasu, Y. Kato: Optimal volume fraction of support material in a heat transfer-enhanced composite for thermochemical energy storage; *HEAT POWERED CYCLES CONFERENCE 2021*, Bilbao, Spain, September 20(19-22), 2021

(8) Yasunari Shinoda, Masakazu Takeuchi, Hikaru Mizukami, Takuya Harada, Hiroki Takasu, Yukitaka Kato, Development of an H2-permeable, PdCu-based, composite membrane by using a reverse build-up method, EES materials / applications #102, *ENERSTOCK*, June 10 (9 -11), 2021, Ljubljana, Slovenia.

(9) Saki Yoshida, Junko Kaneko, Hiroki Takasu, Yukitaka Kato, Reactivity assessment of magnesium chloride and ammonia for chemical heat pump applications, TES material #23, *ENERSTOCK*, June 9 -11, 2021, Ljubljana, Slovenia.

(10) Eriko Minari, Satsuki Kabasawa, Morihiro Mihara, Hitoshi Makino, Hidekazu Asano, Masahiko Nakase, Kenji Takeshita: Impact of Utilization of MOX Fuel in LWRs on the Long-term Safety for Geological Disposal of HLWs; *Proceedings of WM2022, Waste Management symposia 2022*, Phoenix, Arizona, March 6-10, 2022.

(11) Yukihiro Miyakawa, Minho O, Masatoshi Kondo, [17Ce7] Alloying corrosion kinetics of Reduced-activation ferritic (JLF-1) in Liquid metal tin (Sn) for liquid divertor concepts, The 30th International Toki Conference on Plasma and Fusion Research, Book of Abstracts, Nov. 2021.

(12) Ryunosuke Nishio, Masatoshi Kondo, [17Ce3] Experimental study on liquid metal level monitoring by change of cover gas pressure, The 30th International Toki Conference on Plasma and Fusion Research, Book of Abstracts, Nov. 2021.

(13) Atsushi Kawarai, Masatoshi Kondo, [17Ce2] Self-healing behavior of oxide-layer in liquid metal, The 30th International Toki Conference on Plasma and Fusion Research, Book of Abstracts, Nov. 2021.

(14) M. Kondo, M. Onoi, S. Morokoshi, T. Yonemoto, Y. Kitamura, M. Kibayashi, S. Hatakeyama, Y. Miyakawa, N. Oono, S. Ukai, [Invited presentation, 16Ca1] Technological evolution on corrosion resistant materials for liquid Sn divertor of fusion reactors, The 30th International Toki Conference on Plasma and Fusion Research, Book of Abstract, Nov. 2021.

(15) Y.Ueda, R. Kasada, M. Sakamoto, S. Higashijima, N. Ohno, M. Osakabe, M. Kondo, [Invited presentation, 16Caw] Development of Japanese DEMO, The 30th International Toki Conference on Plasma and Fusion Research, Book of Abstract, Nov. 2021.

(16) Y. Kitamura, M. Kibayashi, M. Onoi, S. Morokoshi, T. Yonemoto, Y. Tamai, M. Kondo, [16Ca4] Corrosion characteristics of additive-manufactured FeCrNiAl alloy in liquid metals PbBi, LiPb and Sn, The 30th International Toki Conference on Plasma and Fusion Research, BooK of Abstracts, Nov. 2021.

(17) Masatoshi Kondo, Katsuya Murakami, Yuki Kano, Yukihiro Miyakawa, Nobuhiro Chijiwa, Minho O, Teruya Tanaka, Experimental study on chemical compatibility between liquid metals and concrete materials, 20th International conference on fusion reactor materials (ICFRM-20), Book of Abstract, Oct. 2021.

(18) B. A. Pint, Jiheon Jun, Masatoshi Kondo, Naoko Oono, Kan Sakamoto, Yuji Hatano, COMPATIBILITY OF FeCrAl IN FLOWING Sn AT 400 degree C, 20th International conference on fusion reactor materials (ICFRM-20), Book of Abstract, Oct. 2021.

(19) Tatsuhiro Hosaka, Sato Satoshi, Masami Ando, Takashi Nozawa, Experimental study on corrosion inhibitor for liquid metal heat transfer mediums of A-FNS irradiation capsule, 20th International conference on fusion reactor materials (ICFRM-20), Book of Abstract, Oct. 2021.

(20) Susumu Hatakeyama, Masatoshi Kondo, Naoko Oono, Ryuta Kasada, Kan Sakamoto, Teruya Tanaka, Corrosion resistance of FeCrAl-ODS alloys in impeller induced liquid lead lithium flow, 20th International conference on fusion reactor materials (ICFRM-20), Book of Abstract, Oct. 2021.

(21) Yukihiro Miyakawa, Masatoshi Kondo, Teruya Tanaka, Experimental study on chemical compatibility of liquid tin (Sn) with various steels for liquid divertor concepts, 20th International conference on fusion reactor materials (ICFRM-20),

Boook of Abstract, Oct. 2021.

(22) Masatoshi Kondo, Naoko Oono, Teruya Tanaka, Masafumi Akiyoshi, Ryuta Kasada, Kan Sakamoto, Susumu Hatakeyama, Yukihiro Miyakawa, Bruce Pint, Jiheon Jun, Junichi Miyazawa, Yuji Hatano, Chemical compatibility issues and challenges on advanced liquid metal components of fusion reactors, 20th International conference on fusion reactor materials (ICFRM-20), Book of Abstract, Oct. 2021.

(23) Masatoshi Kondo, Takuya Nagasaka, Yukihiro Miyakawa, Susumu Hatakeyama, Chemical compatibility of dissimilar-metal joint in liquid breeders, 38th JSPF Annual Meeting, Book of Abstract, Nov. 2021.

(24) Yukihiro Miyakawa, Masatoshi Kondo, Naoko Oono, Ryuta Kasada, Yu Hao, Kan Sakamoto, Teruya Tanaka, [1L02] Chemical compatibility of ODS FeCrAl alloys for liquid Sn divertor concepts, The atomic energy society of Japan, 2021 Fall meeting, The atomic energy society of Japan, Fall meeting, Book of Abstract, Sept. 2021.

(25) Tatsuhiro Hosaka, Masatoshi Kondo, Satoshi Sato, Masami, Takashi Nozawa, [1L03] Corrosion behaviors of F82H steel in liquid metal heat transfer mediums Li, Na, and, NaK of A-FNS, The atomic energy society of Japan, 2021 Fall meeting, The atomic energy society of Japan, 2021 Fall meeting, Book of Abstract, Sept. 2021.

(26) Ryunosuke Nishio, Masatoshi Kondo, [1L04] On-line monitoring of liquid metal level through change of static gas pressure, The atomic energy society of Japan 2021 Fall meeting, The atomic energy society of Japan, Book of Abstract, Sept. 2021.

(27) Masatoshi Kondo, Ryunosuke Nishio, Susumu Hatakeyama, Naoko Oono, Teruya Tanaka, [3L02] Investigation of liquid test blanket module for DEMO reactor, (2) Evolution of interface technology for MHD pressure drop reduction in self-cooled LiPb TBM, The atomic energy society of Japan, 2021 Fall meeting, The atomic energy society of Japan, Book of Abstract, Sept. 2021.

(28) Masatoshi Kondo, Masahiro Onoi, Shotarou Morokoshi, *Yoshiki Kitamura, Yoshie Tamai, Tomohiro Yonemoto. [1L01] Liquid metal compatibility with Al-containing steel fabricated by additive manufacturing, The atomic energy society of Japan, 2021 Fall meeting, The atomic energy society of Japan, Book of Abstract, Sept. 2021.

(29) Teruya Tanaka, Masatoshi Kondo, et al., [3L01] Investigation of liquid test blanket module for DEMO reactor (1) Design investigation of self-cooled LiPb module, The atomic energy society of Japan, 2021 Fall meeting, The atomic energy society of Japan, Book of Abstract, Sept. 2021.

(30) Masatoshi Kondo, Ryunosuke Nishio, Susumu Hatakeyama, Naoko Oono, Teruya Tanaka, [3L02] Investigation of liquid test blanket module for

DEMO reactor (2) Evolution of interface technology for MHD pressure drop reduction in self-cooled LiPb TBM, The atomic energy society of Japan, 2021 Fall meeting, The atomic energy society of Japan, Book of Abstract, Sept. 2021 .

(31) Yoshiki Kitamura, Masato Kibayashi, Masatoshi Kondo et al., [1L08] Study on applicability of Additive Manufactured steels for liquid metal components on fusion reactors (2) Corrosion resistance of Al-containing Additive Manufactured steels, The atomic energy society of Japan, The atomic energy society of Japan, 2022 Annual meeting, Book of Abstract, Mar. 2022.

(32) Haruya Masaki, Masatoshi Kondo, Jae-Hwan Kim, Masaru Nakamichi, [1L11] Study on fretting corrosion in solid breeder blanket, The atomic energy society of Japan, The atomic energy society of Japan, 2022 Annual meeting, Book of Abstract, Mar. 2022.

(33) Tatsuhiro Hosaka, Masatoshi Kondo, Satoshi Sato, Masami Ando, [1L03] Experimental study on improvement of material compatibility by using corrosion inhibitor for liquid metal heat transfer mediums of A-FNS irradiation capsule, The atomic energy society of Japan, 2022 Annual meeting, The atomic energy society of Japan Book of Abstract, Mar. 2022.

(34) Susumu Hatakeyama, Yukihiro Miyakawa, Yoshimitsu Hishinuma, Masatoshi Kondo, Teruya Tanaka, Naoko Oono, [1L04] Study on applicability of FeCrAl alloys for liquid metal components in fusion reactors (1) Formation behavior of oxide layer on FeCrAl alloys, The atomic energy society of Japan, 2022 Annual meeting, Mar. 2022.

(35) Ryunosuke Nishio, Masatoshi Kondo, Teruya Tanaka, Naoko Oono, [1L05] Study on applicability of FeCrAl alloys for liquid metal components in fusion reactors (2) Mitigation of MHD pressure drop by self-healing oxide layer, The atomic energy society of Japan, The atomic energy society of Japan, 2022 Annual meeting Book of Abstract, Mar. 2022.

(36) Yukihiro Miyakawa, Masatoshi Kondo, Teruya Tanaka, Naoko Oono, [1L06] Study on applicability of FeCrAl alloys for liquid metal components on fusion reactors (3) Applicability of FeCrAl alloys in liquid diverter concepts, The atomic energy society of Japan, 2022 Annual meeting, The atomic energy society of Japan, 2022 Annual meeting Book of Abstract, Mar. 2022.

(37) Yuga Nakazawa, Hiromi Iinuma, Yoshihisa Iwashita , Yoshiyuki Iwata , Ersin Cicek, Masashi Otani, Naritoshi Kawamura, Ryo Kitamura, Yasuhiro Kondo, Naohito Saito, Yuki Sue, Yusuke Takeuchi, Kazuo Hasegawa, Noriyosu Hayashizaki, Tsutomu Mibe, Takatoshi Morishita, Hiromasa Yasuda, Takayuki Yamazaki, Mitsuhiro Yoshida and Mai Yotsuzuka: Multipacting simulations of coaxial coupler for IH-DTL prototype in muon accelerator; *JPS Conf. Proc.*, **33**, 011128 (2021).

(38) Y. Nakazawa, H. Iinuma, Y. Iwata, M. Otani, N. Kawamura, T. Mibe, E. Cicek, T. Yamazaki, M Yoshida, R. Kitamura, Y. Kondo, T. Morishita, N. Saito, Y. Sue, K. Sumi, M. Yotsuzuka, Y. Takeuchi, N. Hayashizaki, H. Yasuda: Development of an APF IH-DTL in the J-PARC muon g -2/EDM experiment; *Proceedings of the 12th International Particle Accelerator Conference (IPAC'21)*, pp. 2544-2547 (2021).

(39) Yuya Yamashita, Takuya Akiba, Toshihide Iwanaga, Shuichi Date, Hidehiko Yamaoka, Hiroshi Akatsuka: The Plasma Diagnosis of 133 Pa Argon Microwave Discharge Plasma by Optical Emission Spectroscopic Measurement Based on Systematic Excitation-Kinetics Analysis; 4*2nd International Symposium on Dry Process (DPS42)*, ZOOM Meeting, November 18-19, 2021, pp. 57-58, P-9

(40) Yusuke Tsuchiya, Atsushi Nezu, Hiroshi Akatsuka: Effect of Metastable Quenching by Oxygen Admixture on Excited-State Populations of Low-Pressure Ar Plasma; *42nd International Symposium on Dry Process (DPS42)*, ZOOM Meeting, November 18-19, 2021, pp. 59-60, P-10.

(41) Keren Lin, Atsushi Nezu, Hiroshi Akatsuka: Diagnostics of Electron Density and Temperature of Atmospheric Pressure Helium Plasma Based on Collisional-Radiative Model; *42nd International Symposium on Dry Process (DPS42)*, ZOOM Meeting, November 18-19, 2021, pp. 61-62, P-11.

(42) Yuta Kuzuki, Atsushi Nezu, Hiroshi Akatsuka: Effect of Electron Energy Distribution Function on Spectroscopic Measurement of Excited-State Densities of Non-Equilibrium Argon Plasma; *42nd International Symposium on Dry Process (DPS42)*, ZOOM Meeting, November 18-19, 2021, pp. 63-64, P-12.

(43) Takuma Jinnai, Jun Hasegawa: Dependence of Pre-charged Ion Flux from a Laser Ablation Cluster Source on Background Gas Stream Conditions; *The 38th Annual Meeting of Japan Society of Plasma Science and Nuclear Fusion Research*, Nagoya, Nov. 22-25, 23Ap05 (2021).

(44) Kazuhiro Matsuda, Jun Hasegawa: Discharge Analysis of linear Inertial Electrostatic Confinement Plasma with PIC-MCC; *The 37th Annual Meeting of Japan Society of Plasma Science and Nuclear Fusion Research*, Nagoya, Nov. 22-25, 22P-1F-07 (2021).

(45) Yuji Inoue, Jun Hasegawa, Takuma Jinnai, Kazumasa Takahashi, Jun Tamura, Ken Takayama: Characteristics of Highly Charged Carbon Ions from a Laser Ion Source Using a Cryogenic Target; The 37th Annual Meeting of Japan Society of Plasma Science and Nuclear Fusion Research, Nagoya, Nov. 22-25, 22P-1F-07 (2021).

(46) K. Takayama, T. Adachi, T. Kawakubo, K. Okamura, Yosuke Yuri, Jun Hasegawa, K. Horioka, T. Kikuchi, T. Sasaki, K. Takahashi: Review of the Massive Ion Inertial Fusion Driver for Future Inertial Fusion and

our Understanding of Fusion Technology; NIFS Collaborative Research Symposium on "Frontier of Advanced Pulsed Power Technology and its Application to Plasma and Particle Beam", Toki, Jan. 11-12 (2022).

(47) Kazuhiro Matsuda, Jun Hasegawa: Analysis of Inertial Electrostatic Confinement Plasma Using One-Dimensional PIC-MCC Simulation; *NIFS Collaborative Research Symposium on "Frontier of Advanced Pulsed Power Technology and its Application to Plasma and Particle Beam", Toki, Jan. 11-12 (2022).*

(48) Jun Hasegawa, Ken Takayama: Beam loss due to In-beam charge exchange in the massive ion ICF driver; *NIFS Collaborative Research Symposium on "Frontier of Advanced Pulsed Power Technology and its Application to Plasma and Particle Beam"*, Toki, Jan. 11-12 (2022).

(49) Yuji Inoue, Jun Hasegawa, Takuma Zinnai, Kazuhiko Horioka, Kazumasa Takahashi, Jun Tamura, Ken Takayama: Research on Laser Ablation of Cryogenic CO2 Targets; *NIFS Collaborative Research Symposium on "Frontier of Advanced Pulsed Power Technology and its Application to Plasma and Particle Beam"*, Toki, Jan. 11-12 (2022).

(50) Chi Young HAN, Hiroshi SAGARA, Tatsuya KATABUCHI, Hiroshige KIKURA, Yoshihisa MATSUMOTO, Kenji TAKESHITA, Koichiro TAKAO, Satoshi CHIBA. The Advanced Nuclear 3S Education and Training (ANSET) Program of Tokyo Tech: (2) 3S Exercises, The INMM & ESARDA Joint Annual Meeting, Proceedings of the INMM & ESARDA Joint Annual Meeting, Aug. 2021.

(51) Hiroshi SAGARA, Chi Young HAN, Satoshi CHIBA, Yoshihisa MATSUMOTO, Noriyosu HAYASHIZAKI, Masako IKEGAMI, Akira OMOTO, Kenji TAKESHITA, Tatsuya KATABUCHI, Hiroshige KIKURA, Koichiro TAKAO. The Advanced Nuclear 3S Education and Training (ANSET) Program of Tokyo Tech: (1) Overview, The INMM & ESARDA Joint Annual Meeting, Proceedings of the INMM & ESARDA Joint Annual Meeting, Aug. 2021.

(52) S.Kai, H.Takahashi, H.Taniguchi, A.Kawashima, H. Takahashi, K. Jinza, H. Kikura: Study on Decontamination Effect of Shot Blasting and Barrel Polishing System; *The 16th International Symposium on Advanced Science and Technology in Experimental Mechanics (ISEM'21)*, November 3-6,2021, Online Conference.

(53) Z. Zhang, T.Liu, M.Batsaikhan, H.Takahashi, H.Kikura: Development of Ultrasonic Measurement System for Shape and 2D Velocity Field Using Ultrasonic Velocity Profiler and Total Focusing Methods; *28th International Conference on Nuclear Engineering (ICONE28)*, August 4-6,2021, Online Conference, ICONE28-64510.

(54) Z.Zhang, N.Shoji, M.Batsaikhan, H.Takahashi,

W.Wongsaroj, H.Kikura: Telemetry System for 2D Flow Map Using Ultrasonic Velocity Profiler; *2021 IEEE International IOT, Electronics and Mechatronics Conference (IEMTRONICS)*, July 1-4,2021, Online Conference, No.149,pp901.

(55) H.Takahashi, N.Shoji, G.Endo, I.Wakaida, H.Kikura: Fundamental Study on Remote Investigation in Fukushima Daiichi Nuclear Power Plant by Advanced Super Dragon Articulated Robot Arm; 13th *International Symposium on Ultrasonic Doppler Methods for Fluid Mechanics and Fluid Engineering (ISUD13)*, June 13-15,2021, Hybrid Conference, Proceedings pp. AC18.

(56) N.Shoji, H.Takahashi, H.Kikura: Development of Advanced UVP Instruments Applicable to 3-D Velocity Vector Measurement; *13th International Symposium on Ultrasonic Doppler Methods for Fluid Mechanics and Fluid Engineering (ISUD13)*, June 13-15,2021, Hybrid Conference, Proceedings pp.72-76.

(57) W. Wongsaroj, H.Takahashi, N.Thong-Un, H.Kikura: The Development of Ultrasonic Velocity Profiler for Velocity Vector Measurement in Bubbly Flow; *13th International Symposium on Ultrasonic Doppler Methods for Fluid Mechanics and Fluid Engineering (ISUD13)*, June 13-15,2021, Hybrid Conference, Proceedings pp.76-79.

(58) S. Sayidatun Nisa Sailellah, H.Takahashi, H.Kikura: The Development of Soluminescence Elemental Analysis,Case Study: Na and Sr in Aqueous Solution; *13th International Symposium on Ultrasonic Doppler Methods for Fluid Mechanics and Fluid Engineering (ISUD13)*, June 13-15,2021, Hybrid Conference, Proceedings pp.60-63.

(59) T.Moriya, H.Kikura, H.Takahashi: Basic Study on Ultrasonic Remote Leakage Position Estimation Method for Underwater Exploration; *13th International Symposium on Ultrasonic Doppler Methods for Fluid Mechanics and Fluid Engineering (ISUD13)*, June 13-15,2021, Hybrid Conference, Proceedings pp.52-55.

(60) Z. Zhang, M.Batsaikhan, H.Takahashi, H.Kikura: Measurement System for Flow Mapping and Shape Detection using Sectorial Array Sensors; *13th International Symposium on Ultrasonic Doppler Methods for Fluid Mechanics and Fluid Engineering (ISUD13)*, June 13-15,2021, Hybrid Conference, Proceedings pp.96-99.

(61) N.Shoji, H.Takahashi, H.Kikura: Ultrasonic Measurement of Multi-Dimensional Velocity Vector Plofile Using Array Tranceducer; *11th International Conference on Advances in Fluid Dynamics with emphasis on Multiphase and Complex Flow (AFM/MPF 2021)*, April 21-24,2021, Online Conference, WIT Transactions on Engineering Science Vol.132, pp.153-164.

(62) Hiroshi Sagara, "Nuclear nonproliferation and security research and education at Tokyo Tech," *the*

*international forum on peaceful use of nuclear energy, nuclear non-proliferation and nuclear security, "Nuclear Non-proliferation and nuclear security in the post COVID-19 era,"* online, Dec. 15, 2021

(63) Hiroshi SAGARA, Chi Young HAN, Satoshi CHIBA, Yoshihisa MATSUMOTO, Noriyosu HAYASHIZAKI, Masako IKEGAMI, Akira OMOTO, Kenji TAKESHITA, Tatsuya KATABUCHI, Hiroshige KIKURA, and Koichiro TAKAO: The Advanced Nuclear 3S Education and Training (ANSET) Program of Tokyo Tech: (1) Overview; *Proceedings of INMM&ESARDA Joint Annual Meeting*, 2021.

(64) Chi Young HAN, Hiroshi SAGARA, Tatsuya KATABUCHI, Hiroshige KIKURA, Yoshihisa MATSUMOTO, Kenji TAKESHITA, and Koichiro TAKAO, and Satoshi CHIBA: The Advanced Nuclear 3S Education and Training (ANSET) Program of Tokyo Tech: (2) 3S Exercises; *Proceedings of INMM&ESARDA Joint Annual Meeting*, 2021.

(65) Akito Oizumi, Hiroshi Sagara: Material Attractiveness Evaluation of Actinides in Pyroprocessing Facility for Partitioning and Transmutation Cycle; *Proceedings of INMM&ESARDA Joint Annual Meeting*, 2021.

(66) Chin Kim Wei, Hiroshi Sagara, Chi Young, Han: System Design Of Photofission Reaction Ratio With High-energy Bremsstrahlung Photons For Nuclear Security; *Proceedings of INMM&ESARDA Joint Annual Meeting*, 2021.

(67) Natsumi Mitsuboshi, Hiroshi Sagara: Feasibility study on small and medium modular light water reactors with inherent nuclear safety and security features using U3Si2 fuel and MA; *Proceedings of INMM&ESARDA Joint Annual Meeting*, 2021.

(68) Masatoshi Kawashima, Hiroshi Sagara, Koji Morita, "Development of a passive reactor shutdown device to prevent core damage accidents in fast reactors-Feasibility of the innovative device-idea and its nonproliferation features-," *Proc. The 42nd Annual Meeting of INMM Japan Chapter*, #4211, 2021.

(69) Chi Young HAN , Hiroshi SAGARA, Yoshihisa MATSUMOTO, Satoshi CHIBA, Noriyosu HAYASHIZAKI, Masako IKEGAMI, Akira OMOTO, Tatsuya KATABUCHI, Koichiro TAKAO, Hiroshige KIKURA, and Kenji TAKESHITA, "Nuclear Regulation Human Resource Development Program in Tokyo Tech, "The Advanced Nuclear 3S Education and Training (ANSET)" (7) Implementation Status AY2021," *Proc. The 42nd Annual Meeting of INMM Japan Chapter*, #4214, 2021.

(70) Masatoshi Kawashima, Hiroshi Sagara, Koji Morita, "Development of a passive reactor shutdown device to prevent core damage accidents in fast reactors-Feasibility of the innovative device-idea and its

nonproliferation features-," *Proc. The 42nd Annual Meeting of INMM Japan Chapter*, #4211, 2021.

(71) Chi Young HAN , Hiroshi SAGARA, Yoshihisa MATSUMOTO, Satoshi CHIBA, Noriyosu HAYASHIZAKI, Masako IKEGAMI, Akira OMOTO, Tatsuya KATABUCHI, Koichiro TAKAO, Hiroshige KIKURA, and Kenji TAKESHITA, "Nuclear Regulation Human Resource Development Program in Tokyo Tech, "The Advanced Nuclear 3S Education and Training (ANSET)" (7) Implementation Status AY2021," *Proc. The 42nd Annual Meeting of INMM Japan Chapter*, #4214, 2021.

(72) Natsumi Mitsuboshi，Hiroshi Sagara, "Feasibility study on innovative small and medium modular reactor with inherent nuclear safety, security, and non-proliferation features (2) Assessment of Material attractiveness of Np as a target material in (U,Np)3Si2 fuel," Proc. *The 42nd Annual Meeting of INMM Japan Chapter*, P4251, 2021.

(73) Shotaro Terayama , Chi Young Han, Hiroshi Sagara, "The effect of nuclear fuel cycle scenario on TRU material balance and nuclear nonproliferation, " *Proc. The 42nd Annual Meeting of INMM Japan Chapter*, P4252, 2021.

(74) Katsuyoshi Tsuchiya, Hiroshi Sagara, Chi Young Han, "Non-Destructive Assay Technology Using Passive Neutron Emission Tomography -Inhibiting Factor Sensitivity of Tomography Image-," *Proc. The 42nd Annual Meeting of INMM Japan Chapter*, P4253, 2021.

(75) （8） Hong Fatt Chong，Hiroshi Sagara, Natsumi Mitsuboshi, "Design Study of U-TRU Fuel Loaded Gas Cooled Reactor Core for TRU Transmutation with Enhanced Safety and Security (I) U-Np Fuel, " *Proc. The 42nd Annual Meeting of INMM Japan Chapter*, P4257, 2021.

(76) Yuichi Kagayama, Hiroshi Sagara, Chi Young Han,and Yoshiki Kimura, "Nuclear Forensics Signatures of Spent Nuclear Fuel from Light Water Reactors, " *Proc. The 42nd Annual Meeting of INMM Japan Chapter*, P4258, 2021.

(77) Akito Oizumi，Takanori Sugawara，Hiroshi Sagara, "Non-proliferation Features in Partitioning and Transmutation Cycle using Accelerator-driven System(2) Evaluation of Material Attractiveness of Uranium in ADS Fuel Assembly, " *Proc. The 42nd Annual Meeting of INMM Japan Chapter*, P4259, 2021.

(78) Non-proliferation features of Accelerator-Driven System using TRU fuel with separation resistance of an actinide element. Proc. *The 42nd Annual Meeting of INMM Japan Chapter*, P4260, 2021.

(79) Haruka Okazaki, Natsumi Mitsuboshi, Masatoshi Kawashima, Hiroshi Sagara, " Improving nuclear safety and security performance of small and medium scale fast reactors by a passive reactor shutdown device (1) Research Plan, " *Proc. The 42nd*

*Annual Meeting of INMM Japan Chapter*, P4262, 2021.

(80) Kim Wei Chin, Rei Kimura, Hiroshi Sagara, Kosuke Tanabe, "Proposal of numerical method to solve multi-nuclides system based on Photofission Reaction Ratio methodology, " *Proc. The 42nd Annual Meeting of INMM Japan Chapter*, P4263, 2021.

(81) T. Takeda, M. Stefanica: Study on Liquid Jet for Neutron Source of BNCT; *19th International Conference on Nuclear Engineering (ICONE20)*, October 24-25, 2012, Paris, France, ICONE20-45600.

**Oral Presentation in international or domestic conferences**

(1) Y. Shinoda, M. Takeuchi, H. Takasu, Y. Kato: Fabrication of PdCu-based H2-permeable composite membrane by reverse build-up method; *ISIJ 183th Sprng Meeting*, 2022/03/16.

(2) S Kuzukami, S. Tominaga, Y. Kato. H. Takasu: Performance evaluation of CO2 electrolysis of metal supported solid oxide electrolysis cell for carbon recycling technology; *ISIJ 183th Sprng Meeting*, 2022/03/16.

(3) T. Enosawa, S. Yoshida, H. Takasu, Y. Kato: Development of chemical heat pump using magnesium chloride/ammonia for utilization of low-quality waste heat; *ISIJ 183th Spring Meeting*, 2022/03/16.

(4) Saki YOSHIDA, Junko KANEKO, Hiroki TAKASU, Takuya HARADA, Yukitaka KATO, Development of Chemical Heat Storage Materials for Use in Air Conditioning and Hot Water Supply, *JSRAE*, 2021/09/08.

(5) S. Funayana, H. Takasu, Y. Kato、Development of composite materials using calcium hydroxide and silicon carbide porous supports for thermochemical energy storage 、*58th Japan Heat Transfer Symposium,*2021/5/25.On-line.

(6) Y. Kato, Carbon recycling industrial system for low-carbon societies, *346th Plastic Forming Symposium*, 2022/02/04, On-line

(7) Y. Kato, Energy Perspective for Carbon Neutral Industry Creation, *JACI Frontier Committee*, 2021/12/08.

(8) Y. Kato: Innovation and Carbon Neutrality on Ironmaking Processes for Carbon Neutrality; *Yukawa Memorial Lecture at Tohoku Region*, 2021/10/26, Tohoku Univ.

(9) Y. Kato, Carbo Flow for Carbon Neutral Society, *26th Public Lecture of Shinshu University*, 2021/10/28, Nagano

(10) Y. Kato, [Plenary lecture]: Renaissance of Energy Storage Technologies for Carbon Neutral Society; *2nd Asian Conf. on Thermal Science(2nd ACTS)*, 2021/10/04On-line

(11) Y. Kato: Contribution of thermochemical energy storage for carbon neutrality; 3*3th Chugoku-Shikoku Heat Transfer Seminar*, 2021/9/28, On-line

(12) Y. Kato, Carbon recycling ironmaking for carbon neutrality, *ISIJ 11th Ironmaking Committee*, 2021/6/10, On-line

(13) Y. Kato: Expectation of Chemical Industry for carbon dioxide materialization for carbon recycling ironmaking system; *Industry-University Exchange Committee, The Chemical Society of Japan*, 2021/5/18 On-line

(14) Tomohiro Okamura, Akito Oizumi, Kenji Nishihara, Masahiko Nakase, Kenji Takeshita: Development of nuclear fuel cycle scenario code "NMB4.0" for integral analysis from front to back end of nuclear fuel cycle; *Technical Workshop on Fuel Cycle Simulation Edition 2021*, Online, June 29, 2021.

(15) Eriko Minari, Tomohiro Okamura, Masahiko Nakase, Hidekazu Asano, Kenji Takeshita: Scenario study of optimization of disposal method to reduce the amount of waste and disposal area in MOX fuel utilization; *Technical Workshop on Fuel Cycle Simulation Edition 2021*, Online, June 3, 2021.

(16) Masahiko Nakase: Toward the resolve of nuclear issues by innovation of radioactive-nuclei separation and their stable solidification; *IIR week of Institute of Innovative Research Tokyo Institute of Technology*, Online, July 12, 2021.

(17) Kenji Takeshita: Study of Fukushima Reconstruction and Revitalization; *IIR week of Institute of Innovative Research Tokyo Institute of Technology*, Online, July 13, 2021.

(18) Kenji Takeshita, Xiangbiao Yin, Shinta Watanabe, Tatsuya Fukuda, Masahiko Nakase: Development of Subcritical Water Ion Exchange System for Cleaning of Soil contaminated by Radioactive Cesium (1) Ion exchange desorption of $Cs^+$ from vermiculite; *10th annual meeting of the Society for Remediation of Radioactive Contamination in Environment*, Fukushima, August 25, 2021.

(19) Shinta Watanabe, Tatsuya Fukuda, Miki Harigai, Masahiko Nakase, Kenji Takeshita: Development of Subcritical Water Ion Exchange System for Cleaning of Soil contaminated by Radioactive Cesium(2)Theoretical Analysis of Desorption Mechanism of Cs from Vermiculite; *10th annual meeting of the Society for Remediation of Radioactive Contamination in Environment*, Fukushima, August 25, 2021.

(20) Hirokazu Miyatake, Tomo Muranoi, Masahiko Nakase, Kenji Takeshita, Tsuyoshi Shinozaki, Shunji Takagi, Kenichi Arima, Kazuto Endo, Masahiro Osako: technical investigation of the stabilization bodies of spent sorbent (2: Calculation of internal temperature and hydrogen generation); *10th annual meeting of the Society for Remediation of Radioactive Contamination in Environment*, Fukushima, August 25, 2021.

(21) Masahiko Nakase, Miki Harigai, Eriko Wada, Tohru

Kobayashi, Yuji Baba, Kenji Takeshita: Proposal of phosphate waste form of sediment wastes of contaminated water treatment in Fukushima Daiichi Nuclear Power Station and the electronic states analysis of the constated elements by synchrotron XAFS; *JXAFS24*, Online, September 3, 2021.

(22) Kenji Takeshita, Masahiko Nakase, Kazuo Utsumi, Takatoshi Hijikata, Shun Kanagawa, Yoshikazu Koma, Takahiro Mori: Development of stable solidification technique of ALPS sediment wastes by apatite ceramics(6) Project objective and progress; *Atomic Energy Society of Japan 2021 Autumn Meeting*, Online, September 9, 2021.

(23) Masahiko Nakase, Miki Harigai, Eriko Wada, Kazuo Utsumi, Shun Kanagawa, Takatoshi Hijikata, Yoshikazu Koma: Development of stable solidification technique of ALPS sediment wastes by apatite ceramics(7) Characteristics of apatite and phosphate waste forms with doped Cs, Sr and lanthanide; *Atomic Energy Society of Japan 2021 Autumn Meeting*, Online, September 9, 2021.

(24) Shun Kanagawa, Takatoshi Hijikata, Masahiko Nakase, Kazuo Utsumi, Kenji Takeshita: Development of stable solidification technique of ALPS sediment wastes by apatite ceramics(8) Development of apatite solidification process for simulated carbonate waste; *Atomic Energy Society of Japan 2021 Autumn Meeting*, Online, September 9, 2021.

(25) Takatoshi Hijikata, Shun Kanagawa, Masahiko Nakase, Kazuo Utsumi, Kenji Takeshita: Development of stable solidification technique of ALPS sediment wastes by apatite ceramics(9) Engineer scale experiment of apatite solidification from the simulated carbonate waste; *Atomic Energy Society of Japan 2021 Autumn Meeting*, Online, September 9, 2021.

(26) Jun Kato, Takeshi Osugi, Tomoyuki Sone, Ryoichiro Kuroki, Yoshikazu Koma, Masahiko Nakase, Kazuo Utsumi, Kenji Takeshita, Shun Kanagawa, Takatoshi Hijikata: Development of stable solidification technique of ALPS sediment wastes by apatite ceramics(10) Characteristics of hydrogen gas generation from solidified apatite; *Atomic Energy Society of Japan 2021 Autumn Meeting*, Online, September 9, 2021.

(27) Takahiro Mori, Hiroyuki Nagaoka, Kouji Okushi, Naoki Kanno, Takashi Asano, Shun Kanagawa, Takatoshi Hijikata, Masahiko Nakase, Kenji Takeshita: Development of stable solidification technique of ALPS sediment wastes by apatite ceramics(11) Basic design of actual scale processing equipment of apatite solidification; *Atomic Energy Society of Japan 2021 Autumn Meeting*, Online, September 9, 2021.

(28) Eriko Minari, Satsuki Kabasawa, Morihiro Mihara, Hitoshi Makino, Masahiko Nakase, Hidekazu Asano, Kenji Takeshita: Evaluation of long-term safety of geological disposal of high-level waste generated during reprocessing spent MOX-LWR fuels; *Atomic Energy Society of Japan 2021 Autumn Meeting*, Online, September 8, 2021.

(29) Koichi Kakinoki, Takashi Shimada, Naoki Ogawa, Ryoukichi Hamaguchi, Taisuke Tsukamoto, Masahiko Nakase, Miki Harigai, Tomoo Yamamura, Chihiro Tabata, Mariko Konaka: Development of Minor Actinides separation and storage technology by process using flame-retardant and low heat of vaporization diluent and CHON extractant(7) Concept of the separation and storage for Minor Actinides (Part2); *Atomic Energy Society of Japan 2021 Autumn Meeting*, Online, September 1, 2021.

(30) Miki Harigai, Masahiko Nakase, Tomoo Yamamura, Chihiro Tabata, Koichi Kakinoki, Naoki Ogawa, Ryoukichi Hamaguchi, Taisuke Tsukamoto, Takashi Shimada: Development of Minor Actinides separation and storage technology by process using flame-retardant and low heat of vaporization diluent and CHON extractant(8) Extraction behavior of Np; *Atomic Energy Society of Japan 2021 Autumn Meeting*, Online, September 1, 2021.

(31) Tomoo Yamamura, Chihiro Tabata, Mariko Konaka, Masahiko Nakase, Miki Harigai, Koichi Kakinoki, Naoki Ogawa, Ryoukichi Hamaguchi, Taisuke Tsukamoto, Takashi Shimada: Development of Minor Actinides separation and storage technology by process using flame-retardant and low heat of vaporization diluent and CHON extractant(9) Productions of uranium-based solid matrix containing lanthanide by distillation and heating processes; *Atomic Energy Society of Japan 2021 Autumn Meeting*, Online, September 1, 2021.

(32) Chihiro Tabata, Masahiko Nakase, Miki Harigai, Kenji Shirasaki, Tomoo Yamamura, Koichi Kakinoki, Naoki Ogawa, Ryoukichi Hamaguchi, Taisuke Tsukamoto, Takashi Shimada: Development of Minor Actinides separation and storage technology by process using flame-retardant and low heat of vaporization diluent and CHON extractant(10) Synthesis of fluorite-structured metal oxides by low-temperature hydrothermal method; *Atomic Energy Society of Japan 2021 Autumn Meeting*, Online, September 1, 2021.

(33) Yuma Dotsuta, Liu Jiang, Toru Kitagaki, Tomoaki Kato, Masahiko Nakase, Kenji Takeshita, Toshihiko Ohnuki: Microbiological flora around Fukushima Daiichi Nuclear Power Plant area and its change by contact with fuel debris; *Institute for Environmental Sciences International Symposium 2021 "Environmental Dynamics of Radionuclides and Biological Effects of Low Dose-Rate Radiation"*, Online, September 27, 2021.

(34) Masahiko Nakase: [Invited] Study on solution chemistry, thermodynamics and extraction separation of Actinide elements in Oarai and alpha laboratories; *Institute for Materials Research,*

*Tohoku University Oarai / Alpha Joint meeting*, Miyagi, September 29, 2021.

(35) Yuji Sasaki, Masashi Kaneko, Yasutoshi Ban, Masahiko Matsumiya, Masahiko Nakase, Kenji Takeshita: Separation of An from Ln by Multi-Stage Extraction Using DGA and DTPA Extraction System; The 40th Symposium on Solvent Extraction of Japan Association of Solvent Extraction, *The 35th Symposium on Japan Society of Ion Exchange*, Online, October 21, 2021.

(36) Masahiko Nakase, Tomoo Yamamura, Miki Harigai, Kenkji Shirasaki, Shingo Sugawara, Chihiro Tabata: Establishment of Acquisition Protocol of Thermodynamic Data of Actinium and Its Solvent Extraction Behavior; *The 40th Symposium on Solvent Extraction of Japan Association of Solvent Extraction, The 35th Symposium on Japan Society of Ion Exchange*, Online, October 21, 2021.

(37) Kenji Takeshita: [Award Lecture] Study on Extraction Technology for Volume Reduction and Radiotoxicity Reduction of Nuclear waste; *The 40th Symposium on Solvent Extraction of Japan Association of Solvent Extraction, The 35th Symposium on Japan Society of Ion Exchange*, Online, October 21, 2021.

(38) Tomofumi Sakuragi, Tomohiro Okamura, Ryo Hamada, Hidekazu Asano, Eriko Minari, Masahiko Nakase, Kenji Takeshita, Toshiro Oniki, Midori Uchiyama: Optimal Waste Loading in HLW glass from High Burn-up Spent Fuel for Reduction of Waste Volume and Footprint of Geological Disposal; *45th Symposium on Scientific Basis for Nuclear Waste Management (SBNWM2021)*, Online, October 24, 2021.

(39) Masahiko Nakase: Challenge of Novel Hybrid-waste-solidification of Mobile Nuclei Generated in Fukushima Nuclear Power Station and Establishment of Rational Disposal Concept and its Safety Assessment; *Fukushima Research Conference (FRC) FY2021 2nd Wisdom Project Workshop*, Online, November 8, 2021.

(40) Takuhi Hara, Masahiko Nakase, Miki Harigai, Kenji Takeshita: Cesium adsorption behaviors and thermal study using functional porous glass; *International Symposium on Porous Materials 2021*, Online, November 4, 2021.

(41) Toshihiko Ohnuki, Jiang Liu, Yuma Dotsuta, Toru Kitagaki, Takehiro Sumita, Masayuki Morihira, Atsushi Ikeda-Ohno, Masahiko Nakase, Koichiro Takao, Takehiko Tsukahara, Kenji Takeshita: Study on degradation of fuel debris by combined effects of radiological, chemical, and biological functions; *The 2021 International Chemical Congress of Pacific Basin Societies*, Online, December 16, 2021.

(42) [Invited] Masahiko Nakase: Relationship between oil-water dispersion and extraction performance in a liquid-liquid centrifugal contactor with Taylor-vortices; *Atomic Energy Society of Japan "Reprocessing Technology for Future Nuclear Systems" Research Committee*, Tokyo, December 24, 2021.

(43) Kazuki Minowa, Sou Watanabe, Masahiko Nakase, Yasutoshi Ban, Haruaki Matsuura: Local structural analysis of rare earth elements in alkyldiamideamine adsorbent; *The 15th Student Research Presentation of Atomic Energy Society of Japan Kanto-Koetsu Branch*, Online, March 1, 2022.

(44) [Invited] Masahiko Nakase, Miki Harigai, Shingo Sugawara, Kenji Shirasaki, Shinta Watanabe, Tomoo Yamamura: Exploring the Thermodynamic Properties of Actinium in Solution State by Utilization of Solvent Extraction Technique; *Summit of Materials Science 2022 & GIMRT User Meeting 2022*, Miyagi, March 2, 2022.

(45) Masahiko Nakase: Relationship of recognition property of light Actinide and chemical properties by synthesis of novel phthalocyanine derivatives and substitution of functional group Relationship; *Kyoto University Multidisciplinary Research Seminar "Physical Chemistry of Actinides and Their Applications"*, Online, March 3, 2022.

(46) Kenji Takeshita, Masahiko Nakase, Kenji Nishihara, Hitoshi Makino, Tatsuro Matsumura: Study on nuclear utilization scenario towards the second half of the 21st century(1)Study on the integration of nuclear fuel cycle for the establishment of the advanced nuclear energy system; *Atomic Energy Society of Japan 2022 Spring Annual Meeting*, Online, March 16, 2022."

(47) Tomohiro Okamura, Kenji Nishihara, Ryota Katano, Akito Oizumi, Masahiko Nakase, Kenji Takeshita: Study on nuclear utilization scenario towards the second half of the 21st century(2) NMB4.0: Development and Release of Integrated Nuclear Fuel Cycle Simulator from front- to back-end processes; *Atomic Energy Society of Japan 2022 Spring Annual Meeting*, Online, March 16, 2022.

(48) Eriko Minari, Morihiro Mihara, Hitoshi Makino, Tomohiro Okamura, Akito Oizumi, Kenji Nishihara, Masahiko Nakase, Kenji Takeshita: Study on nuclear utilization scenario towards the second half of the 21st century(3) Evaluation of long-term safety of geological disposal of vitrified MOX-LWR high-level waste; *Atomic Energy Society of Japan 2022 Spring Annual Meeting*, Online, March 16, 2022.

(49) Kenji Nishihara, Akito Oizumi, Tomohiro Okamura, Masahiko Nakase, Kenji Takeshita: Study on nuclear utilization scenario towards the second half of the 21st century(4) Transmutation scenario for MA from LWR spent fuel; *Atomic Energy Society of Japan 2022 Spring Annual Meeting*, Online, March 16, 2022.

(50) Hidekazu Asano, Tomofumi Sakuragi, Ryo Hamada, Chi Young Han, Masahiko Nakase, Tatsuro Matsumura, Go Chiba, H.Sagara, Kenji Takeshita:

Study on Nuclear Energy System Considering Environmental Load Reduction of Waste Disposal in Diversification of Nuclear Fuel Cycle Conditions (5) Integrated evaluation of the environmental burden of the variational condition of nuclear fuel cycle; *Atomic Energy Society of Japan 2022 Spring Annual Meeting*, Online, March 16, 2022.

(51) Naoya Shigekiyo, Masahiko Nakase, Hidekazu Asano, Tomofumi Sakuragi, Ryo Hamada, Kenji Takeshita: Study on Nuclear Energy System Considering Environmental Load Reduction of Waste Disposal in Diversification of Nuclear Fuel Cycle Conditions (8)Survey of existing technology from the viewpoint of simplified Minor Actinide separation; *Atomic Energy Society of Japan 2022 Spring Annual Meeting*, Online, March 16, 2022.

(52) Masahiko Nakase, Miki Harigai, Shinta Watanabe, Takashi Kajitani, Tohru Kobayashi, Kota Matsui, Chihiro Tabata, Tomoo Yamamura, Koichi Kakinoki, Takashi Shimada: Exploration of Fluorinated Super-Solvent for Minor Actinide extraction(1)General Plan; *Atomic Energy Society of Japan 2022 Spring Annual Meeting*, Online, March 16, 2022.

(53) Miki Harigai, Masahiko Nakase, Shinta Watanabe, Chihiro Tabata, Tomoo Yamamura, Tohru Kobayashi, Kota Matsui, Taisuke Tsukamoto, Koichi Kakinoki, Takashi Shimada: Exploration of Fluorinated Super-Solvent for Minor Actinide extraction(2)Extraction behavior of Lanthanide ions by various kinds of solvent; *Atomic Energy Society of Japan 2022 Spring Annual Meeting*, Online, March 16, 2022.

(54) Chihiro Tabata, Masahiko Nakase, Miki Harigai, Shinta Watanabe, Tomoo Yamamura, Kota Matsui, Koichi Kakinoki, Taisuke Tsukamoto, Takashi Shimada: Exploration of Fluorinated Super-Solvent for Minor Actinide extraction(3)Acquisition of Chemical and Physical Property Data for Materials Informatics to Explore Fluorinated Super Solvents; *Atomic Energy Society of Japan 2022 Spring Annual Meeting*, Online, March 16, 2022.

(55) Kota Matsui, Masahiko Nakase, Miki Harigai, Shinta Watanabe, Chihiro Tabata, Tomoo Yamamura, Tohru Kobayashi, Taisuke Tsukamoto, Koichi Kakinoki, Takashi Shimada: Exploration of Fluorinated Super-Solvent for Minor Actinide extraction(4)Prospects of Machine Learning Approach on Exploration of Fluorinated Super-Solvent for Minor Actinide extraction; *Atomic Energy Society of Japan 2022 Spring Annual Meeting*, Online, March 16, 2022.

(56) Koichi Kakinoki, Takashi Shimada, Masahiko Nakase, Miki Harigai, Shinta Watanabe, Takashi Kajitani, Tohru Kobayashi, Kota Matsui, Chihiro Tabata, Tomoo Yamamura: Exploration of Fluorinated Super-Solvents for Minor Actinide extraction(5)Consideration of safety requirements and issues for processes using Fluorinated Super-Solvents; *Atomic Energy Society of Japan 2022 Spring Annual Meeting*, Online, March 16, 2022.

(57) Masahiko Nakase: Evaluation of the current nuclear fuel cycle based on the light water reactor; *Atomic Energy Society of Japan 2022 Spring Annual Meeting*, Online, March 16, 2022.

(58) Tomoo Yamamura, Chihiro Tabata, Masahiko Nakase, Miki Harigai, Koichi Kakinoki, Naoki Ogawa, Ryoukichi Hamaguchi, Taisuke Tsukamoto, Takashi Shimada: Development of Minor Actinides separation and storage technology by process using flame-retardant(11)Crystal structural analysis of solid solution of rare earth and uranium oxides in stabilization process; *Atomic Energy Society of Japan 2022 Spring Annual Meeting*, Online, March 16, 2022.

(59) Yuji Sasaki, Masashi Kaneko, Yasutoshi Ban, Daiki Nomizu, Yusuke Tsuchida, Masahiko Matsumiya, Masahiko Nakase, Kenji Takeshita, Takahiro Shimosaka, Tatsuya Suzuki: Complexation of actinides and lanthanides with water-soluble amides and carboxylic acids and their tetrad effect; *Atomic Energy Society of Japan 2022 Spring Annual Meeting*, Online, March 16, 2022.

(60) Aki Murata, Shota Ikeda, Kunihiro Fujita, Yasuo Wakabayashi, Hideaki Yamauchi, Masashi Masuoka, Yoshie Otake, Noriyosu Hayashizaki: Development of a Next Generation Accelerator-driven Compact Neutron Source for Infrastructure Inspection; *The 18th Annual Meeting of Particle Accelerator Society of Japan*, August 9-12, 2021, QST-Takasaki Online, Japan.

(61) Shota Ikeda, Yoshie Otake, Tomohiro Kobayashi, Noriyosu Hayashizaki, Hideaki Yamauchi, Masashi Masuoka: High power test of 500 MHz-RFQ linac for compact neutron source RANSIII; *The 18th Annual Meeting of Particle Accelerator Society of Japan*, August 9-12, 2021, QST-Takasaki Online, Japan.

(62) Takahiro Shinya, Kohei Sakurai, Kai Masuda, Noriyosu Hayashizaki, Tetsuo Abe, Hitoshi Kobayashi, Ken Takayama, Francesco Scantamburlo and Andrea De Franco: Present Status of Linear IFMIF Prototype Accelerator (LIPAc), (2) Particle Simulations of Multipactering in RF Coupler; *2022 Annual Meetings of the Atomic Energy Society of Japan*, March 16-18, 2022, online, Japan.

(63) Saburo MATUNAGA, Hiroshi FURUYA, Yoichi YATSU, Noriyosu HAYASHIZAKI, Yasuyuki MIYAZAKI, Keiichi OKUYAMA, Kazuyuki NAKAMURA, Akihito WATANABE, Toshihiro CHUJO, Kiyona MIYAMOTO: Activities of Research and Development Center of Smart Space Components and Systems for Creation of New Space Industries; *MoViC/SEC'21*, December 9-10, 2021, online, Japan.

(64) Thijs van der Gaag, Hiroshi Akatsuka: Arbitrary Electron Energy Distribution Determination from the Continuum Emission Spectrum for Atmospheric-Pressure Plasma Electron Diagnostics; *74th Annual Gaseous Electronics Conference (GEC2021)*, ZOOM Meeting, October 4-8, 2021, Bull. Am. Phys. Soc. Vol.**66**, No.7, KW73.00003, The American Physical Society.

(65) Keren Lin, Atsushi Nezu, Hiroshi Akatsuka: Development of Atmospheric Pressure Helium Collisional-Radiative Model by Including Atomic Collisions; *74th Annual Gaseous Electronics Conference (GEC2021)*, ZOOM Meeting, October 4-8, 2021, Bull. Am. Phys. Soc. Vol.**66**, No.7, GT61.00059, The American Physical Society.

(66) Hiroshi Akatsuka: Low-Temperature Plasma Measurement: Line Spectrum for Low-pressure Plasmas and Continuum Spectrum for Atmospheric-pressure Plasmas; *The 12th Asia-Pacific International Symposium on the Basics and Applications of Plasma Technology (APSPT-12)*, National Taiwan University of Science and Technology with hybrid ZOOM Meeting, December 9-11, 2021, Plenary Lecture 2.

(67) Keren Lin, Atsushi Nezu, Hiroshi Akatsuka: Diagnosis of Electron Density and Temperature of Atmospheric Pressure Helium Plasma Based on Collisional-Radiative Model; *The 12th Asia-Pacific International Symposium on the Basics and Applications of Plasma Technology (APSPT-12)*, Taipei with hybrid ZOOM Meeting, December 9-11, 2021, O19-2.

(68) Thijs van der Gaag, Hiroshi Akatsuka: A Machine Learning Approach to Determine Arbitrary EEDF of Atmospheric Pressure Plasma from OES Measurement; *The 12th Asia-Pacific International Symposium on the Basics and Applications of Plasma Technology (APSPT-12)*, National Taiwan University of Science and Technology with hybrid ZOOM Meeting, December 9-11, 2021, O17-2.

(69) Yuya Yamashita, Takuya Akiba, Toshihide Iwanaga, Shuichi Date, Hidehiko Yamaoka, Hiroshi Akatsuka: Electron Temperature, Density, and Energy Distribution Function Diagnostics of the Argon Low Pressure Plasma Generated by an Etching Unit Based on Optical Emission Spectroscopic Measurement, *The 82nd JSAP Autumn Meeting 2021*, ZOOM Meeting, September 10-13, 2021, p. 07-002, 10a-S301-2.

(70) Ryo Ishizuka, Atsushi Nezu, Hiroshi Akatsuka: Measurement of Electron Temperature and Electron Density by Emission Spectroscopy in Ar&$N_2$ Mixed Atmospheric Pressure Non-Equilibrium Plasma; *The 82nd JSAP Autumn Meeting 2021*, ZOOM Meeting, September 10-13, 2021, p. 07-003, 10a-S301-3.

(71) Takuma Takimoto, Hiroshi Akatsuka: Discussion on Excitation Temperature of Non-Equilibrium Plasma by Collisional-Radiative Model and Rényi's Entropy; *JPS 2021 Autumn Meeting, The Physical Society of Japan*, ZOOM Meeting, September 20-23, 2021, p. 739, 22pB1-3.

(72) Rei Togashi, Atsushi Nezu, Hiroshi Akatsuka: Spectroscopic Study on Optical Emission Spectrum of NH A-X Transition in $N_2$-$H_2$ Plasma; *The 38th JSPF Annual Meeting 2021*, ZOOM Meeting, November 22-25, 2021, 22Ap06.

(73) Tomoya Izumida, Kiyoyuki Yambe, Hiroshi Akatsuka: Comparison of Non-Thermal Equilibrium Argon and Helium Plasmas at Atmospheric Pressure by Continuum Radiation Analysis; *2021 Annual Meeting of Niigata Division, Tokyo Branch, Institute of Electrical and Electronic Engineers Japan (IEEJ)*, Niigata, December 4, 2021, NGT-21-033.

(74) Kenya Suganami, Atsushi Nezu, Hiroshi Akatsuka: Optical Spectroscopic Measurement of Fulcher-α Band and Reconsideration of Rotation Constant of Hydrogen Molecule $H_2$; *The 39-th Symposium on Plasma Processing/The 34-th Symposium on Plasma Science for Materials (SPP-39/SPSM34)*, ZOOM Meeting, January 24-26, 2022, pp. 74 - 75, LO25-AM-B-02.

(75) Yuya Yamashita, Shuichi Date, Hidehiko Yamaoka, Takuya Akiba, Takayuki Shibuya, Toshihide Iwanaga, Hiroshi Akatsuka: Diagnostics of Vibrational and Rotational Temperature of OH Radical of Argon-Oxygen Low Pressure Inductively Coupled Plasma; *The 69th JSAP Spring Meeting 2022*, Sagamihara with hybrid ZOOM Meeting, March 22-26, 2022, p. 7-009, 22p-E105-8.

(76) Masaki Takemura, Atsushi Nezu, Hiroshi Akatsuka: Dependence of Discharge Properties on the Power-Supply Frequency in Non-Equilibrium Atmospheric-Pressure Ar Plasma; T*he 2022 Annual Meeting IEE of Japan*, ZOOM Meeting, March 21-23, 2022, p. 64, 1-047.

(77) Hiroshi Akatsuka: Optical Emission Spectroscopy (OES) Measurement and Atomic/Molecular Processes of Diatomic Molecular Gas-Discharge Plasma; *The 234th Technical Meeting of Silicon Technology Division, Japan Society of Applied Physics*, ZOOM Meeting, March 15, 2022, Plenary (2).

(78) Satoshi Chiba, Chen Jingde, Chikako Ishizuka and Akira Ono: A theoretical challenge to the ternary fission based on antisymmetrized molecular dynamics; *JEFF meeting,* April 27-29, 2021.

(79) Satoshi Chiba: Interplay of various shell closures in fission of actinides to SHN studied by Langevin model; *COSNAP Colloquium, No. 16.,* June 1, Tue, 2021, 15:00 - 16:30 (Beijing, CST).

(80) Tatsuya Katabuchi: Activity report of research committee for nuclear data in the fiscal years of 2019 and 2020, Human Resource Development for Nuclear Data Research, *2021 Fall Meeting of Atomic Energy Society of Japan*, Online, Sep. 8-10, 2021,

2F_PL02.

(81) Chi Young HAN, Hiroshi SAGARA, Yoshihisa MATSUMOTO, Satoshi CHIBA, Noriyosu HAYASHIZAKI, Masako IKEGAMI, Akira OMOTO, Tatsuya KATABUCHI, Koichiro TAKAO, Hiroshige KIKURA, Kenji TAKESHITA: Nuclear Regulation Human Resources Development Program in Tokyo Tech "The Advanced Nuclear 3S Education and Training (ANSET)" (4) Implementation Status FY2020, *The 42th Annual Meeting of INMM Japan Chapter*, 2021.

(82) Hideto Nakano, Tatsuya Katabuchi, Gerard Rovira Leveroni, Yu Kodama, Kazushi Terada, Atsushi Kimura, Shoji Nakamura, Shunsuke Endo: Neutron Capture Cross Section Measurement of 107Pd in the Resonance Energy Region, *2022 Annual Meeting of the Atomic Energy Society of Japan*, Online, March 16-18, 2021.

(83) T.Moriya, H.Takahashi, H. Kikura: Basic Study on Ultrasonic Investigation System for Decommission of Nuclear Reactor; *2022 Annual Meeting of Atomic Energy Society of Japan*, Online Conference, March 16-18, 2022, 1H02.

(84) S.Kai, H.Takahashi, H.Taniguchi, A. Kawashima, H.Takahashi, K. Jinza, H.Kikura: Fundamental Study on Mechanism of Blasting Decontamination Device for Small Diameter Pipe (Part5); *2022 Annual Meeting of Atomic Energy Society of Japan*, Online Conference, March 16-18, 2022, 3H07.

(85) H.Takahashi, G.Endo, I.Wakaida, H.Kikura: Development of Remote Inspection Method using Advanced Super Dragon Articulated Robot Arm (1)Project Outline and Measurement Method Development; *2022 Annual Meeting of Atomic Energy Society of Japan*, Online Conference, March 16-18, 2022, 3H02.

(86) G.Endo, T.Nagai, A.Takata, H.Kikura H.Takahashi: Development of Remote Inspection Method using Advanced Super Dragon Articulated Robot Arm (2)Development of an Articulated Robot Arm with Telescopic Structure; *2022 Annual Meeting of Atomic Energy Society of Japan*, Online Conference, March 16-18, 2022, 3H03.

(87) K.Fujihira, H.Takahashi, H.Kikura; Study on visualization of gas-liquid mass transfer using laser-induced fluorescence; *2022 Annual Meeting of Atomic Energy Society of Japan Student Poster Session,* Online Conference, March 16-17, 2022, 2-31.

(88) S.Kai, H.Takahashi, H.Taniguchi, A. Kawashima, H.Takahashi, K. Jinza, H.Kikura; Study on Clarification of Decontamination Mechanism of Small-Diameter Pipe in Dry-type Decontamination Machine; *2022 Annual Meeting of Atomic Energy Society of Japan Student Poster Session,* Online Conference, March 16-17, 2022, 1-10.

(89) T.Numata, Tran Tri Vien, H.Takahashi, H.Kikura; Fundamental Study on Flow Characteristics of Venturi Nozzle for High Efficiency Filtered Containment Venting System; *2022 Annual Meeting of Atomic Energy Society of Japan Student Poster Session,* Online Conference, March 16-17, 2022, 2-32.

(90) N.Shoji, S.Kai, H.Takahashi, H.Kikura: Fundamental Study on Ultrasonic Signal Processing for In-pipe Fluid Measurement; *The 15th Student Research Meeting of the Atomic Energy Society of Japan Kanto-Koetsu Branch,* Online Conference, *March 1, 2022,* B5-3.

(91) M.Moto, N.Shoji, H.Takahashi, H.Kikura: Fundamental Study for Development of Gas Heat Flow Measurement of Steam Flow using Tunable Diode Laser Absorption Spectrometry; *The 15th Student Research Meeting of the Atomic Energy Society of Japan Kanto-Koetsu Branch,* Online Conference, March 1, 2022, A5-2.

(92) H.Tanabe, N.Shoji, H.Takahashi, H.Kikura: Study on Object Shape Reconstruction and Water Level Measurement by Air-coupled parametric ultrasound; *The 15th Student Research Meeting of the Atomic Energy Society of Japan Kanto-Koetsu Branch,* Online Conference, March 1, 2022, B4-5.

(93) K.Fujihira, H.Takahashi, H. Kikura; Development of Laser-induced Fluorescence Method toward Understanding Source Term Gas-Liquid Migration Behavior; *The 15th Student Research Meeting of the Atomic Energy Society of Japan Kanto-Koetsu Branch,* Online Conference, March 1, 2022, B2-3.

(94) Z.Zhang, T.Moriya, N.Shoji, H.Takahashi, H.Kikura: Fundamental Study on Development of Microchip-laser Induced Breakdown Spectroscopy System for Remote Analysis; *The 5th Visualization Workshop*, Online Conference, February 24,2022, P13.

(95) Y.Iijima H.Nagasaka, H.Takahashi, H.Kikura: Visualization Sutdy on Fluid Vibration modes Due to Direct-Contact Condensation in an Upward-Facing Nuzzle; *The 5th Visualization Workshop*, Online Conference, February 24,2022,P15.

(96) R.Ikeda , K.Shimada , H.Takahashi, H.Kikura: Fundamental Study on Tactile Sensing Technique and Enrgy Harvesting Using Magnetic Fluid Rubber and its Application to Radiation Environment; *2021 JSMFR Conference*, Online Conference, December 9-10, 2021, 5.

(97) R.Ikeda, K.Shimada, H.Takahashi, H.Kikura; A Study of Development of Tactile Sensing and Enrgy Harvesting Technologies in Nuclear Field Utilizing Magnetic Compound Fluid Rubber; *The 20th Young Researchers and Engineers Presentation and Discussion*, Online Conference, November 29,2021, V-2.

(98) T.Tri Vien T. Narabayashi, H.Takahashi, H.Kikura:

UVP Measurement of Fluid Behavior in Advanced Venturi Scrubber Nozzle of Filtered Containment Venting System; *JSME the 99th Fluid Engineering Division Conference*, Online Conference, November 9-10, 2021, OS14-04.

(99) N. S. Sardini Sayidatun，H.Takahashi, H.Kikura; Effect of Ultrasonic Sonoluminescence Spectroscopy on Flow; *JSME the 99th Fluid Engineering Division Conference*, Online Conference, November 9-10, 2021, OS14-06.

(100) T.Nakada, N.Shoji, H.Takahashi, H.Kikura; Fundamental Study on Portable Ultrasonic Velocity Profiler Using Smart Glasses; *JSME the 99th Fluid Engineering Division Conference,* Online Conference, November 9-10, 2021, OS-05.

(101) Y.Oishi, D.Sasayama, H.Kawai, H. Kikura: Evaluation of Characteristics of Water-in-Oil Emulsion by Taylor-Couette Flow with Small Aspect Ratio using UVP; *49th Symposium on Visualization,* Online Conference, September 9-10, 2021, OS6.

(102) N.Shoji, H.Takahashi, H.Kikura; Three-dimensional Visualization of Leakage Flow by Pulsed Ultrasound; *49th Symposium on Visualization*, Online Conference, September 9-10, 2021, OS6.

(103) K.Fujihira, H.Takahashi, H.Kikura; VVisualization of CO2 Dissolution Process from a Bubble into Water by LIF Measurement Using HPTS; *49th Symposium on Visualization*, Online Conference, September 9-10, 2021, OS2

(104) R.Inoue, H.Tanabe, N.Shoji , H.Takahashi ,H.Kikura; Study on Object Shape Reconstruction Technique using Camera and Ultrasonic Sensor; *49th Symposium on Visualization,* Online Conference, September 9-10, 2021, OS6.

(105) T. Nakada, M.Muto, N.Shoji, H.Takahashi, H.Kikura; Fundamental Study on Development of Pipe Flow Smart Visualization System using UVP; *49th Symposium on Visualization*, Online Conference, September 9-10, 2021, OS6.

(106) H.Tanabe, N.Shoji, H.Kikura, H.Takahashi: Study on Object Shape Reconstruction by Parametric Ultrasound; *49th Symposium on Visualization,* Online Conference, September 9-10, 2021, OS6.

(107) S.Kai, R.Ikeda, H. Takahashi, H. Taniguchi, A. Kawashima, H. Takahashi, K.Jinza, H. Kikura: Fundamental Study on Mechanism of Blasting Decontamination Device for Small Diameter Pipe (Part 4); *AESJ 2021 Fall Meeting*, Online Conference, September 8-10, 2021, 3C08.

(108) A.Takata, H.Nabae, K.Suzumori, H.Kikura, H.Takahashi, G. Endo: Stability Analysis of Wire Interference Driven Articulated Arm with Synthetic Fiber Rope; *39th RSJ Conference(RSJ2021),* Online Conference, September 8-11, 2021, 212-07.

(109) S. Kai, H.Takahashi, H.Taniguchi, A.Kawashima,H.Takahashi, H. Kikura;

Experimental study on the decontamination effect and mechanism of dry decontamination system; *2021 Annual Meeting of JSEM*, Online Conference, August 25-27, 2021, A301.

(110) M.Muto, N.Shoji, H.Takahashi, Y.Deguchi, H. Kikura: Fundamental Experiment for Development on Temperature and Velocity Measurement of Steam Flow using Tunable Diode Laser Absorption Spectroscopy; *2021 Annual Meeting of JSEM*, Online Conference, August 25-27, 2021, B109.

(111) Hiroshige KIKURA: Revitalizics for SDGs -Cross Linear Solar Concentration (CL-CSP) and Cross Over Sun-Tracking Solar System (CRO)-; *The 3rd Engneering physics International Conference (EPIC)*, Online Conference ,August 24-25,2021.

(112) T. Narabayashi, H.Kikura, H.Takahashi: Development of virus removal system using Venturi Scrubber nozzles for   Filtered Containment Venting System; *2021 JSMF Symposium,* Online Conference, August 22-24, 2021, E0147.

(113) H.Sagara, C.Young Han, S.Chiba, Y.Matsumoto, N.Hayashizaki, M.Ikegami, A.Omoto, K.Takeshita, T.Katabuchi, H.Kikura, K.Takao: The Advanced Nuclear 3S Education and Training (ANSET) Program of Tokyo Tech: (1) OVERVIEW OF YEAR 5; *INMM &ESARDA Annual Meeting*; Online Conference ,August 23-26,2021.

(114) C.Young Han, H.Sagara, T.Katabuchi, H.Kikura, Y.Matsumoto, K.Takeshita, K.Takao, S.Chiba: The Advanced Nuclear 3S Education and Training (ANSET) Program of Tokyo Tech: (2) 3S EXERCISES; *INMM &ESARDA Annual Meeting*; Online Conference ,August 23-26,2021.

(115) H. Takahashi, N. Shoji, G.Endo, H.Kikura: New Direction of Ultrasonic Non-destructive Measurement Technology Research in Remote Environment for Fukushima Revitalization and Decommissioning; *2021 JSNDI Symposium*, Online Conference, June 22-23, 2021,UT Part.

(116) H.Kikura, H.Takahashi: Practical Science of "Revitalizics" for Decommission of Fukushima Dai-ichi Nuclear Power Plant ～Innovation with ultrasonic measurement technique and robotic system ～; *The 11th Vietnam-Japan Resarch &HRD Forun on Nuclear Technology*, Online Conference, June 22-24,2021.

(117) H.Kikura: Practical Science of "Revitalizics" for Decommission of Fukushima Dai-ichi Nuclear Power Plant ～ Innovation with ultrasonic measurement technique and robotic system ～ ; *Vietnam/Japan Research/HRD Forum on Nuclear Technology-XI*, Online Conference, June 22-24, 2021,S1-2-J.

(118) Z.Zhang, T.Miyabe, T.Moriya, M.Batsaikhan, H.Takahashi, H. Kikura: A Study on Object Shape Reconstruction using Monocular Camera and Ultrasonic Sensor; *The 27th Symposium on Sensing*

*via Image Information*, Online Conference, Jun 9-11, 2021, IS1-05.

(119)    A.Takata, H. Nabae, K.Suzumori, H.Kikura, H.Takahashi, G.Endo: Position Accuracy of a Long-reach Coupled Tendon-driven Robot Arm "Super Dragon" in a Full-scale Exploration Test; *The Robotics and Mechatronics Conference 2021 in Osaka*, Online Conference, Jun 6-8, 2021, 2A1-O03.

(120)    H.Tei, H.Nabae, K.Suzumori, H.Kikura, H.Takahashi, G. Endo: Development of Lightweight Telescopic boom for Reactor Pressure Vessel Research; *The Robotics and Mechatronics Conference 2021 in Osaka*, Online Conference, Jun 6-8, 2021, 2A1-O02.

(121)    A. Itoh, M. Kurata, D. Luxat, M. Barrachin: Understanding of $UO_2$/Zircaloy interaction with updated thermodynamic database and application to simplified modelling for SA-code analysis; *JAEA/CLADS in collaboration with OECD/NEA TCOFF final workshop*, online, Dec. 14-16, 2021.

(122)    A. Itoh: Improvement of materials interaction models and the application to SA-analysis code; *JAEA/CLADS in collaboration with OECD/NEA TCOFF final workshop*, online, Dec. 14-16, 2021.

(123)    A. Itoh, R. Hagiwara, S. Yasui, Y. Kobayashi: Mass transport of the Zr-O-(Fe,Cr,Ni) system during the SUS316-Zircaloy4 reaction at high temperatures under the severe accident condition of light water reactor; *2021 the 183th ISIJ (Iron and Steel Institute of Japan) meeting*, online, Sep. 2-4, 2021.

(124)    A. Itoh, S. Yasui, Y. Kobayashi, K. Sakamoto, M. Mizokami, M. Hirai, K. Ito: Initial melting reaction mechanism of BWR structural material with Zircaloy/Steel or Inconel; *2022 AESJ (Atomic Energy Society Japan) Annual meeting*, online, Mar. 16-18, 2022.

(125)    S. Sakuma, A. Itoh, S. Yasui, Y. Kobayashi, M. Mizokami, M. Hirai, K. Ito: Investigation of re-distribution of B in SUS304-$B_4C$ alloy under high temperature steam simulating BWR severe accident; *2022 AESJ (Atomic Energy Society Japan) Annual meeting*, online, Mar. 16-18, 2022.

(126)    Taro Kanbe, Kenta Nakagawa: Development of Liquid Target for Neutron Capture Therapy Using Accelerator, (1) An outline of the target for NCT; *2012 Annual Meeting of Atomic Energy Society of Japan*, Fukui, March 30-35, 2012, K46.    （例）

(127)    R. Nakazawa, Y. Kobayashi: Thermodynamics of the Sm-Fe-O ternary system for the development of high coercivity magnet material; The 170th meeting of Japan Institute of Metals Mar. 2022.

(128)    Y. Kobayashi: Precipitation of copper sulfide and segregation ehavior of elements in low carbon steel cast with variation in cooling rate; The 183rd ISIJ Meeting Mar. 2022.

(129)    Y. Liu, Y. Kobayashi: Determination of activity of chromium oxide in molten slag in high purity chromium steel refining process; The 183rd ISIJ Meeting Mar. 2022.

(130)    Mikio Shimada, Kaima Tsukada, Kotaro Saikawa, Tomoko Miyake, Ryoichi Hirayama, Yoshihisa Matsumoto. High LET irradiation induceds multipplar cell division in human induced pluripotent stem cells, 64th Annual meeting of Japanese Radiation Research Association, Sept. 2021.

(131)    Rikiya Imamura, Mizuki Saito, Mikio Shimada, Masamichi Ishiai, Yoshihisa Matsumoto. The role of hereditary disease factor APTX in DNA replication and replication stress, 64th Annual meeting of Japanese Radiation Research Association, Sept. 2021.

(132)    Hideki Matsumoto, Yoshiya Shimada, Asako Nakamura, Noriko Usami, Mitsuaki Ojima, Shizuko Kakinuma, Mikio Shimada, Masaaki Sunaoshi, Ryoichi Hirayama, Hroshi Tauchi. Activities of commision for corresponding to radiation disaster of the Japanese radiation research society in reconstitution assistance from Fukushima Daiichi Nuclear Plant: Issuance of "health effects riggerd by tritium", 64th Annual meeting of Japanese Radiation Research Association, Sept. 2021.

(133)    Hiroyasu Mochizuki: Verification of Neutronics-Thermalhydraulics Couping UDF for FLUENT Code using MSRE Experiment -Analyses of Pump Startup and Trip Experimens-; *2021 Annual Meeting of Atomic Energy Society of Japan*, On-Line, March 17-19, 2021, 1C05.

(134)    Hiroyasu Mochizuki: Study of a Fuel-Salt to Coolant-Salt Heat Exchanger for Molten Salt Fast Reactor; *2012 Fall Meeting of Atomic Energy Society of Japan*, On-Line, September 8-10, 2021, 3J06.

(135)    Yoshihisa Tahara, Satoshi Chiba, Hiroyasu Mochizuki: Evaluation of burnup performance of transuranic elements by a small chloride molten salt fast reactor; 2*022 Annual Meeting of Atomic Energy Society of Japan*, On-Line, March 16-18, 2022, 1D07.

(136)    Hiroyasu Mochizuki: Analysis of Reactivity Insertion Tests of MSRE using RELAP5-3D; 2*022 Annual Meeting of Atomic Energy Society of Japan*, On-Line, March 16-18, 2022, 2E05.

(137)    Toru Obara; "Toward construction of cross-organizational education system for nuclear engineering: activities ofglobal nuclear human resource development initiative program by MEXT (3) Activity in International Group Meeting": *Proc. of 2022 Annual meeting of Atomic Energy Society of Japan*, 1L_PL03 (2022).

(138)    Toru Obara, Van Khanh Hoang, Odmaa Sambuu, Jun Nishiyama;"Feasibility of rotational fuel shuffling lead cooled Breed-and-Burn fast reactor": *Proc. of 2022 Annual meeting of Atomic Energy Society of Japan*, 1D06 (2022).

(139)    Toru Obara, Van Khanh Hoang, Odmaa

Sambuu, Jun Nishiyama; "Conceptual design of rotational fuel shuffling sodium cooled Breed-and-Burn fast reactor": *Proc. of 2021 Autumn meeting of Atomic Energy Society of Japan*, 3K13 (2021).

(140) K. Kobayashi, S. Mouri, T. Udo, Y. Kebukawa, H. Mita, H. Fukuda, Y. Oguri, V.S. Airapetian: The Role of Solar Energetic Particles in Habitability of the early Earth: Experimental approach; *EANA 2021 Virtual Conference*, European Astrobiology Network Association, September 7-10, 2021 (online).

(141) H. Liu, N. Hagura, Y. Oguri, H. Miyake, K. Enoki, A. Komori, K. Ueda: Particle Trajectory Optimization of PIG Negative-Ion Source in Electrostatic Tandem Accelerator; *2021 Fall Meeting of Atomic Energy Society of Japan*, September 8-10, 2021, 1G03, online (2021).

(142) Hiroshi Sagara: The advanced Nuclear 3S Education and Training(ANSET) Program of Tokyo Tech; Webinar series: Education as a Key to Addressing the Gender Equality Gap in Global Nuclear Security, Women in Nuclear Security Initiative, IAEA, March 7, 2022.

(143) Saki Yamaguchi, Akito Oizumi, Hiroshi Sagara, "Neutronics and Non-proliferation features of Accelerator-Driven System using TRU fuel with separation resistance of an actinide element, " AESJ 2022 Annual Mtg., online, 2022.

(144) Daisuke Hara, Hiroshi Sagara, "Development Of Proliferation Resistance Evaluation Methodology And Its Applicability For The Offshore Floating Nuclear Power Plant," AESJ 2022 Annual Mtg., online, 2022.

(145) Hidekazu Asano, Tomofumi Sakuragi, Ryo Hamada, Chi Young Han, Masahiko Nakase, Tatsuro Matsumura, Go Chiba, Hiroshi Sagara and Kenji Takeshita, "Study on advanced nuclear energy system based on the environmental impact of radioactive waste disposal (5) Integrated environmental load assessment for diversifying nuclear fuel cycle conditions" AESJ 2022 Annual Mtg., online, 2022.

(146) Chi Young HAN, Hiroshi SAGARA and Hidekazu ASANO, "Study on Advanced Nuclear Energy System Based on the Environmental Impact of Radioactive Waste Disposal (7) Development of an Assessment Program of the Environmental Load of Radioactive Wastes for NFCSS," AESJ 2022 Annual Mtg., online, 2022.

(147) Koji Morita, Wei Liu, Tatsumi Arima, Yuji Arita, Isamu Sato, Haruaki Matsuura, Yoshihiro Sekio, Hiroshi Sagara and Masatoshi Kawashima, "Development of a passive safety shutdown device to prevent core damage accidents in fast reactors (3) Overview of overall project progress through FY2020," AESJ 2021 Fall Mtg., online, 2021.

(148) Hiroshi Sagara, Koji Morita, Masatoshi Kawashima, Tatsumi Arima, Wei Liu, Yuji Arita, Isamu Sato, "Development of a passive safety shutdown device to prevent core damage accidents in fast reactors (6) Specification of the device assembly design effective in the reactivity control by its material relocation," AESJ 2021 Fall Mtg., online, 2021.

(149) Yuichi Kagayama, Hiroshi Sagara, Chi Young HAN, Yoshiki Kimura, "Nuclear Forensics Signatures of Spent Nuclear Fuel -Signatures for discriminating reactor and fuel types-," AESJ 2021 Fall Mtg., online, 2021.

(150) Katsuyoshi Tsuchiya, Hiroshi Sagara and Chi Young HAN, "Applicability of Passive Neutron Emission Tomography to spent nuclear fuel assemblies (2) The effect of Water Rod on the tomography" AESJ 2021 Fall Mtg., online, 2021.

(151) Atsushi Nonaka, Hiroaki Tsutsui, Shunji Tsuji-Iio: Measurement of poloidal magnetic field distribution inside plasma using magnetic probe in tokamak device PHiX; *2012 Annual Meeting of Japan Society of Plasma Science and Nuclear Fusion Research*, online, November 22-25, 2021, 24P-3F-13.

(152) Shin Naito, Yasuhiro Suzuki, Hiroaki Tsutsui: Analysis of vertical position stabilizing effect by local coils using TERPSICHORE code; *2012 Annual Meeting of Japan Society of Plasma Science and Nuclear Fusion Research*, online, November 22-25, 2021, 24P-2F-17.

(153) WANG Jingting, TSUTSUI Hiroaki, NAKAMURA Kazuo, ONCHI Takumi, HASEGAWA Makoto, MITARAI Osamu: Analysis of Vertical Position Feedback Control of Divertor Plasma in Ohmic Discharge of QUEST; *2012 Annual Meeting of Japan Society of Plasma Science and Nuclear Fusion Research*, online, November 22-25, 2021, 24P-3F-08.

(154) Sejung Jang, Hiroaki Tsutsui: Prediction of Plasma Vertical displacement by Using LSTM Recurrent Neural Network; *2012 Annual Meeting of Japan Society of Plasma Science and Nuclear Fusion Research*, online, November 22-25, 2021, 24P-1F-04.

(155) Ying Chung, Katsumi Yoshida, Anna Gubarevich: Sintering of SiC Ceramics with Boron or Aluminum Additives using Polycarbosilane, *45th International Conference and Expo on Advanced Ceramics and Composites (ICACC2021, Virtual)*, February 8, 2021, Online, 3476652.

(156) Kenji Miyashita, Katsumi Yoshida, Yukio Kishi, Kento Matsukura: $Cl_2$ plasma exposure behavior of yttrium oxyfluoride ceramics, *45th International Conference and Expo on Advanced Ceramics and Composites (ICACC2021, Virtual)*, February 9, 2021, Online, 3478077.

(157) Tsubasa Watanabe, Anna Gubarevich, Katsumi Yoshida: Sinterability of $Al_4SiC_4$ ceramics by hot pressing and their mechanical properties; *8th International Congress on Ceramics (ICC8)*, April 25-30, 2021, Virtual, Korea, 8-2936.

(158) Katsumi Yoshida, Anna Gubarevich, Masaki Kotani: Coating Process of Carbon and Hexagonal-Boron Nitride Interphases for SiC$_f$/SiC Composites Using Electrophoretic Phenomenon, *8th International Congress on Ceramics (ICC8)*, April 25-30, 2021, Virtual, Korea, 7-0586 (Invited).

(159) Ying Chung, Anna Gubarevich, Katsumi Yoshida: Sintering of Silicon Carbide Ceramics with Boron and Aluminum Additives Using Polymeric Precursor; *8th International Congress on Ceramics (ICC8)*, April 25-30, 2021, Virtual, Korea, 11-3254.

(160) Daichi Sakakibara, Anna Gubarevich, Katsumi Yoshida, Kotani Masaki: Mechanical Properties of Unidirectional SiC$_f$/SiC Composites Using Boron Nitride-Coated SiC Fibers Prepared by Electrophoretic Deposition Process; *8th International Congress on Ceramics (ICC8)*, April 25-30, 2021, Virtual, Korea, 12-3826.

(161) Yu Wei Wu, Anna Gubarevich, Katsumi Yoshida: Mechanical properties of microstructure-controlled $Al_2O_3$/$LaPO_4$ composites; *The 12th International Conference on the Science and Technology for Advanced Ceramics (STAC-12)*, July 6, 2021, Zoom Webinar.

(162) Anna Gubarevich, Tsubasa Watanabe, Toshiyuki Nishimura, Katsumi Yoshida: Induction Heating-Assisted Combustion Synthesis and Mechanical Properties of $Al_4SiC_4$ Ceramics; *The 12th International Conference on the Science and Technology for Advanced Ceramics (STAC-12)*, July 6, 2021, Zoom Webinar.

(163) Ying Chung, Anna Gubarevich, Katsumi Yoshida: Fabrication of porous silicon carbide ceramics using in-situ grain growth with addition of aluminum and boron; *The 12th International Conference on the Science and Technology for Advanced Ceramics (STAC-12)*, July 6, 2021, Zoom Webinar.

(164) Daichi Sakakibara, Katsumi Yoshida, Anna Gubarevich, Masaki Kotani: Evaluation of Mechanical Properties of Unidirectional SiCf/SiC Composites with BN Interphase Formed by Electrophoretic Deposition; *The 12th International Conference on the Science and Technology for Advanced Ceramics (STAC-12)*, July 6, 2021, Zoom Webinar.

(165) Riyo Yamanaka, Anna Gubarevich, Katsumi Yoshida: Adsorption of Volatile Siloxane Compounds on Porous Materials for Prevention of Surface Contamination; *The 12th International Conference on the Science and Technology for Advanced Ceramics (STAC-12)*, July 6, 2021, Zoom Webinar.

(166) Katsumi Yoshida, Anna Gubarevich, Masaki Kotani: Application of Electrophoretic Phenomenon for Interphase Formation of SiC$_f$/SiC Composites, *Korea-Japan Joint Workshop on Ceramic Matrix Composites at KCerS 2021 Fall Meeting*, November 4, 2021, Virtual (Hybrid) (Invited).

(167) Shunya Yamamoto, Anna Gubarevich, Katsumi Yoshida, Tetsuya Goto, Akinobu Teramoto: Plasma irradiation behavior of Y-Al-O ceramics; *42nd International Symposium on Dry Process (DPS2021)*, November 19, 2021, Online, P-7.

(168) Riyo Yamanaka, Anna Gubarevich, Katsumi Yoshida: Study on Desorption of Methyl Siloxane from Porous Materials by Thermogravimetry with Evolved Gas Analysis; *The International Chemical Congress of Pacific Basin Societies 2021*, December 18, 2021, Online, 3591014.

(169) Ying Chung, Anna Gubarevich, Katsumi Yoshida: Fabrication of SiC ceramics with Boron or Aluminum Additive using Polycarbosilane, *The 59th Symposium on Basic Science of Ceramics*, January 7-8, 2021, Online, CBS2021-H09.

(170) Riyo Yamanaka, Anna Gubarevich, Katsumi Yoshida: Research on Materials for Siloxane Adsorption under Extreme Environment, The 101st CSJ Annual Meeting (2021), March 19, 2021, Online Meeting, A28-1pm-05.

(171) Ying Chung, Anna Gubarevich, Katsumi Yoshida: Effect of Boron Addition on Properties of Silicon Carbide Ceramics," *Annual Meeting of The Ceramic Society of Japan, 2021*, March 23, 2021, on-line, 1PA008.

(172) Riku Akatsu, Anna Gubarevich, Katsumi Yoshida: Formation of graphene and $Ti_3SiC_2$ interphase for SiC$_f$/SiC composites by electrophoretic deposition and their mechanical properties, *Annual Meeting of The Ceramic Society of Japan, 2021*, March 24, 2021, on-line, 2A04.

(173) Takahiro Sugizaki, Anna Gubarevich, Katsumi Yoshida: Formation of $Al_4SiC_4$ interphase of SiC$_f$/SiC composites by electrophoretic deposition method and their mechanical properties, *Annual Meeting of The Ceramic Society of Japan, 2021*, March 24, 2021, on-line, 2A05.

(174) Daichi Sakakibara, Anna Gubarevich, Katsumi Yoshida, Masaki Kotani: Fracture behavior of SiC$_f$/SiC composites with BN interphase formed by electrophoretic deposition method, *Annual Meeting of The Ceramic Society of Japan, 2021*, March 24, 2021, on-line, 2A07.

(175) Takaya Sawahiraki, Shotaro Yoshii, Shinji Ogihara, Takuya Aoki, Toshio Ogasawara, Katsumi Yoshida: Fabrication and bending behavior of CMC by melt-infiltration method using Si-V-Cr alloy, *Annual Meeting of The Ceramic Society of Japan, 2021*, March 24, 2021, on-line, 2A09.

(176) Shunya Yamamoto, Kenji Miyashita, Anna Gubarevich, Katsumi Yoshida: Mechanical properties of sintered bulk of Y-Al-O Ceramics, *Annual Meeting of The Ceramic Society of Japan, 2021*, March 25, 2021, on-line, 3A02.

(177) Yu Wei Wu, Anna Gubarevich, Katsumi

Yoshida: Fabrication of microstructure-controlled $Al_2O_3$-based composites with $LaPO_4$, *The 34th Fall Meeting of The Ceramic Society of Japan*, September 2, 2021, on-line, 2H03.

(178) Hiroaki Ashizawa, Katsumi Yoshida: Investigation of fluoride behavior of yttria coatings prepared by aerosol deposition method, *The 34th Fall Meeting of The Ceramic Society of Japan*, September 2, 2021, on-line, 2H22.

(179) Ryoto Takizawa, Hiroaki Ashizawa, Masakatsu Kiyohara: Evaluation for material properties and wear-resistance characteristics of Zirconium oxide coatings by AD method, *The 34th Fall Meeting of The Ceramic Society of Japan*, September 2, 2021, on-line, 2H24.

(180) Katsumi Yoshida, Mayuko Kasakura, Anna Gubarevich, Masaki Kotani: Fabrication and mechanical properties of $SiC_f$/SiC composites with BN interphase formed by electrophoretic deposition method using flaked BN suspension, *The 34th Fall Meeting of The Ceramic Society of Japan*, September 3, 2021, on-line, 3H14.

(181) Daichi Sakakibara, Katsumi Yoshida, Anna Gubarevich, Masaki Kotani: Evaluation of tensile strength of bundle $SiC_f$/SiC composites with BN interphase layer formed by EPD method, *The 34th Fall Meeting of The Ceramic Society of Japan*, September 3, 2021, on-line, 3H15.

(182) Tohru S. Suzuki, Shota Azuma, Tetsuo Uchikoshi, Katsumi Yoshida: Fabrication of textured $B_4C$ with aligned tubal pores by using a magnetic field, *The 34th Fall Meeting of The Ceramic Society of Japan*, September 3, 2021, on-line, 3H19.

BULLETIN OF THE
LABORATORY FOR ZERO-CARBON ENERGY

Vol.1                                                    2022